LIQUID CRYSTALS:

Structure - Properties Relationship

THESIS SUBMITTED FOR THE DEGREE OF
DOCTOR OF PHILOSOPHY (SCIENCE)
OF THE
UNIVERSITY OF NORTH BENGAL

September, 1999

by

Sajal Kumar Giri

LIQUID CRYSTAL RESEARCH LABORATORY
Department of Physics
University of North Bengal
Raja Rammohanpur
Darjeeling - 734 430
West Bengal, India

STOCK TAKING - 2011

Dedicated to my parents

DEPARTMENT OF PHYSICS
UNIVERSITY OF NORTH BENGAL
P.O. NORTH BENGAL UNIVERSITY
DIST. DARJEELING (WB)
PIN : 734430 INDIA

Railway Station : New Jalpaiguri (NFR)
Airport : Bagdogra
Phone : 0353-450414* Fax : 0353-450546*
E-mail : root @ nbu. ernet. in

**local : omit 0353*
**International : replace 0353 by +91353*

Date: 27.09.99

This is to certify that the research work reported in this thesis entitled "Liquid Crystals: Structure - Properties Relationship" by Mr Sajal Kumar Giri has been carried out by the candidate himself under our joint supervision and guidance. He has fulfilled all the requirements for the submission of the thesis for PhD degree of the University of North Bengal. Some parts of the research work presented in this dissertation have been performed in collaboration with others. However, major work has been performed by him and his contribution is very substantial. In character and disposition Mr Sajal Kumar Giri is fit to submit the thesis for PhD degree.

Sukla Paul

(Sukla Paul)
Reader in Physics

(Pradip Kumar Mandal)
Reader in Physics

"A matter that becomes clear ceases to concern us".

— Nietzsche

CONTENTS

ACKNOWLEDGEMENTS

At the outset, I am expressing my profound sense of gratitude to Dr (Mrs.) S. Paul, Reader in Physics, North Bengal University, by whose efficacious and vivacious supervision and constant helping I have come into possession of such a rare facility. Her through and through cogitation about my scientific work beggars description. To my co-supervisor, Dr P. K. Mandal, Reader in Physics, North Bengal University, an additional measure of thanks is due for his meticulous attention to my research work. He has played a key role at every stage of my work and I am grateful to him for his wise decisions.

I pay my tribute to Dr R. Paul, Professor of Physics, North Bengal University, a man of profound learning and a celebrity of science, for his apropos analysis and expounding his verdict in many facets of my research work.

Special thanks go to Dr M. Mitra, Lecturer in Physics, Bangabashi College, Calcutta, whose words were a great source of encouragement to me and helped me to reach this milestone in my life.

I wish to express my appreciation to Professor R. Dabrowski, Military University of Technology, Warsaw, Poland for supplying good quality liquid crystal samples.

I am also thankful to all the members of the Department of Physics, North Bengal University. My exquisite thanks go to Dr M. K. Das, Dr B. Adhikari, Dr N. K. Pradhan, Mr P. Sarkar, Ms S. Ghosh for their helpful co-operation in my research work.

I am moved at the co-operative behaviour and technical suggestions of Mr S. Sarkar, a person of real sense of commitment to the job. I hope my action would express my gratitude to him more than any word could do. The staff members of University Science and Instrumentation Centre are gratefully acknowledged for their help.

I am expressing my thanks to Department of Atomic Energy, India for awarding me a Junior Research Fellowship.

During my research period many special people have helped me in a variety of ways and have given mental support to me. My heartfelt thanks are due to all of them.

Finally, I owe my debt of gratitude to my family, specially my parents, who by giving me the necessary impetus, have aroused in me the interest to do this scientific work. Their love and proper guidance help me to reach here.

Date: University of North Bengal
September 28, 1999

Sajal Kumar Giri
(Sajal Kumar Giri)

Chapter - 1

INTRODUCTION

1.1 LIQUID CRYSTALS

> *"I venture to ask you to investigate somewhat closer the physical isomerism of the two enclosed substances. Both substances show such striking and beautiful phenomena that I can hopefully expect that they will also interest you to a high degree...."*

This is from a letter of Friedrich Reinitzer, the Austrian botanist, written to Otto Lehmann, the German physicist in 1888[1] — while discovering '**Liquid Crystals**', a term latter coined by Lehmann[2]. Not only to Lehmann but also it has grown interest to a large section of scientific community. Liquid Crystals, usually organic or organometalic compound[3-5], represent a different state of matter in which the degree of molecular order lie intermediate between the perfect long-range positional and orientational order found in solid crystals and the statistical long-range disorder found in ordinary isotropic liquids and gases. It can flow like a liquid and form droplets, yet it is anisotropic, which is reminiscent of crystals. Now-a-days, following Friedel's[6,7] suggestion the term 'mesomorphic phase' or 'mesophase' meaning intermediate phase, are also used along with the term liquid crystals.

An important factor governing the formation of a mesophase is molecular shape[5,8]. The molecules are usually geometrically anisotropic. Mesogens which are formed by the molecules elongated in one dimension i.e., rod-like or reed-like are called calamitic and which are formed by the molecules extended in two dimensions i.e., disk-like or lath-like are called columnar or discotic. The molecular shape may even be bowl-shaped[9], sofa-shaped, banana-shaped[10-13], U[11], Y[14], H[15] and T[16] -shaped.

1.2 CLASSIFICATION OF LIQUID CRYSTALS

Liquid crystals are divided into two main subgroups:

1.2.1. Lyotropic Liquid Crystals

Lyotropic liquid crystals (LLC)[17-21] are mixtures of an anisotropic amphiphilic compound (surfactant) and one or more polar solvents such as water. Amphiphilic compound has two groups — a hydrophilic polar head and a

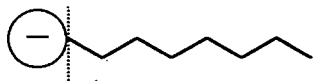

Polar head hydrocarbon chain

hydrophobic hydrocarbon chain. It is highly soluble in water. The temperature range of the mesophase of a LLC is determined by its concentration. At low concentration the solute molecules are distributed randomly throughout the solvent. Below certain concentration LLC will not form. This concentration is called critical concentration. In LLC solute-solvent interaction plays a major role to maintain long-range ordering. Here solute-solute interaction is secondary. The lyotropic liquid crystalline phases have relevance to biological systems. Biological membrane consists of lipids and water and usually also proteins which have liquid crystalline properties. Moreover, Lyotropic systems, are usually as sensitive to changes in temperature as thermotropic systems. There are different types of LLCs but as this dissertation is not concerned with LLC, it shall not be discussed any further.

1.2.2. Thermotropic Liquid Crystals

Depending on the molecular structure, a particular compound may pass through one or more mesophases before it is transformed from low temperature solid into the high temperature isotropic liquid or vice-versa. They are commonly designated as thermotropic. Thermotropic liquid crystals (TLC) can be classified into three main types: A) nematic, B) smectic and C) columnar phases[7,8,17,21-23].

A) Nematics

The word 'nematic' comes from a Greek word *νημα* means 'thread' and it indicates thread-like defects in this type of mesophase. The properties are as follows:

i) Nematic liquid crystals have no translational or positional order.

ii) They have long-range orientational order about the molecular long-axis.

iii) Molecules are aligned along time averaged preferred direction, labelled by a unit vector (called director) **n**.

iv) The direction of **n** may be determined by some minor forces such as surface force.

v) The states of the director **n** and - **n** are indistinguishable. If the individual molecules carry a permanent electric dipole there are just as many dipoles 'up' as there are dipoles 'down'.

vi) It is optically uniaxial.

vii)The molecules are either optically inactive or, if they are optically active, right and left handed molecules must be racemic (1:1).

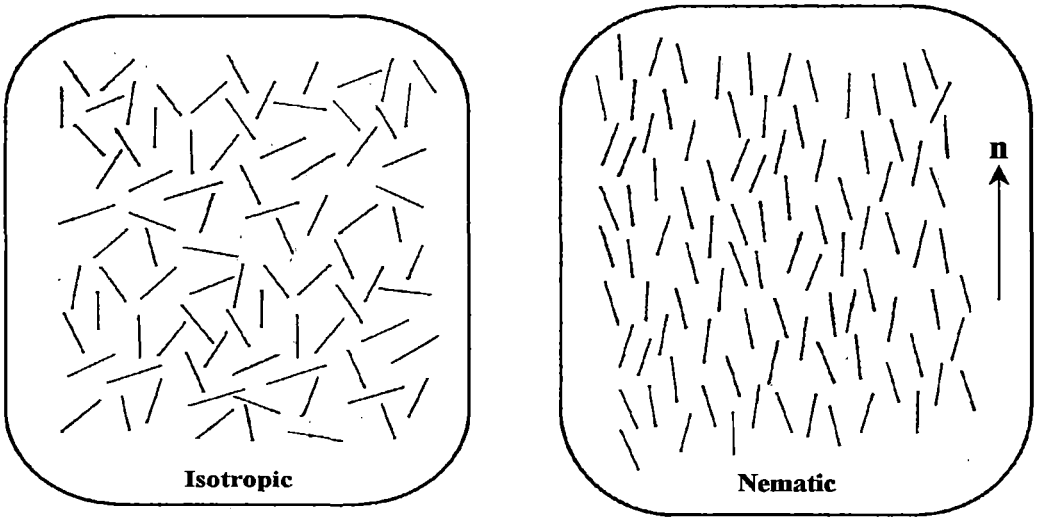

Fig.- 1.1 Schematic diagram of molecular order in the isotropic and nematic phase.

Apart from ordinary nematics two other nematic phases are common. These are a) cholesteric or chiral type nematic and b) cybotactic nematic.

a) Cholesteric or chiral-nematics

Cholesteric (N* or N_{ch}) are very similar to a nematic material[22]. The centre of gravity have no long-range order and the molecular orientation shows a preferred axis labelled by a director **n**. However, **n** is not constant in space. The preferred conformation, shown in Fig.-1.2, is helical. If we call the z-axis the helical axis, we have the following structure for **n**

$n_x = \cos(q_0 z + \varphi)$; $n_y = \sin(q_0 z + \varphi)$; $n_z = 0$.

Both the helical axis (z) and the value of φ are arbitrary. The structure is periodic along z and (since the states **n** and **-n** are again equivalent) the spatial period L is equal to one-half of the pitch:

$L = \pi / |q_o|$.

Both the magnitude and sign of q_o are meaningful. The sign distinguishes between right- and left-handed helices; a given sample at a given temperature always produces helices of the same sign. Magnitude of q_o depends on temperature and concentration.

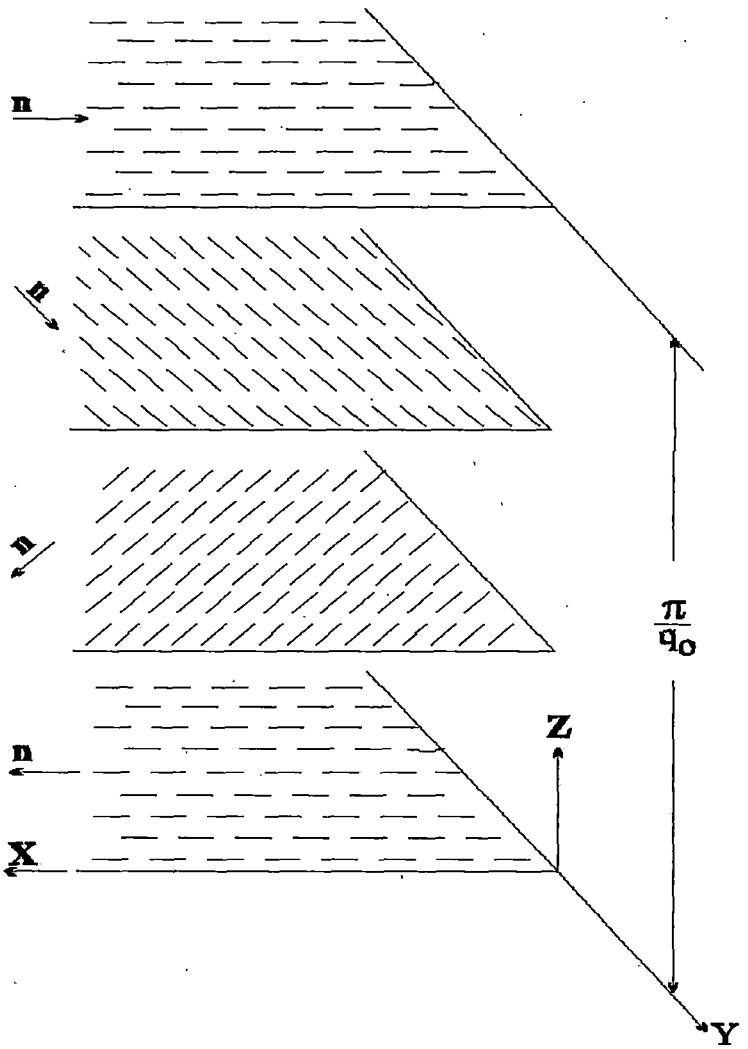

Fig.- 1.2 Schematic representation of the helical structure of the cholesteric liquid crystals.

b) Cybotactic nematic

This phase was first observed by de Vries[24,25] from x-ray studies. It contains a groups of molecules and the molecular centre in each group lie in a well defined plane. When molecular long-axis is arranged perpendicular to the plane or tilted with respect to the plane, the phases are called normal or skewed cybotactic nematic phase respectively. This phase looks like nematics with smectic fluctuation.

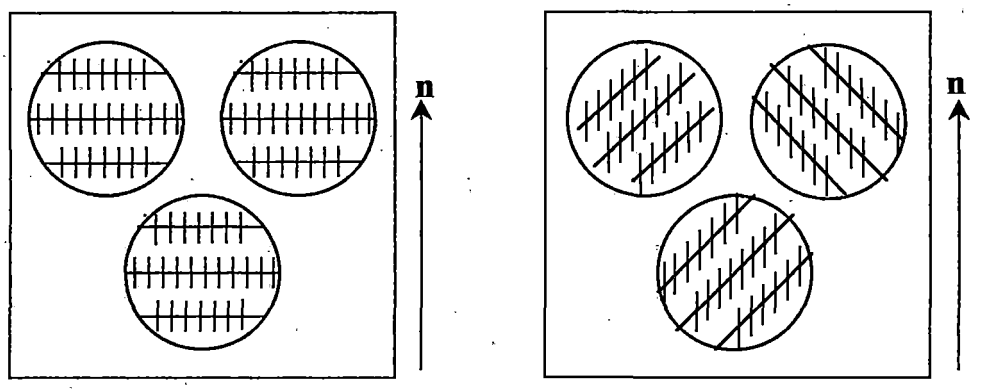

Normal Cybotactic (S_A type) **Skewed Cybotactic (S_C type)**

(a) **(b)**

Fig. - 1.3 Schematic representation showing molecular arrangements in cybotactic nematic phase

Although biaxial nematic was theoretically predicted by Freiser in 1971 it has been observed in mid 80's in polymeric as well as low molecular weight thermotropic systems[22,26-28].

B) Smectics

The properties of smectic mesophases (Sm) are as follows:

i) This type of mesophases have a lamellar structure

ii) Within each layer molecules are mobile in two directions and can rotate about one axis in some cases.

iii) Inter layer attraction forces are weaker than the lateral forces among molecules within a layer and thus the layers can easily slide over one another.
iv) Molecules may be normal to the plane of the layers or inclined.
v) This phase is more viscous than nematic.
vi) For a given material usually occur at temperatures below the nematic domain.

Though Friedel[23] recognised only one type of smectic, now called smectic A, over the years a large number of different smectic phases have been identified[8,22,29-38]. These have been tabulated in Tables - 1.1–1.2. Only those smectic phases which are relevant to the present work described below.

Smectic A (SmA)

i) Molecular long axes are normal to the plane of the layer.
ii) The centres of mass of the molecules possess short-range one-dimensional translational periodicity along the layer normal.
iii) Within each layer molecules have only orientational ordering.
iv) The phase is optically uniaxial.

SmA_1: This phase is a monolayer phase arranged in a liquid like fashion with the dipolar heads oriented up and down randomly within each layer. It produces the periodicity d equal to l, the molecular length.

SmA_2: It is a bi-layer phase. This is attributed to a preferential up-down ordering of the dipolar heads within each layer, which alternates from layer to layer producing a periodicity d equal to twice the molecular length, 2l.

SmA_d: This is an intermediate phase of SmA_1 and SmA_2 characterised by the layer thickness between one and two molecular lengths (i.e., $l < d < 2l$) due to head to tail association of molecules with some overlapping, contrast to no overlapping as in SmA_2 phase. Thus this is a partially bilayer phase, indistinguishable with SmA_2 phase in context of microscopic symmetries.

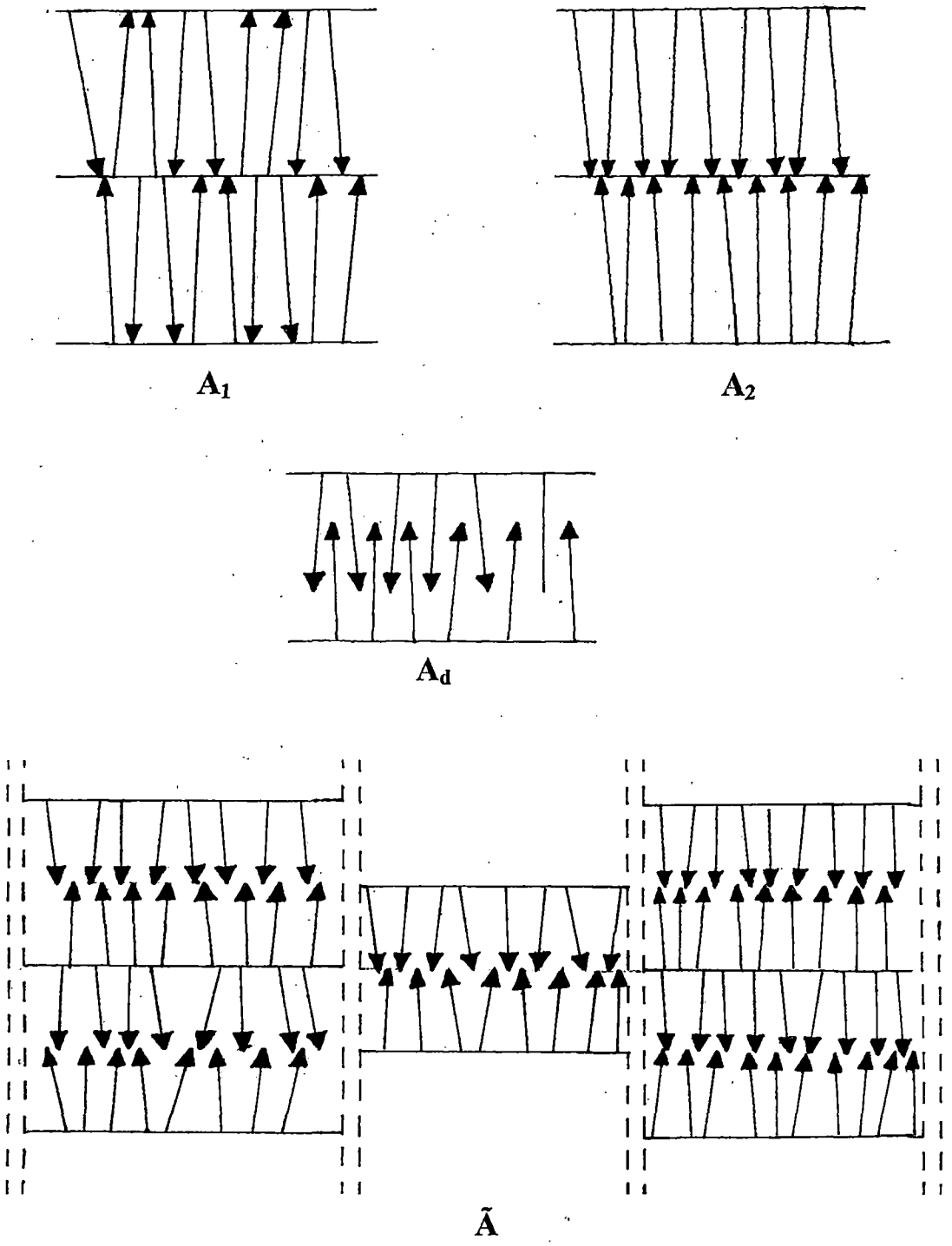

Fig. - 1.4 Schematic representation of the molecular arrangement in the different forms of smectic A phase composed of polar molecules; monolayer A_1, bilayer A_2, partially bilayer A_d and antiphase Ã.

SmÃ: This is actually a two dimensionally ordered bilayer smectic phase, called antiphase, with modulation in the direction perpendicular to the layer normal[39].

There is a new type of SmA phase denoted by SmA_{ic}[40] which intervenes between the SmA_d and SmA_2 phases. This phase has two collinear incommensurate density modulations.

Smectic C (SmC)

The properties of SmC phase are as follows:

i) Molecules in a strata are arranged in a tilted manner with respect to the layer normal. Each layer is a 2-D liquid.

ii) Tilt angle may be constant or temperature dependent[34].

iii) The phase is optically biaxial.

Further it is classified into three subgroups, viz., C_1, C_2 and C_3 depending on the nature of tilt angles.

Smectic B (SmB)

The properties of SmB phase are as follows:

i) Within a layer molecular long axes are parallel to the layer normal but the centres of mass of the molecules are arranged in hexagonal symmetry.

ii) It is optically uniaxial.

This mesogen is reclassified into CrB (or L phase) and hexatic B phases. Both the phases exhibit long range bond orientational order but CrB (or L) shows inter and intra layer long range translational order whereas hexatic B exhibits quasi long range inter layer and short range intra layer translational order.

1.3 FEW OTHER MESOPHASES

Discotic

In 1977 S. Chandrasekhar et al.[41] first reported discotic phase mesophase in

a system of disc like molecule. Two distinct phases are observed in this case — columnar and nematic. There are several columnar mesophases exhibited by discotic materials; these arise because of the different symmetry claseses of the two - dimentional lattice of columns and order or disorder of the molecular stacking within the columns. In recent years, significant amount of research works have been performed in this section[42-45].

Blue phase

Some cholesteric liquid crystal materials having cubic symmetry and short pitch (<7000 Å) show a specific bluish - violet colour at a very short temperature region (~ 0.1 – 0.5^0C) below its clearing temperature. These mesophases are called 'blue phase' due to its colour[44-48]. From thermodynamic and optical studies it is confirmed that these phases are stable in a narrow temperature interval. Three principal types of blue phases (I, II and III) have been observed depending upon their helical pitch. In increasing the pitch, phase III is the first to lose the stability, then phase II and at last phase I. These mesophases do not exhibit optical birefringence[49] but show optical activity and selective reflection of circularly polarised light.

Re-entrant phase

In liquid crystalline compounds different phases appear in a fixed sequences as a function of temperature. The sequence of the mesophases during cooling from isotropic phase is given below:

Iso→Blue→N→A→C→B(hex)→I→B(Cr.)→F→J→G→E→K→H→Solid Crystal.

However, there is no single compound which exhibits all the phases. When temperature is changed if any phase reappears after normal occurrence in the above sequence, then that phase is called re-entrant phase. Re-entrant nematic (N_r) phase sequence (N – S – N_r) was first observed by P. E. Cladis[50], in a binary mixture of two polar cyano compounds. Later this behaviour is observed in many systems

either in mixtures, in pure state, under pressure or some combination of these three conditions[51]. Multiple re-entrant behaviour has also been observed[52]. Cladis explained the re-entrance phenomenon in system of polar molecules in terms of dipole-dipole interaction. de Gennes gave simple models based on mean-field arrangements to explain single and double re-entrance behaviour[22]. The re-entrant phenomenon in mixtures and in pure compounds, according to Brodzik and Dabrowski[47], is due to the change in an equilibrium between associated and non-associated forms of the molecules as a result of change in temperature and the competition between short and long range order.

Induced and enhanced Smectic phases

Sometimes binary mixtures of two purely nematic compounds show smectic phase depending upon the charge distribution of individual compounds. This type of smectic phase is known as induced smectic phase. One of the components of the mixture be a strongly polar compound and other is non-polar or weakly polar[53-68].

Components of binary mixture, having smectic phase in their pure states may exhibit a smectic phase over wider temperature region for certain concentrations. This phase in binary mixture is known as enhanced smectic phase.

The formation of induced smectic A_d phase may be explained by mean field approximation model of Longa and de Jeu[69] or Berker's frustrated spin glass model[70]. In both the models molecular association due to dipole-dipole interaction and role of alkyl chain length are important.

Chiral tilted smectic phase

Within various types of smectic liquid crystals seven viz., C, I, F, J, G, K and H have tilted structure. Since the molecules are tilted with respect to the layer normal, the rotation of the molecules about the director is anisotropic, resulting in a non-compensated macroscopic component of the molecular dipole moment. In addition to this if a chirality is present in the molecules they can give rise to spontaneous polarisation. These are called ferro-electric liquid crystals and are denoted by C*, I*, F*, J*, G*, K* and H*[56].

Table - 1.1

Classification of Liquid Crystals

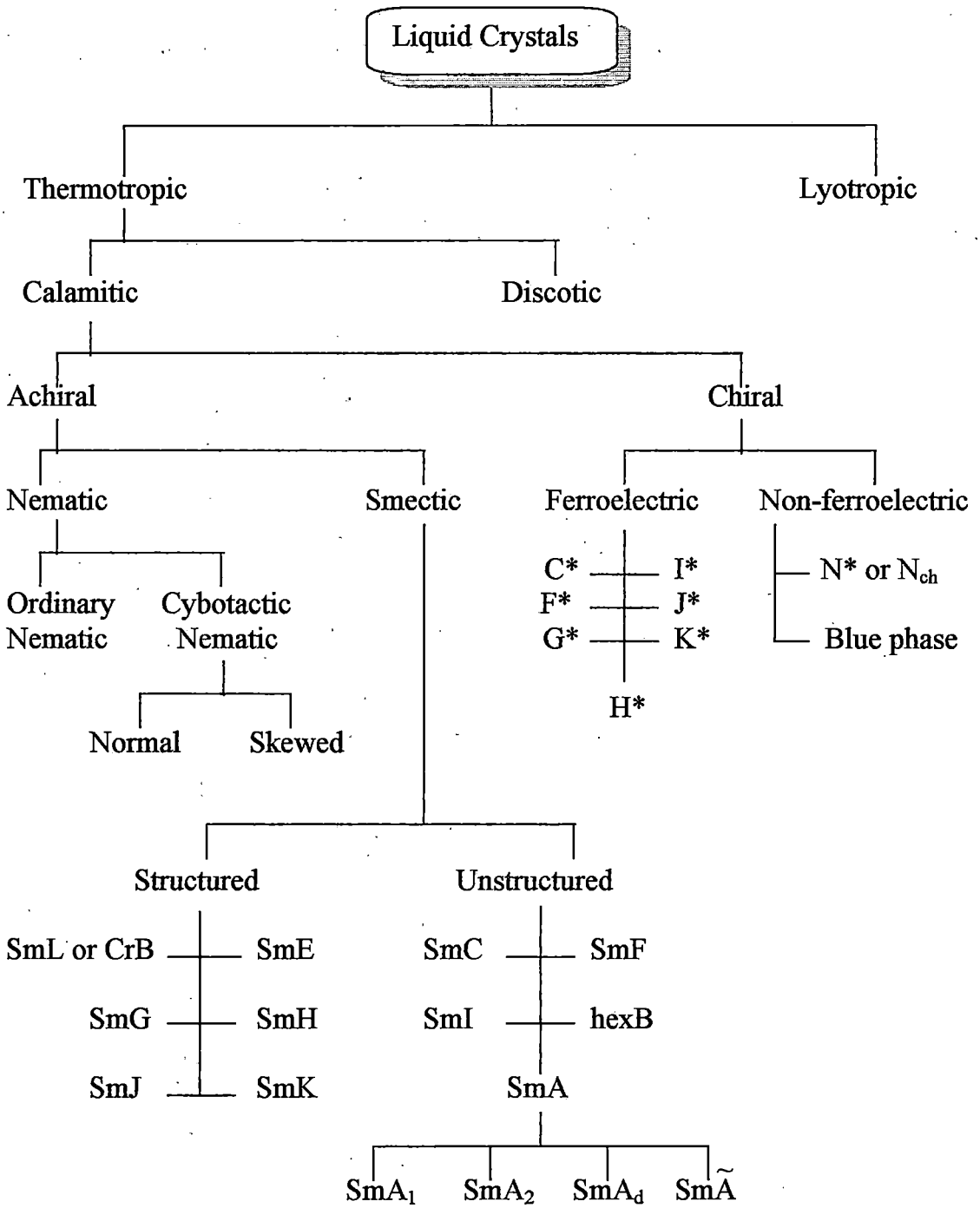

Table - 1.2

Phase type and ordering

Phase type	Molecular orientation	Molecular packing	Molecular orientational ordering	Bond orientational ordering	Positional ordering	
					Normal to the layer	within the layer
N	parallelism of long molecular axis	random	LRO	Nil	Nil	Nil
S_A	orthogonal	random	LRO	SRO	QLRO	SRO
S_C	tilted	random	LRO	SRO	QLRO	SRO
hex B	orthogonal	hexagonal	LRO	LRO	QLRO	SRO
S_I	tilt to apex of hexagon	pseudo hexagonal	LRO	LRO	QLRO	SRO
S_F	tilt to side of hexagon	pseudo hexagonal	LRO	LRO	QLRO	SRO
S_L	orthogonal	hexagonal	LRO	LRO	LRO	LRO
S_J	tilt to apex of hexagon	pseudo hexagonal	LRO	LRO	LRO	LRO
S_G	tilt to side of hexagon	pseudo hexagonal	LRO	LRO	LRO	LRO
S_E	orthogonal	ortho- rhombic	LRO	LRO	LRO	LRO
S_K	tilted to side a	mono-clinic	LRO	LRO	LRO	LRO
S_H	tilted to side b	mono-clinic	LRO	LRO	LRO	LRO

SRO : short range order, LRO : long range order, QLRO : quasi-long range order

Chapter - 2

THEORETICAL BACKGROUND OF DIFFERENT EXPERIMENTAL TECHNIQUE

2.1 INTRODUCTION

Scientist had been trying to develop some theories to understand the behaviour of liquid crystals over many years. One of the theory is molecular field approximation proposed by Born[71] who treated the medium as an assembly of permanent electric dipoles and demonstrated the possibility of a transition from an isotropic to an anisotropic phase when temperature is lowered. Though this result is important qualitatively but the main objections against it are (1) permanent dipole moments are not necessary for the occurrence of liquid crystal phase and (2) resulting anisotropic phase in most cases not ferroelectric as the theory predicts.

In 1937 Landau[72] made an elegant and far-reaching speculation about the functional dependence of the free energy density on the order parameter. It is a quantitative measure of how well formed the phase is.

Considering the molecule as a long hard rod, later Onsager[73] proposed a theory based on an exact density expansion for the free energy. But his theory also fails to explain the observed behaviour of order parameter near the nematic–isotropic phase transition.

Most acceptable and widely used theories based on molecular field approximation are given by Maier-Saupe[74] for nematics and McMillan[75] for smectic A though both the theories have also some limitations. I have compared my experimental data with the theoretical values obtained from these theories and I am, therefore, describing these two theories in short.

2.2 MAIER-SAUPE MEAN FIELD THEORY OF NEMATIC PHASE OF ROD LIKE MOLECULES

A microscopic approach that has proved to be useful in developing a theory of long range orientational order and some of related properties of the nematic phase is that due to Maier and Saupe[74]. It is based on mean-field approximation. They assumed that

- the molecules are up-down symmetric about their long axis and with respect to a given molecule the distribution of the remaining molecules may be taken to be cylindrically symmetric.

• the alignment of the molecules are caused by dispersion forces. Repulsive interaction is not considered.

Here alignment of the molecules with respect to a preferred axis, called the director, is described by an orientational order parameter $S = \langle P_2(\cos\theta) \rangle$ or $\langle P_2 \rangle$, where θ is the average angle between molecular long axis and the director, where $\langle \ldots \rangle$ means statistical average aver all orientations in the system.

The single particle orientational potential energy would be proportional to $-\cos^2\theta$ (or, $P_2(\cos\theta)$), where $P_2(\cos\theta)$ is second order Legendre Polynomial.

$\therefore \quad U(\cos\theta) \propto -P_2(\cos\theta)$

Again mean field should be directly proportional to the degree of alignment and we have,

$$U(\cos\theta) \propto \langle P_2(\cos\theta) \rangle$$

$$\therefore \quad U(\cos\theta) \propto -\langle P_2(\cos\theta) \rangle P_2(\cos\theta)$$

$$= -(A / V^2) S P_2(\cos\theta)$$

$$= -v_2 S P_2(\cos\theta) \qquad 2.1$$

where V is the mean molecular volume, A is a constant characteristic of the molecule, independent of pressure, volume and temperature and $v_2 = A / V^2$.

Humphries et al[76] developed a more comprehensive concept by including higher order terms in the mean field potential for cylindrically symmetric molecules. Their result is

$$U(\cos\theta) = \sum_{L \text{ even}} U_L P_L(\cos\theta) \langle P_L(\cos\theta) \rangle \qquad (L \neq 0) \qquad 2.2$$

2.2.1 Orientational distribution function

Orientational distribution function $f(\cos\theta)$ gives the probability of finding molecule whose axis makes an angle θ with the director **n**.

The distribution function for the molecular arrangement is

$$f(\cos\theta) = Z^{-1} \exp[-\beta U(\cos\theta)] \qquad 2.3$$

where Z is the single molecular partition function given by

$$Z = \int_0^1 \exp[-\beta U(\cos\theta)]\, d(\cos\theta) \qquad 2.4$$

Here $\beta = 1 / kT$, k is Boltzmann's constant, T is the temperature in absolute scale.

Therefore, the average value of the order parameter is

$$\langle P_2(\cos\theta)\rangle = \int_0^1 P_2(\cos\theta)\, f(\cos\theta)\, d(\cos\theta) \qquad 2.5$$

$$= \frac{\int_0^1 P_2(\cos\theta) e^{v_2 \langle P_2\rangle P_2(\cos\theta)/kT}\, d(\cos\theta)}{\int_0^1 e^{v_2 \langle P_2\rangle P_2(\cos\theta)/kT}\, d(\cos\theta)}$$

$$= \frac{\int_0^1 P_2(\cos\theta) e^{\langle P_2\rangle P_2(\cos\theta)/T^*}\, d(\cos\theta)}{\int_0^1 e^{\langle P_2\rangle P_2(\cos\theta)/T^*}\, d(\cos\theta)} \qquad 2.6$$

where $T^* = kT / v_2$ is called the reduced temperature.

Equation 2.6 is a self-consistent equation for the determination of the temperature dependence of $\langle P_2\rangle$. The value of $\langle P_2\rangle = 0$ is a solution at all temperatures, which represents a disordered phase, the normal isotropic liquid. In addition, for temperature $T^* < 0.22284$ two more solutions of $\langle P_2\rangle$ appear. One is $\langle P_2\rangle$ greater than zero which tend to unity at $T = 0$ means almost perfectly aligned molecule. Other value of $\langle P_2\rangle$ is negative which has not yet been observed experimentally for calamitic systems.

The laws of thermodynamics state that the stable phase, will be the one having the minimum free energy. Applying this stability condition, we get the region $0 \le T^* \le 0.22019$, where $\langle P_2\rangle$ is greater than zero which corresponds an anisotropic nematic phase and for $T^* > 0.22019$, the isotropic phase with $\langle P_2\rangle = 0$ is the stable state.

The order parameter $\langle P_2\rangle$ varies from 1 at $T^* = 0$ to 0.4289 at $T^* = 0.22019$. The transition from nematic to isotropic phase is first order as $\langle P_2\rangle$ value jumps from 0.4289 to 0 suddenly.

2.3 McMILLAN'S THEORY FOR SMECTIC PHASE

The structure of smectic phase is different from nematic. There is an extra positional order i.e., one dimensional periodicity along one direction (taken as Z axis).

Therefore, the single particle distribution function can be written as

$$f(z,\cos\theta) = \sum_{\substack{l=0 \\ \text{even}}} \sum_{n=0} A_{l,n}\, P_l(\cos\theta) \cos\left(\frac{2\pi n z}{d}\right) \qquad 2.7$$

where d is the layer thickness. McMillan[75] developed the theory of smectic A liquid crystals starting from the Kobayashi[77,78] form of potential. For simplicity, neglecting higher order terms McMillan wrote the mean field potential as

$$V_1(z,\cos\theta) = -v_0\left[\delta\alpha\tau \cos\left(\frac{2\pi z}{d}\right) + \left\{S + \sigma\alpha \cos\left(\frac{2\pi z}{d}\right)\right\} P_2(\cos\theta)\right] \qquad 2.8$$

where v_0 and δ are constants characterising the strengths of the anisotropic and isotropic parts of the interaction respectively. Here

orientational order parameter $S = \left\langle\left(\frac{3}{2}\cos^2\theta - \frac{1}{2}\right)\right\rangle$,

translational order parameter $\tau = \left\langle \cos\left(\frac{2\pi z}{d}\right)\right\rangle$,

mixed order parameter $\sigma = \left\langle P_2(\cos\theta)\cos\left(\frac{2\pi z}{d}\right)\right\rangle$

and α is a parameter which depends on the core length and molecular length.

Then

$$f_1(z,\cos\theta) = Z^{-1} \exp\left[-\beta V_1(z,\cos\theta)\right] \qquad 2.9$$

Z is the single molecular partition function given by

$$Z = \int_0^d dz \int_0^1 \exp\left[-\beta V_1(Z,\cos\theta)\right] d(\cos\theta)$$

in which range of dispersion interaction, r_o, is of the order of the length of the rigid core of the molecule. δ is another parameter of potential.

The order parameters are given by,

$$\left.\begin{aligned} S &= \int_0^1 \int_0^d P_2(\cos\theta)\, f_1(\cos\theta, z)\, dz\, d(\cos\theta) \\ \tau &= \int_0^1 \int_0^d \cos\left(\frac{2\pi z}{d}\right) f_1(\cos\theta, z)\, dz\, d(\cos\theta) \\ \sigma &= \int_0^1 \int_0^d P_2(\cos\theta) \cos\left(\frac{2\pi z}{d}\right) f_1(\cos\theta, z)\, dz\, d(\cos\theta) \end{aligned}\right\} \quad 2.10$$

There are a self consistent equations for the three order parameters as functions of temperatures.

The expression of S, σ and τ exhibit three types of solutions:

i) $\tau = \sigma = S = 0$, no order characteristic of the isotropic liquid phase;

ii) $\tau = 0$, $\sigma = 0$, $S \neq 0$, orientational order only, the theory reduces to the Maier-Saupe theory of the nematic phase; and

iii) $\tau \neq 0$, $\sigma \neq 0$, $S \neq 0$, orientational and translational order characteristic of the smectic A phase.

One can also predict the nature of the smectic to nematic phase transition observing McMillan ratio (T_{NA}/T_{NI}). (T_{NA}/T_{NI}) $\rangle$ 0.87 represents first order and (T_{NA}/T_{NI}) $\langle$ 0.87 represents second order SmA – N transition. T_{NA} and T_{NI} are the Sm – N and N – I transition temperature respectively.

2.4 X-RAY SCATTERING

The general formula for the intensity of scattering from a system of molecules is

$$I(\mathbf{S}) = \sum_k \sum_l \sum_m \sum_n \left\langle f_{km}(\mathbf{S}) f_{ln}^*(\mathbf{S}) \exp\left[i\mathbf{S}.(\mathbf{r}_k - \mathbf{r}_l)\right] \exp\left[i\mathbf{S}.(R_{ln} - R_{km})\right] \right\rangle \quad 2.11$$

where the brackets indicate an average over the liquid is involved. $\mathbf{r}_k$ is the centre of mass of the k^{th} molecule, f_{km} is the atomic scattering factor of the m^{th} atom in the k^{th} molecule and R_{km} is the position of the m^{th} atom in the k^{th} molecule.

S is the scattering vector and $\mathbf{S} = \mathbf{K}_s - \mathbf{K}_i$.

$\mathbf{K}_s$ = scattered wave vector, $\mathbf{K}_i$ = incident wave vector.

For elastic scattering $|\mathbf{K}_s| = |\mathbf{K}_i| = 2\pi / \lambda$.

The intensity can be written as

$I(\mathbf{S}) = I_m(\mathbf{S}) + D(\mathbf{S})$

$I_m(\mathbf{S})$ is the molecular structure factor and $D(\mathbf{S})$ is called the interference function.

$$I_m(\mathbf{S}) = \sum_k \left\langle \sum_{m,n} f_{km}(\mathbf{S})\, f_{kn}^*(\mathbf{S}) \exp\left[i\mathbf{S}\left(R_{kn} - R_{km}\right)\right] \right\rangle$$

$$= N\left\langle \left| \sum_m f_{kn} \exp\left(-i\mathbf{S}R_{km}\right) \right|^2 \right\rangle$$

$$D(\mathbf{S}) = \left\langle \sum_{k\neq l}^{m} \exp\left(i\mathbf{S}.\mathbf{r}_{kl}\right) \sum_{m,n} \left\langle f_{km}(\mathbf{S}) f_{ln}^*(\mathbf{S}) \exp\left[i\mathbf{S}.\left(R_{ln} - R_{km}\right)\right] \right\rangle \right\rangle \qquad 2.12$$

$$\mathbf{r}_{kl} = \mathbf{r}_k - \mathbf{r}_l$$

The term $I_m(\mathbf{S})$ gives the scattered intensity which would be observed from a random distribution of identical molecules.

$D(\mathbf{S})$ contains information regarding

a) Molecular packing
b) Orientational distribution function
c) Order parameters $\langle P_2 \rangle$, $\langle P_4 \rangle$ ... etc.
d) Apparent molecular length
e) Average lateral distance between the molecules
f) Layer thickness in Smectics
g) Layer order parameters τ and $\langle z^2 \rangle$ in SmA
h) Correlation lengths
i) Tilt angle
j) Bond orientational order parameter
k) Critical exponents.

2.5 EXPERIMENTAL TECHNIQUE AND DATA ANALYSIS BY X-RAY DIFFRACTION STUDIES

Small angle x-ray scattering is a best tool for structural determination of condensed matter. The x-ray set-up was designed and fabricated by Jha and Paul[79] in our laboratory. The schematic representation of the whole set-up is shown in Fig. - 2.1

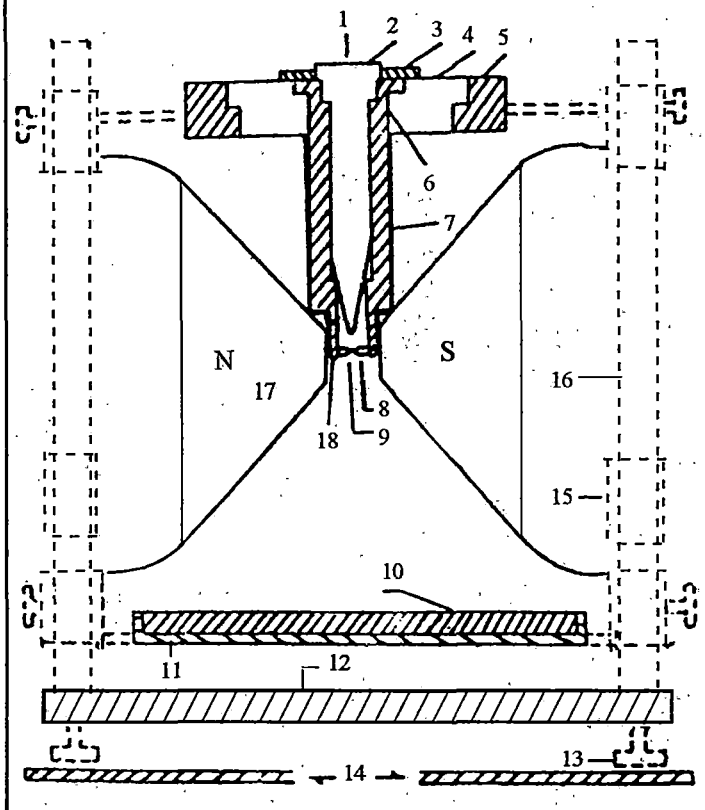

Fig. 2.1 Sectional diagram of the X-ray diffraction camera

1. Entrance of x-ray beam,
2. Collimator,
3. Brass ring,
4. Ring of syndanyo board,
5. Brass ring,
6. Cylindrical Brass chamber,
7. Asbestos insulation and heater winding,
8. Specimen holder and thermocouple,
9. Sample position,
10. Film cassette,
11. Film cassette holder,
12. Base plate,
13. Levelling screw,
14. Brass plates over the coils of the electromagnet,
15. Removable spacer,
16. Supporting brass stand,
17. Pole pieces,
18. Asbestos insulation.

In experiment sample is taken in a lindemann glass capillary of ~0.1 mm. diameter and then seal both the ends of it. The sample is placed inside a thermostated block. Slow and controlled cooling from isotropic state or a very high temperature mesophase to required temperature in the presence of magnetic field makes the sample aligned along the direction of magnetic field. X-ray photograph is

taken with nickel filtered Cu K_α radiation, x-ray beam being perpendicular to the magnetic field.

X-ray photographs of oriented samples are of different types depending upon the mesophase. Fig.- 2.2 shows small angle x-ray diffraction pattern of ordinary nematic and smectic A phases aligned along the applied magnetic field. Here the circular outer halo splits into two crescents having maxima along the equatorial direction. These crescents are formed due to intermolecular scattering and the corresponding diffraction angle is a measure of lateral intermolecular distance.

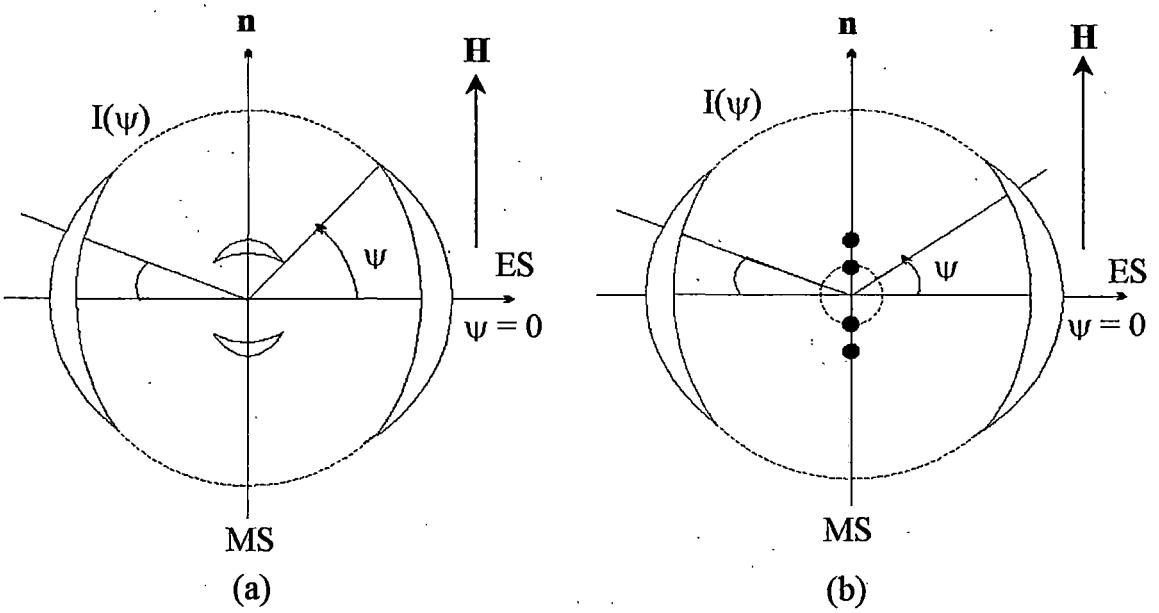

ES : Equatorial section, MS : Meridional section

Fig. - 2.2 Schematic representation of the x-ray diffraction pattern of an oriented (a) nematic and (b) smectic phase.

At much lower scattering angle intensity peaks usually in the shape of short bar are in the meridional direction. Measuring the corresponding angle of diffraction we get the value of apparent molecular length.

In case of cybotactic nematic these bars break up into spots[80].

Photographic nature of SmA phase is different. Unlike nematic phase inner diffraction peaks usually change to two sharp spots. Sometimes second order spots also appear. τ, the translational order parameter can be determined from these spots.

From the equatorial arcs of x-ray diffraction pattern, orientational order parameters and intermolecular distance can be calculated. Full circular scanning of optical density (O.D) is performed with the help of microdensitometer (CARL ZEISS JENA MD 100) at required intervals considering the maximum O.D position at an angle $\psi = 0^\circ$. These O.D data are converted to intensity data with the help of a calibration curve[81]. Thus we get angle (ψ) vs. angular intensity distribution I (ψ) curve. From the value of I (ψ) [for $\psi = 0^\circ$ to 90°], we can calculate the orientational distribution function f(β) using the relation[82] of Leadbetter and Norris.

The relation between f(β) and I (ψ) is

$$I(\psi) = C\int_{\beta=\psi}^{\pi/2} f(\beta)\sec^2\psi\left[\tan^2\beta - \tan^2\psi\right]^{-1/2}\sin\beta\, d\beta \qquad 2.13$$

where β is the angle between director **n** and molecular long axis.

As molecular distribution in the nematic phase is centrosymmetric, the distribution function and the intensity can be expanded as even cosine power series.

$$I(\psi) = \sum_{n=0}^{r} a_{2n}\cos^{2n}\psi \qquad 2.14$$

$$f(\beta) = \sum_{n=0}^{r} b_{2n}\cos^{2n}\beta \qquad 2.15$$

The series converge rapidly. Retaining eight terms in the truncated series, a least square fitting was made with the observed I(ψ) values to get the coefficients of 2.14. These values of a_{2n} were then used to calculate the coefficients of b_{2n}.

Orientational order parameter $\langle P_2\rangle$ and $\langle P_4\rangle$ were then calculated using the following equation

$$\langle P_l\rangle = \frac{\int_0^1 P_l(\cos\beta)\, f(\beta)\, d(\cos\beta)}{\int_0^1 f(\beta)\, d(\cos\beta)} \qquad 2.16$$

Necessary computer program was written in our laboratory. The errors in calculation of $\langle P_2 \rangle$ and $\langle P_4 \rangle$ in my experiment are estimated to be within $\pm$ 0.02.

Linear scanning of outer halo gives average intermolecular distance (D). Corresponding equation is

$$2D\sin\theta = k\lambda \qquad 2.17$$

where θ is the Bragg angle for equatorial diffraction, λ is the wavelength of CuK_α line and k is a constant varying with order parameter[83]. For perfectly ordered state k = 1.117 as given by de Vries[25].

Linear scanning of inner halo or spot gives the apparent molecular length (for N phase) or layer thickness (for Sm phase). For this we use the Bragg equation

$$2d\sin\theta = \lambda \qquad 2.18$$

2.6 OPTICAL BIREFRINGENCE STUDY

When light falls on a uniaxial aligned liquid crystal sample, double refraction can be observed. One principal refractive index is n_o or $n_\perp$, corresponding to the 'ordinary' ray with the electric vector oscillating perpendicular to the optic axis of the molecule (generally taken as director of **n**) and another is n_e or $n_\parallel$, of the 'extraordinary' ray with electric vector oscillating parallel to the axis.

Thus the optical anisotropy or birefringence is given by

$$\Delta n = n_e \sim n_o = n_\parallel \sim n_\perp$$

which depends on the wavelength and temperature. For positive uniaxial mesogen Δn is positive i.e., $n_e > n_o$ and it is negative for negative uniaxial mesogen.

Birefringence of liquid crystals was first determined experimentally by E. Dorn[84] for nematogen. Subsequently Δn was also measured in smectic phases[85-88].

The existence of Δn is related to molecular polarisability (α) which originates due to π electrons and delocalised electrons not participating in chemical bonds of the organic sample. This α can be determined by knowing the value of internal field. As the internal field is anisotropic in nature for mesogens, Lorentz–Lorentz force, valid for liquid state, is not applicable here. I follow, the Neugebauer[89] and Vuks'[90] modified formula for calculation of α.

2.6.1 Neugebauer Method

Neugebauer used anisotropic internal field constant. The effective molecular polarisabilities α_o and α_e are related to n_o and n_e by the following equations:

$$n_e^2 - 1 = 4\pi N\alpha_e\left(1 - N\alpha_e\gamma_e\right)^{-1} \qquad 2.19$$

and

$$n_o^2 - 1 = 4\pi N\alpha_o\left(1 - N\alpha_o\gamma_o\right)^{-1} \qquad 2.20$$

where N is the number of molecules per c.c. and γ_e and γ_o are the respective internal field constants for extraordinary and ordinary rays. The relevant equations for calculating polarisabilities α_o and α_e obtained from the above equations are as follows:

$$\frac{1}{\alpha_e} + \frac{2}{\alpha_o} = \frac{4\pi N}{3}\left[\frac{n_e^2 + 2}{n_e^2 - 1} + \frac{2\left(n_o^2 + 2\right)}{n_o^2 - 1}\right] \qquad 2.21$$

and

$$\alpha_e + 2\alpha_o = \frac{9}{4\pi N}\left[\frac{n^2 - 1}{n^2 + 2}\right] \qquad 2.22$$

where n is the mean refractive index and is given by

$$n^2 = \frac{1}{3}\left(2n_o^2 + n_e^2\right)$$

2.6.2 Vuks' method

Vuks considered that the internal field is independent of molecular interaction and the corresponding relations are :

$$\frac{n_o^2 - 1}{n^2 + 2} = \frac{4\pi N}{3}\alpha_o \qquad 2.23$$

and

$$\frac{n_e^2 - 1}{n^2 + 2} = \frac{4\pi N}{3}\alpha_e \qquad 2.24$$

2.6.3 Calculation of orientational order parameter from refractive index measurement

The degree of order of the mesogenic molecule has been determined using α-values obtained from the above two methods. The relation between orientational order parameter S and effective polarisabilities (α_o, α_e) are given by de Gennes[91] as:

$$\alpha_e = \bar{\alpha} + \frac{2}{3}\alpha_a S \qquad 2.25$$

and

$$\alpha_o = \bar{\alpha} - \frac{1}{3}\alpha_a S \qquad 2.26$$

where, $\bar{\alpha} = (2\alpha_o + \alpha_e)/3$, is the mean polarisability and $\alpha_a = (\alpha_{\parallel} - \alpha_{\perp})$, is the molecular polarisability anisotropy where $\alpha_{\parallel}$ and $\alpha_{\perp}$ are the principal polarisabilities, parallel and perpendicular to the molecular long axis in the crystalline state.

From equation 2.25 and 2.26 we obtain,

$$S = \frac{\alpha_e - \alpha_o}{\alpha_{\parallel} - \alpha_{\perp}} . \qquad 2.27$$

It is very difficult to measure α_a in the crystalline state. So we use well known Haller's extrapolation method[92]. A graph was plotted with log ($\alpha_e - \alpha_o$) vs. log ($T_c - T$) to get a straight line. This was extrapolated up to log (T_c) where T_c is the N – I transition temperature. At T = 0 K, i.e., in crystalline state, S is considered to be 1 and then ($\alpha_{\parallel} - \alpha_{\perp}$) is equal to ($\alpha_e - \alpha_o$). Once we know the value of α_a, we can calculate S as a function of temperature.

2.6.4 Measurement of refractive index

Optical birefringence was measured by thin prism whose refracting angle was around 1°. These prisms have been made by using optically flat glass slides. Techniques of preparation of prism have already been reported by Zemindar et al[93]. Special care has been taken for cleaning of glass slides. Conc. HNO_3 was used primarily to clean the impurities. Then washed it with water several times till there

is no acid reagent. After drying, it was dipped in acetone to clean any type of oily substances. Soap or detergent solution was avoided for cleaning because it might be adsorped by glass resulting a non-washable white layer on it. One side of each glass slides were then coated with dilute solution (~ 1%) of Poly Venyl Alcohol (PVA) and rubbed several times on bond paper in same direction to obtain a preferred direction on the substrate. A prism was constructed using high temperature adhesive placing the treated surfaces inside and rubbing direction parallel to the refracting edge of the prism. A thin glass spacer was introduced in one side to get a prism of required angle. It was then placed on a cleaned glass plate. Liquid crystal sample was introduced into the prism from its top open side. The system was alternately heated to isotropic phase and cooled slowly so that liquid crystals were perfectly aligned with its optical axis parallel to the reflection edge of the prism. The prism was then placed into thermostated brass oven and refractive indices were measured (n_e, n_o) for different wavelengths by means of a precision spectrometer, a wavelength selector and a nicol prism. Measurement of densities of the mesogens were performed with the help of single tube dilatometer. The accuracy of density data were within $\pm$ 0.1%.

STRUCTURE AND CHEMICAL NAME OF THE LIQUID CRYSTALS STUDIED

Name and structural formulae of the liquid crystalline compounds studied in this investigation are given below:

1. 4-cyanobiphenyl- 4′-yl 4-heptylbiphenyl -4- carboxylates (7CBB in short)

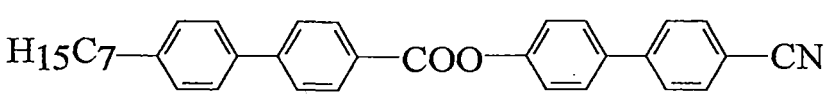

2. 4- alkyloxy -4′- cyanobiphenyls (nOCB in short)
   n = 5, 6, 7, 8

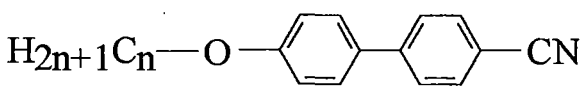

3. p-ethoxyphenyl trans - 4- butyl cyclohexane carboxylate (EPBCC in short)

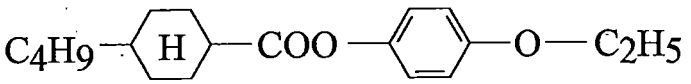

4. 4-n-pentyl 4′cyanobiphenyl (5CB in short)

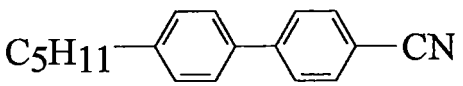

5. 4-n-pentyl phenyl 4-n′ hexyloxy benzoate (ME6O.5 in short)

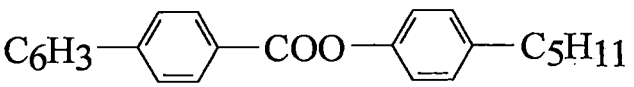

6. 5-(trans-4-alkylcyclohexyl)-2- (4-cyanophenyl) pyrimidine
   n = 2 (EPPCC in short) and n = 7 (HCCPP in short)

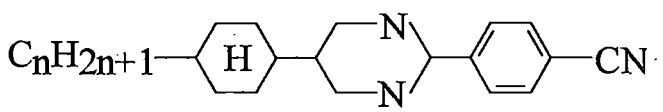

7. 3E-n-butane-phenyl- (4-cyclohexane-4′-n-alkane) -ether
   n = 3 (3CPOD(3)1 in short) and n =5 (5CPOD(3)1 in short)

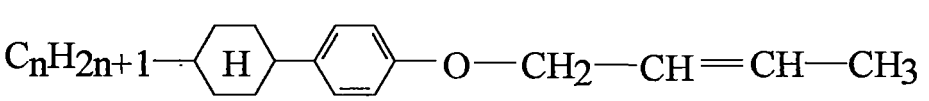

Chapter - 3

SMALL ANGLE X-RAY DIFFRACTION STUDY AND OPTICAL BIREFRINGENCE MEASUREMENTS ON MIXTURES SHOWING RE-ENTRANT NEMATIC AND INDUCED SMECTIC PHASE

3.1 INTRODUCTION

In this chapter I have presented results on investigation by x-ray diffraction and refractive indices measurements of three binary systems of mixture of two polar compounds, one being 7CBB (4-cyanobiphenyl- 4′-yl 4-heptylbiphenyl -4-carboxylates) and other a member of the homologous series nOCB (4- alkyloxy -4′-cyanobiphenyls). Recently Brodzik and Dabrowski[94-96] have shown that four ring nCBB compounds when mixed with two ring polar compounds such as nOCB or nCB (4-alkyl -4′- cyanobiphenyls) give phase diagrams with unusual shape. In the mixtures with higher ($n \geq 8$) homologues of nOCB or nCB strong enhancement of the SmA_d phase is observed and for shorter ($n \leq 7$) homologue induction of SmA_d phase is observed. Induced or enhanced SmA_d phase forms an eliptical 'island' or 'semi-island' surrounded by nematic 'sea'. In such cases, re-entrant nematic phase can be observed over a short concentration range of the mixture. Phase transition diagram, Fig. 3.1, depicts this type of observation.

According to Brodzik et al[94] pure nCBB compounds, for $n<8$, have a nematic phase above SmA_1 phase and SmA_d phase is not formed, since the monomer concentration is high. But when these molecules are in proper environment (for example in the presence of nOCB or nCB) the dimer concentration rises and conditions for formation of SmA_d phases are more favourable. The results also show the influence of the alkyl chain length of two ring component on the smectic layer spacing of the induced SmA_d phase as well as on apparent molecular length in nematic and re-entrant nematic phases. The experiments results and the theoretical explanation of re-entrant phenomena in liquid crystals have been discussed in literature by many authors[68,97-105]. The theories try to explain the re-entrant phenomena in mixtures and in pure compounds by assuming thermal variation of equilibrium between monomers and dimers and their steric properties.

Three bicomponent systems, 7CBB-6OCB (mixture A), 7CBB-7OCB (mixture B) and 7CBB-8OCB (mixture C) were studied by me. Part of this work has already been published[68].

3.2 EXPERIMENTAL

The pure samples 7CBB (Cr 123 SmA_1 136 N 350 I); 6OCB (Cr 57 N 75.5 I); 7OCB (Cr 53.5 N 75 I) and 8OCB (Cr 54.5 SmA_d 67 N 80 I) were prepared at the Institute of Chemistry, Military University of Technology, Warsaw, Poland and supplied to us by Prof. Dabrowski. I have used these samples without further purification. The structural formulae are given below.

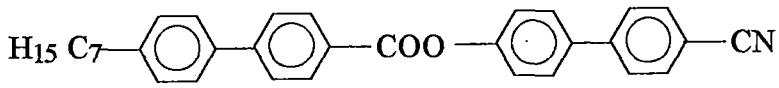

7CBB

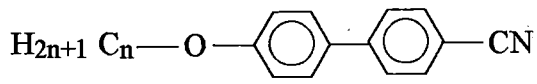

n = 6, **6OCB**
n = 7, **7OCB**
n = 8, **8OCB**

The mixtures of 7CBB and 6OCB (mixture A) were prepared with five different compositions (x_{6OCB} = 0.1585; 0.2977; 0.3973; 0.5043; 0.9105), the mixtures of 7CBB and 7OCB (mixture B) were prepared with seven different compositions (x_{7OCB} = 0.1505; 0.2875; 0.4089; 0.5183; 0.6175; 0.7077; 0.7902) and the mixtures of 7CBB and 8OCB (mixture C) were prepared with five different compositions (x_{8OCB} = 0.1182; 0.3029; 0.5067; 0.7055; 0.9466). Mixtures were investigated at different temperatures and in different phases. Observed transition temperatures are given below in °C, with super cooling temperatures being shown in parentheses.

Mixtures:

A_1 - mole fraction x_{6OCB} = 0.1585 [phase transitions: Cr 115.7 (100) N_r 155.1 S_{Ad} 216 N ~320 I]

A_2 - mole fraction x_{6OCB} = 0.2977 [phase transitions: Cr 107.2 (95) S_{Ad} 211 N ~300 I]

A_3 - mole fraction x_{6OCB} = 0.3973 [phase transitions: Cr 99.3 S_{Ad} 190.4 N 296.2 I]

A_4 - mole fraction x_{6OCB} = 0.5043 [phase transitions: Cr 79.8 S_{Ad} 179 N 273.8 I]

A_5 - mole fraction x_{6OCB} = 0.9105 [phase transitions: Cr 51.8 N 110.5 I]

B_1 - mole fraction x_{7OCB} = 0.1505 [phase transitions: Cr 116 (98.3) N_r 154 S_{Ad} 241.3 N ~320 I]

B_2 - mole fraction x_{7OCB} = 0.2875 [phase transitions: Cr 106.2 (92.5) S_{Ad} 245.2 N ~300 I]

B_3 - mole fraction x_{7OCB} = 0.4089 [phase transitions: Cr 98.4 S_{Ad} 194.8 N 269.3 I]

B_4 - mole fraction x_{7OCB} = 0.5183 [phase transitions: Cr 86.8 S_{Ad} 177.9 N 238.9 I]

B_5 - mole fraction x_{7OCB} = 0.6175 [phase transitions: Cr 67.3 S_{Ad} 174 N 209 I]

B_6 - mole fraction x_{7OCB} = 0.7077 [phase transitions: Cr 59 S_{Ad} 102 N 181.8 I]

B_7 - mole fraction x_{7OCB} = 0.7902 [phase transitions: Cr 49 S_{Ad} 69.1 N 148.6 I]

C_1 - mole fraction x_{8OCB} = 0.1182 [phase transitions: Cr 116.8 (97) N_r 155.7 S_{Ad} 235.4 N ~330 I]

C_2 - mole fraction x_{8OCB} = 0.3029 [phase transitions: Cr 108.3 S_{Ad} 233 N 296 I]

C_3 - mole fraction x_{8OCB} = 0.5067 [phase transitions: Cr 89 S_{Ad} 187.8 N 241 I]

C_4 - mole fraction x_{8OCB} = 0.7055 [phase transitions: Cr 62 S_{Ad} 135.6 N 186.9 I]

C_5 - mole fraction x_{8OCB} = 0.9466 [phase transitions: Cr 55 S_{Ad} 76.4 N 100.1 I]

Only mixtures A_1, B_1 and C_1 have shown N_{re}, SmA_d and N phases. In all other mixtures SmA_d and N phases have been observed except mixture A_5 which shows only N phase. The transition temperatures of the sample were determined with Mettler FP80/82 thermo system by studying textures under a polarising microscope. All the transition temperatures agreed with the previously published results[106]. X-ray photographs were taken using a flat plate camera having a high temperature attachment[79]. Some of the photographs are shown in Fig. - 3.1a. The photographs were scanned by a densitometer and data were analysed to obtain orientational order parameters $\langle P_2 \rangle$ and layer thickness d (or apparent molecular length l) in smectic (or nematic) phase. Optical birefringence study was possible only for mixture B_1. For all other mixtures this experiment could not be performed due to absorption of light

by the samples. Details of all the experimental techniques and data analysis are described in chapter 2.

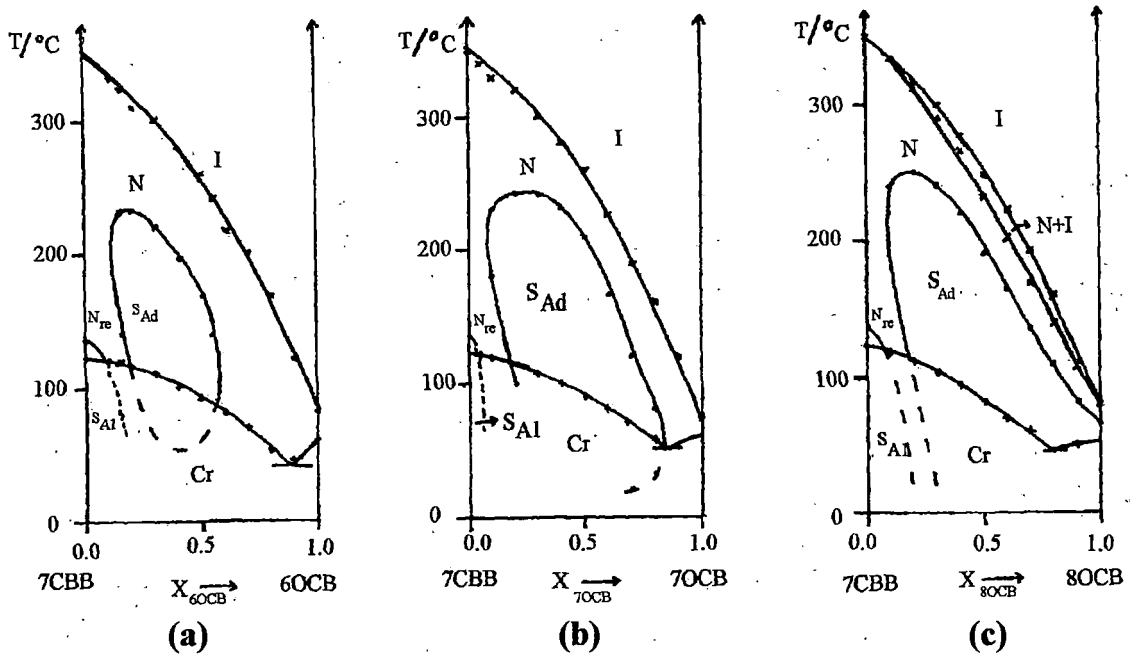

Fig. 3.1 Phase diagram of bicomponent mixtures a) 6OCB + 7CBB, b) 7OCB + 7CBB and c) 8OCB + 7CBB with marked compositions investigated by x-ray technique.

3.3 RESULTS AND DISCUSSIONS

Fig. - 3.2 shows the concentration variation of the layer thickness d (both experimental and calculated) in mixtures A, B and C respectively. For this mixtures A and B were studied at constant temperature 100°C and mixtures C were studied at 110°C, however where smectic phase does not exist at those temperatures diffraction studies were made at nearest possible temperatures and those data are marked by different symbols. It should be noted that the layer thickness of all the mixtures studied, covering the entire range of mole fractions, is between 34.8 to 37.0 Å for mixtures A, between 33.9 to 37.0 Å for mixtures B and between 32.0 to

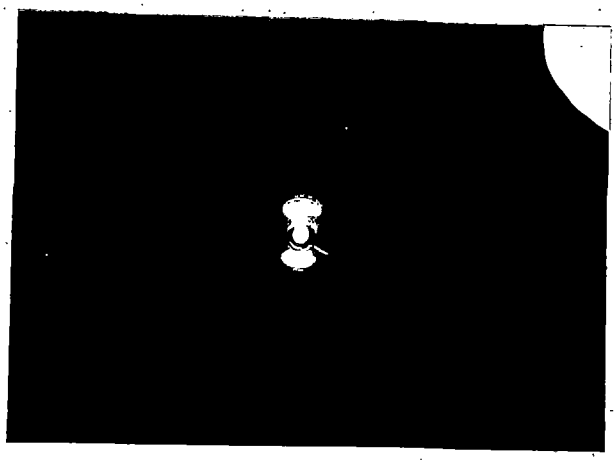

(a)

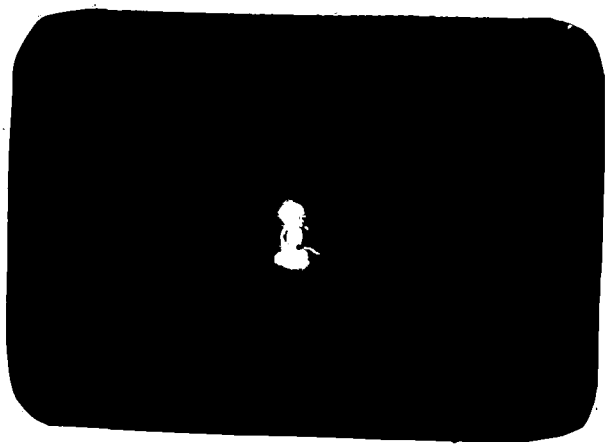

(b)

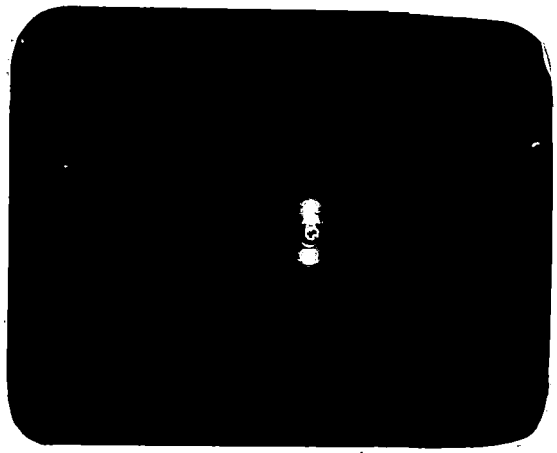

(c)

Fig. 3.1a X-ray photographs of mixture C_1 (8OCB+7CBB):
a) in N_{re} phase at temperature 130°C, b) in SmA_d phase at temperature 170°C and c) in N phase at temperature 240°C

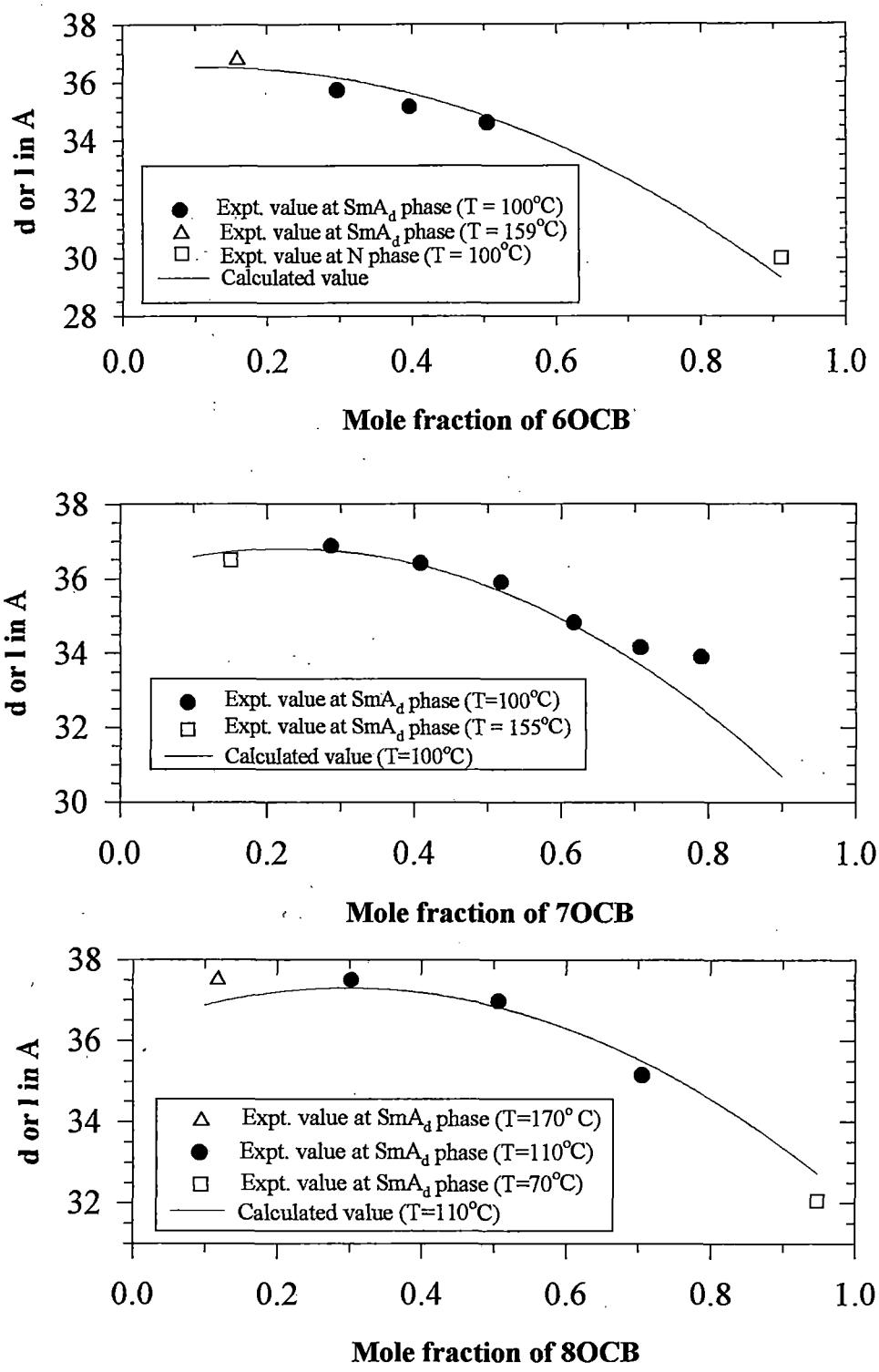

Fig. 3.2 Variation of layer thickness or apparent molecular length with composition of mixture a) 6OCB+7CBB, b) 7OCB +7CBB and c) 8OCB+7CBB

37.5 Å for mixtures C. Layer thicknesses are much larger than the most extended molecular model lengths of the components (see Table 3.1) indicating that the enhanced and induced smectic phases are of the partially bilayer type. The nature of variation of d with composition is similar in all the mixtures. Beyond a certain composition d is found to decrease quite rapidly with concentration. From Fig. - 3.2 it seems that there is a broad flat maxima in the layer thickness, in mixture A at mole fraction $x_{6OCB} \sim 0.2$, in mixture B at mole fraction $x_{7OCB} \sim 0.25$ and in mixture C at mole fraction $x_{8OCB} \sim 0.3$. About these three compositions the thermal stability of the smectic A_d phases of the respective mixtures are maximum. These results are in agreement with our previous observations[68].

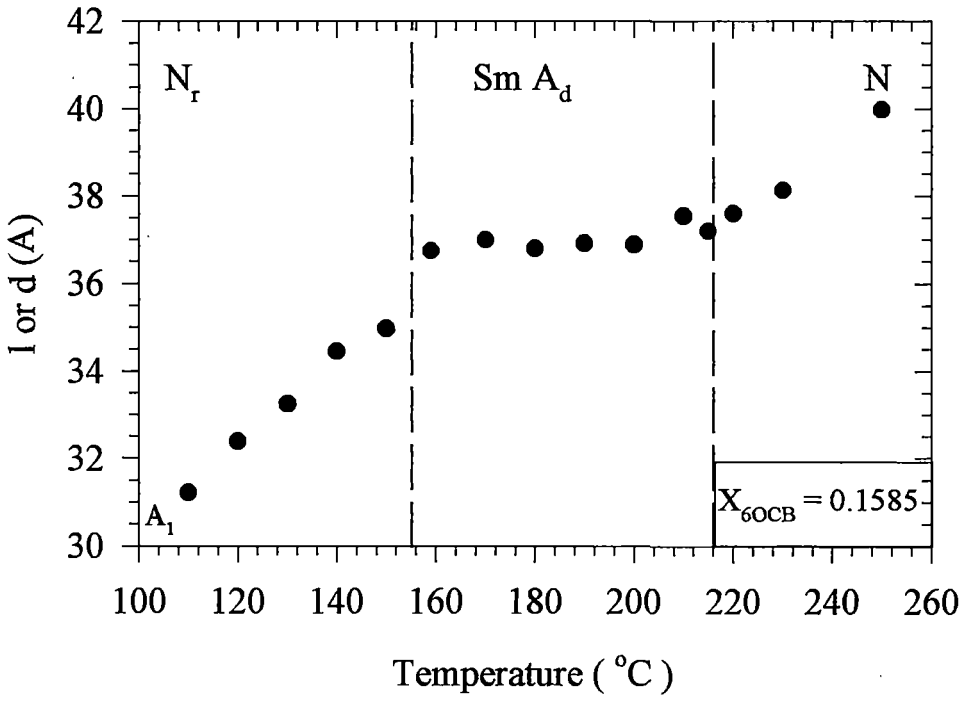

Fig. 3.3a Temperature variation of apparent molecular length / layer thickness of Mixture A_1 (6OCB +7CBB)

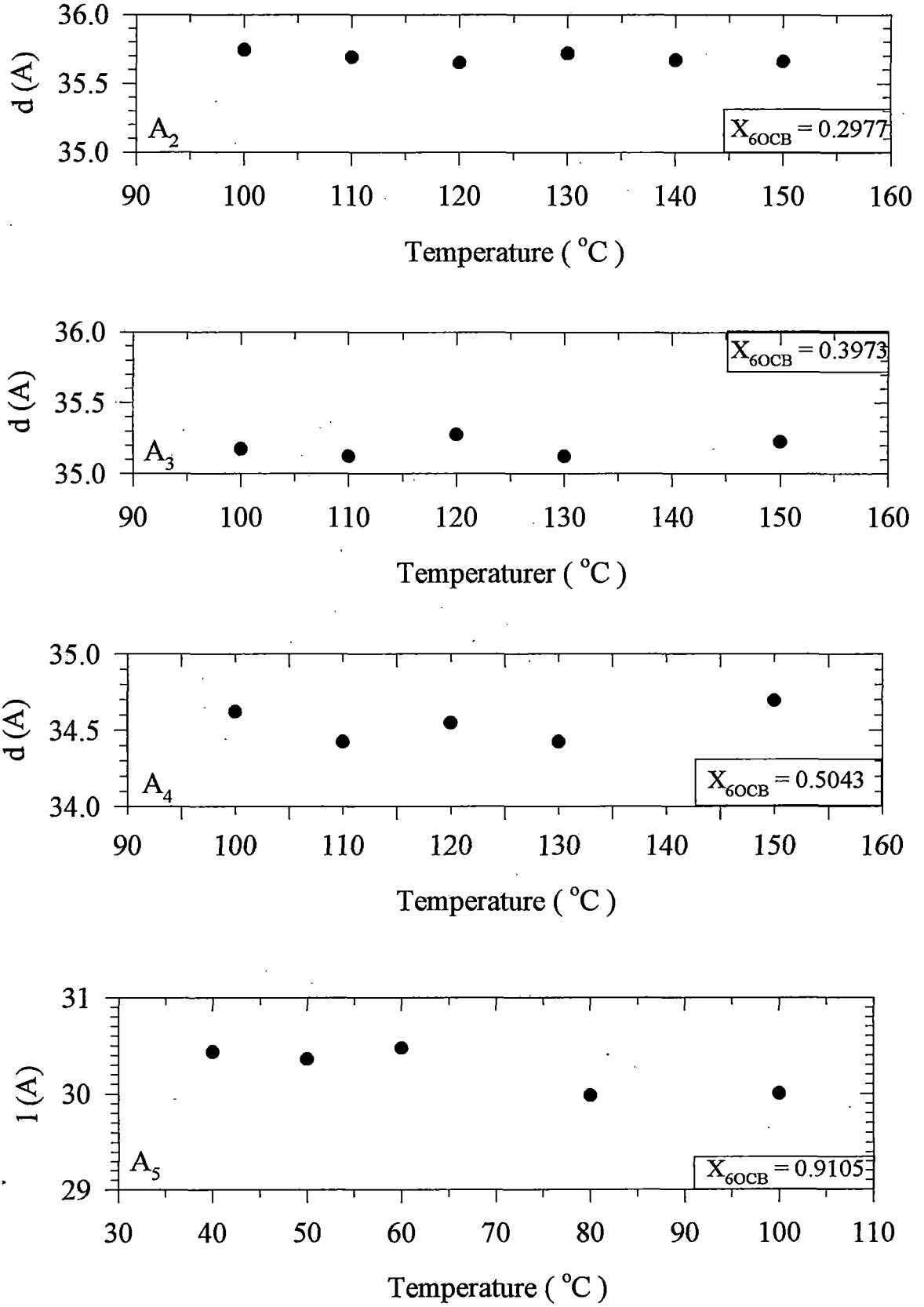

Fig. 3.3b Temperature variation of apparent molecular length / layer thickness of Mixture (6OCB+7CBB)

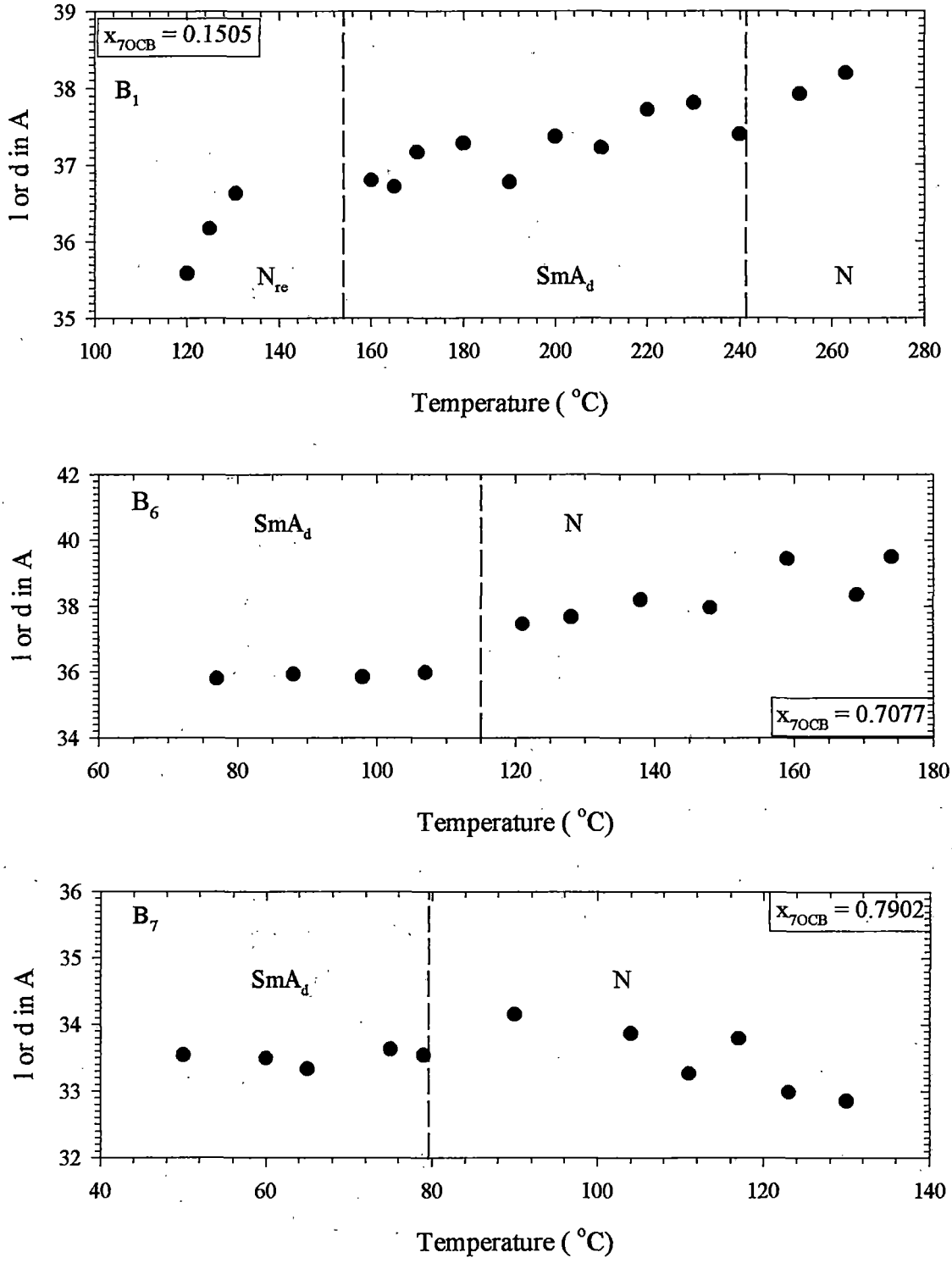

Fig. 3.4 Temperature variation of apparent molecular length/layer thickness of Mixture B (7OCB + 7CBB)

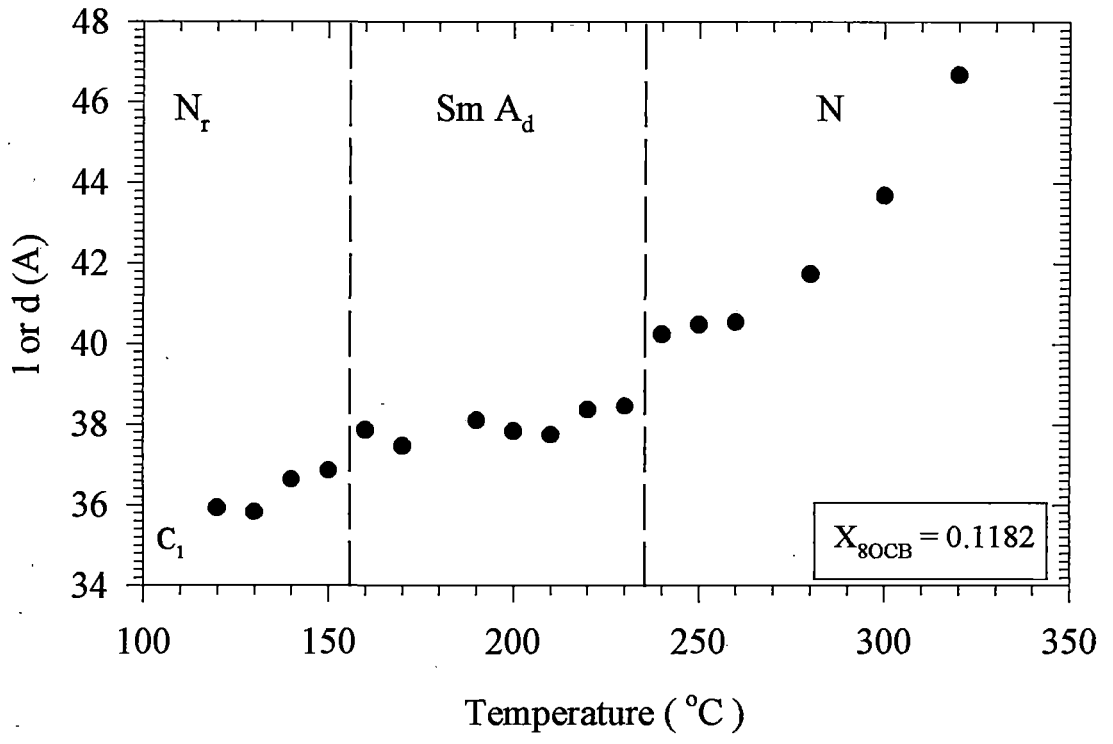

Fig. 3.5a Temperature variation of apparent molecular length / layer thickness of Mixture C_1 (8OCB+7CBB)

Temperature variation of layer thickness and apparent molecular length for mixtures A, B and C are shown in Fig. - 3.3 — 3.5. Except in mixture B_1 layer thickness values are almost temperature independent but apparent molecular length varies with temperature. Mixtures B_2, to B_5 and C_5 were studied only at three different temperatures. Temperature variations of d for these mixtures are not appreciable and hence have not been shown graphically. The average layer thickness of mixture A_1, B_1 and C_1 are 37.0, 37.3 and 37.9 Å respectively. Considering the lengths of monomers, antiparallel homo- and hetero- dimers in side by side configurations I find that average d values are 0.5 to 1.4 Å more than the side by side antiparallel homo-dimers of 7CBB molecules. Also it is noted from

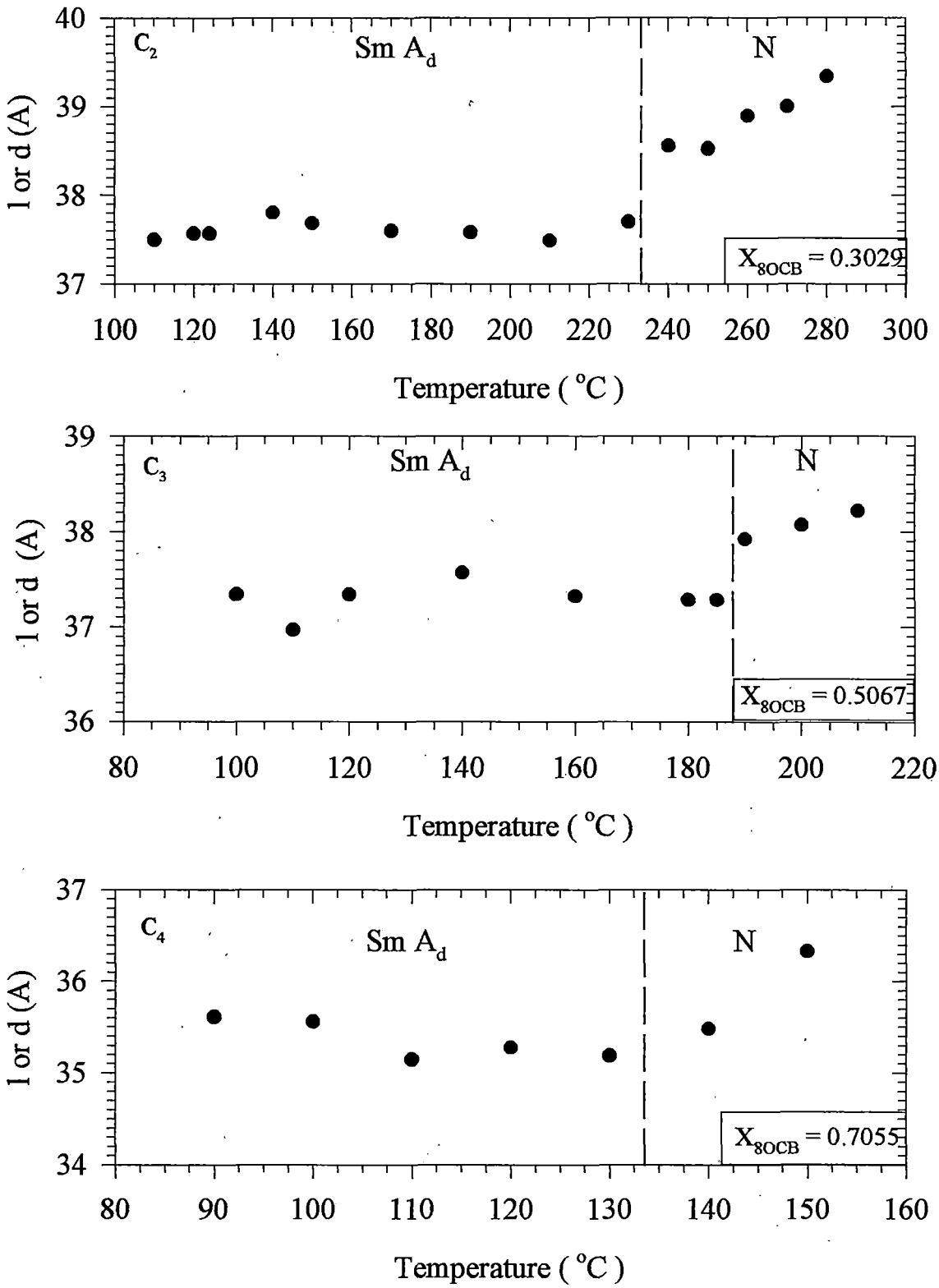

Fig. 3.5b Temperature variation with apparent molecular length / layer thickness of Mixture (8OCB+7CBB)

Fig. - 3.2 that the d values decrease quite rapidly with concentration of nOCB. So I infer that at the lowest concentration of nOCB, the homo-dimer concentration of nCBB is maximum but concentration of nOCB homo-dimers increases rapidly with increasing concentration of nOCB. This observation is corroborated by Fig. - 3.6a which shows the concentrations of monomers and dimers in mixture of 7OCB and 7CBB as a function of mole fraction of 7OCB, calculated according to the theory given later on. Calculated d values fits nicely with the observed values, supports the above conclusion.

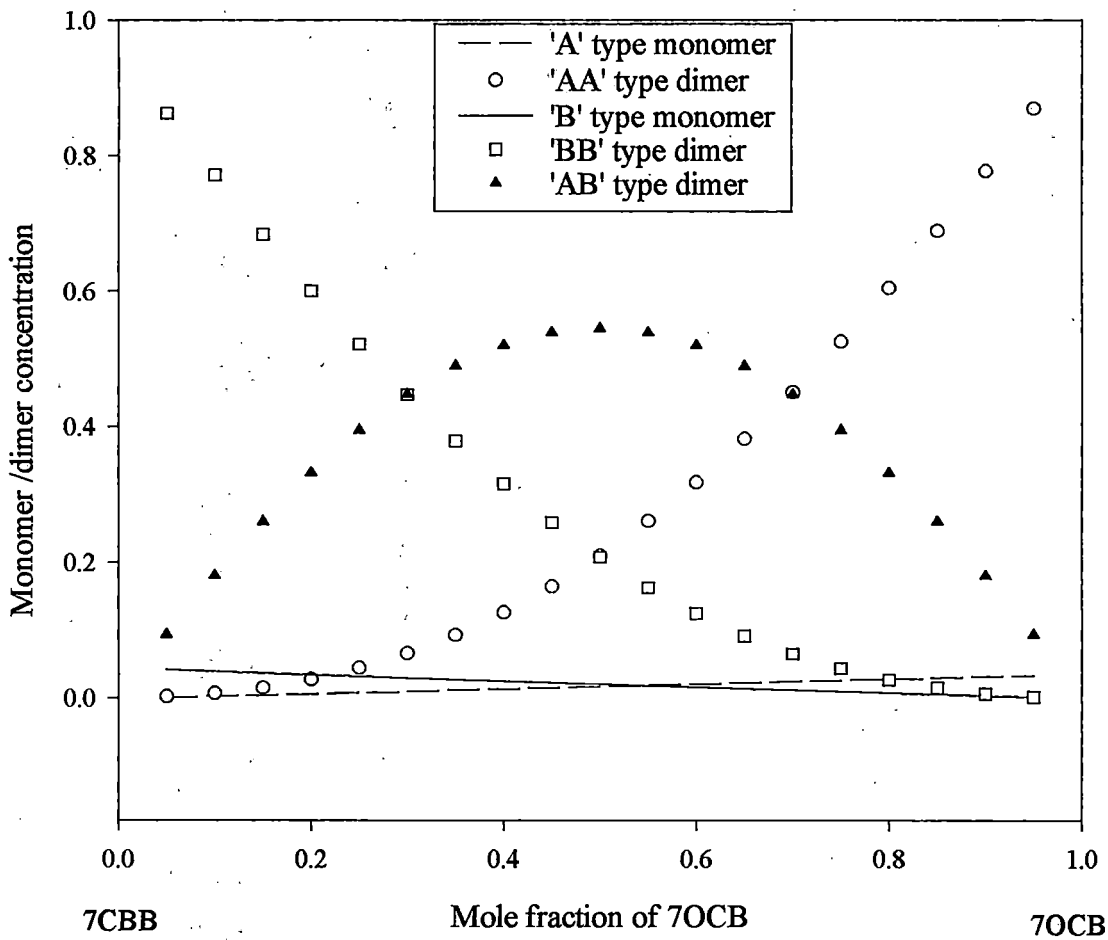

'A' type molecule - 7OCB; 'B' type molecule - 7CBB

Fig. 3.6a Variation of concentrations of monomers and dimers in mixture 7OCB + 7CBB, with mole fraction of 7OCB

The layer thickness and apparent molecular length in the mixtures are calculated by assuming the formation of two types of monomers and three types of dimers from nOCB (A molecule) and 7CBB (B molecule) viz., A, B, AA, BB and AB. The different types of molecules (monomers and dimers) are in equilibrium. If total number of molecules, all considered as monomers, is N then

$$N = n_a + 2n_{aa} + 2n_{bb} + 2n_{ab} + n_b \qquad 3.1a$$

where, n_a = number of 'A' type molecule

n_b = number of 'B' type molecule

n_{aa} = number of 'AA' type dimer

n_{bb} = number of 'BB' type dimer

n_{ab} = number of 'AB' type dimer.

Dividing both sides of equation 3.1a by N we get

$$\therefore \quad x_a + 2x_{aa} + 2x_{bb} + 2x_{ab} + x_b = 1, \text{ where } x_a = n_a / N \text{ etc.} \qquad 3.1b$$

Three different equilibrium constants K_a, K_b and K_m are chosen respectively for three types of association:

$$A + A \overset{K_a}{\rightleftharpoons} AA, \qquad B + B \overset{K_b}{\rightleftharpoons} BB, \qquad A + B \overset{K_m}{\rightleftharpoons} AB$$

Therefore, from first of these association equations:

$$n_{aa} = \frac{1}{K_a} n_a^2$$

which gives $$x_{aa} = \frac{N}{K_a} x_a^2 = P_a x_a^2 \qquad 3.2$$

where $P_a = N / K_a$.

Similarly, from other two association equations, we get

$$x_{bb} = P_b x_b^2 \qquad 3.3$$

and

$$x_{ab} = P_m x_a x_b \qquad 3.4$$

where $P_b = N / K_b$ and $P_m = N / K_m$.

From experimental view point, in bicomponent mixtures two types of monomers having mole fractions C_a and C_b are mixed,

$\therefore \quad C_a + C_b = 1$

where $C_a = x_a + x_{ab} + 2x_{aa}$ 3.5a

and $C_b = x_b + x_{ab} + 2x_{bb}$ 3.5b

Hence, assuming certain value of P_a, P_b and P_m, the value of five unknowns, viz., x_a, x_b, x_{aa}, x_{bb} and x_{ab} can be calculated from the five independent equations 3.1b, 3.2, 3.3, 3.4 and 3.5a. Fig. - 3.6a shows the calculated values of x_a, x_b, x_{aa}, x_{bb} and x_{ab} for the mixture 7OCB and 7CBB.

The mean layer thickness or apparent molecular length may be written as[103]

$$d_{mix} = x_a d_a + x_{aa} d_{aa} + x_b d_b + x_{bb} d_{bb} + x_{ab} d_{ab}. \quad 3.6$$

Here, d_a = molecular length in extended form of 'A' molecule

d_b = molecular length in extended form of 'B' molecule

d_{aa} = length of the dimers of 'A' molecules

d_{bb} = length of the dimers of 'B' molecules

d_{ab} = length of hetero dimers of 'A' and 'B' molecules

The value of d_{mix} can be calculated provided the values of respective molecular length are known. The length of monomers (d_a and d_b) have been estimated from their respective molecular model lengths. The values of d_{aa} and d_{bb} have been calculated from the x-ray diffraction patterns obtained from pure A and pure B chemicals respectively. For d_{aa} I have used Bhattacharjee et al[107], Das et al[108] and Brownsey et al[109] x-ray data. For d_{bb}, i.e., for 7CBB dimer lengths, I have taken the values obtained by Brownsey and Leadbetter[109]. They have obtained two characteristic lengths viz., 29.6 Å and 36.5 Å from x-ray diffraction studies on 7CBB. Obviously, the longer length corresponds to the dimer of 7CBB (d_{bb}). However, I have taken d_b to be equal to 31.5 Å, which is its model molecular length. The experimental value of 29.6 Å is somewhat shorter than the model length, probably because of thermal vibration of the long chain part of the molecule. To estimate the value of d_{ab} I have assumed that the molecular overlap (d_o) is the same for both nOCB + nOCB and nOCB + 7CBB dimers. The assumed molecular configurations for these dimers (for n = 6) are shown in the Fig.-3.6b. The assumption is plausible, since the main interaction causing the formation of dimer is the dipole-dipole interaction and the main dipolar contribution in both the

molecules nOCB and 7CBB come from the cyanobiphenyl part of the molecule. Hence, the overlap (please refer Fig. - 3.6b)

$$d_o = 2d_a - d_{aa}$$

and

$$d_{ab} = d_a + d_b - d_o.$$

It may be mentioned here that d_o as estimated by us increases slowly with increase in the length of the alkyl chain in nOCB. According to the figure, however, the value of d_o should be independent of the length of the alkyl chain. This may be due to dipole - induced dipole interaction between cyanobyphenyl group of one molecule with the alkyl chain of the other molecule, which increases in magnitude as the alkyl chain length increases. This interaction shifts the cyanobyphenyl group more towards the alkyl chain and thereby increases the overlap length, d_o.

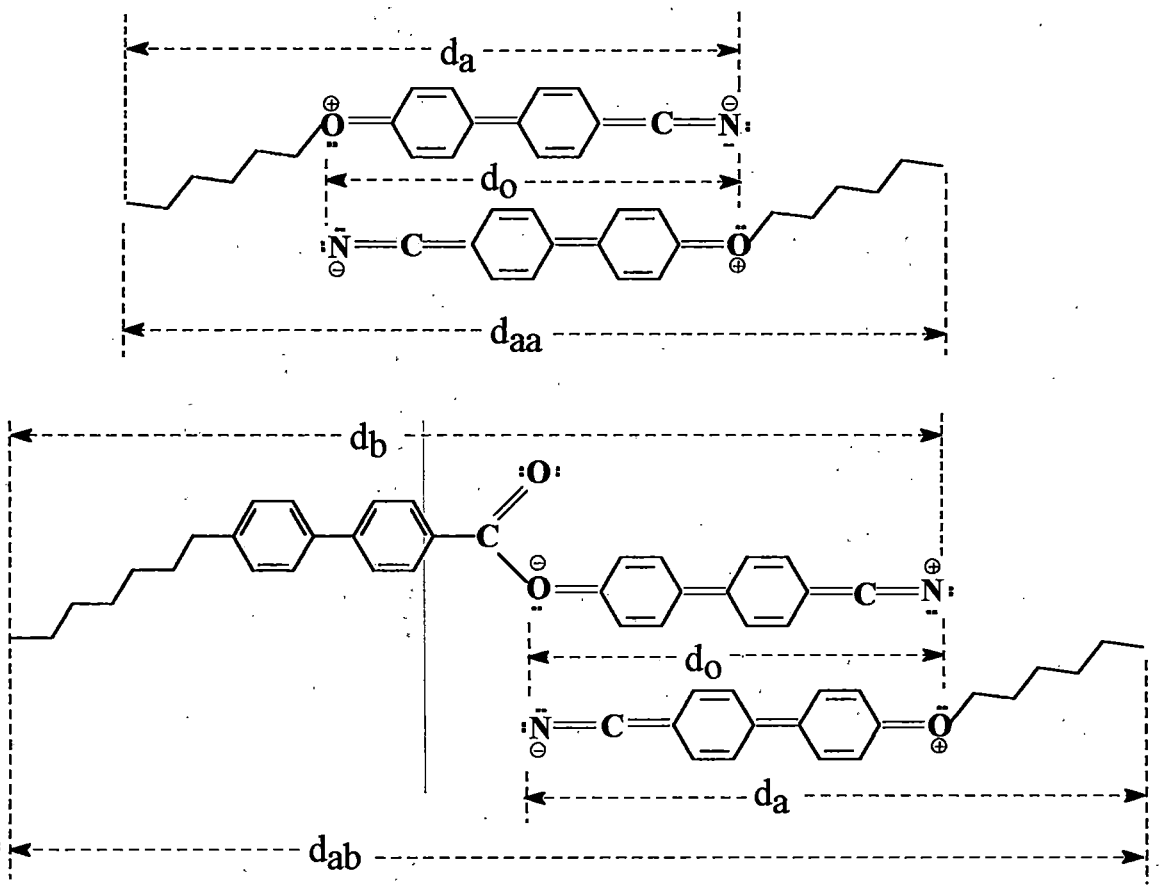

Fig. 3.6b Assumed configuration of dimers; 6OCB + 6OCB dimer (above)
6OCB + 7CBB dimer (below)

The values of d_a, d_b, d_{aa}, d_{bb} and d_{ab} are tabulated in Table - 3.1.

Table - 3.1

Length of monomers and dimers

Monomer or dimer type	Length in Å
d_a (nOCB), n = 6, 7, 8	20.5, 22, 23.2
d_b (7CBB)	31.5
d_{aa} (nOCB +nOCB), n = 6, 7, 8	27.7, 29.2, 31.9
d_{bb} (7CBB + 7CBB)	36.5
d_{ab} (nOCB + 7CBB), n = 6, 7, 8	38.7, 38.7, 40.2

The d_{mix} values are calculated using equation 3.6 assuming certain values of P_a, P_b and P_m. The value of P_a, P_b and P_m are changed till we get a good agreement with the experimental data. However, we keep P_b same for all the three mixtures, since molecule B is always 7CBB. The values of P_a, P_b and P_m which give the best fit are given in Table - 3.2.

Table -3. 2

Value of P_a, P_b and P_m for different mixture systems

Mixtures	P_a	P_b	P_m
A (6OCB + 7CBB)	3000	1000	3000
B (7OCB + 7CBB)	1500	1000	3200
C (8OCB + 7CBB)	1300	1000	2000

It is also noted that in both N_{re} and N phases 1 decreases quite rapidly with lowering temperature. Diffractometric study on mixture B_1 in the re-entrant phase region by J. Przedmojski[68] confirmed the formation of two different cybotactic

structures due to nucleation process — one having apparent molecular length equal to antiparallel dimers of 7CBB molecules (~ 36.5 Å) and second one with length of single 7CBB molecules (30.2 Å). It was seen that these two structures exist in an equilibrium in the whole range of re-entrant nematic phase, but the concentration of dimers decreases quickly with decreasing temperature. I also observe similar behaviour in N_{re} phase. This decrease in apparent molecular length with decreasing temperature may also be caused by preponderance of parallel dimers over antiparallel ones at greater densities (i.e., lower temperature) for highly polar compounds with long alkyl chains[110-112]. The parallel dimers are shorter than antiparallel dimers, hence the apparent molecular length decreases with decreasing temperature.

Variation of $\langle P_2 \rangle$ with temperature through N_{re} and N phases are shown in the Fig.-3.7 and 3.8 for mixtures A_1 and C_1 respectively. As the samples could not be aligned with magnetic field at our disposal (~ 3 Kilogauss) in SmA_d phase, so, I have not tried to fit the data with theoretical calculation. Temperature variations of $\langle P_2 \rangle$ for mixture B_1 throughout the range is shown in Fig.-3.9. It can be seen that the

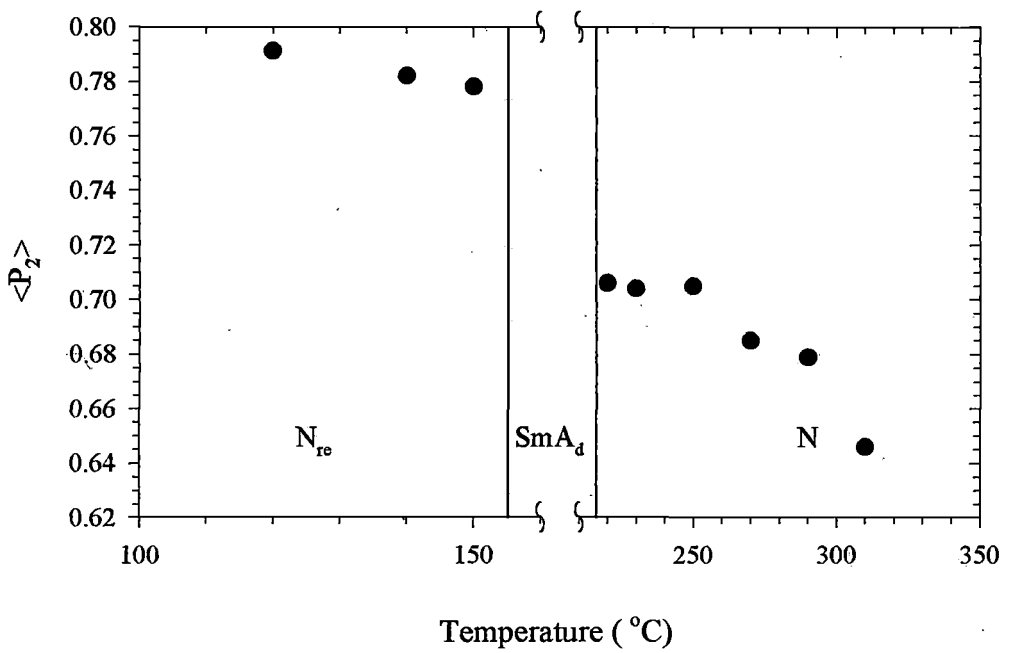

Fig. 3.7 Temperature variation of order parameter of Mixture A_1 (6OCB+7CBB)

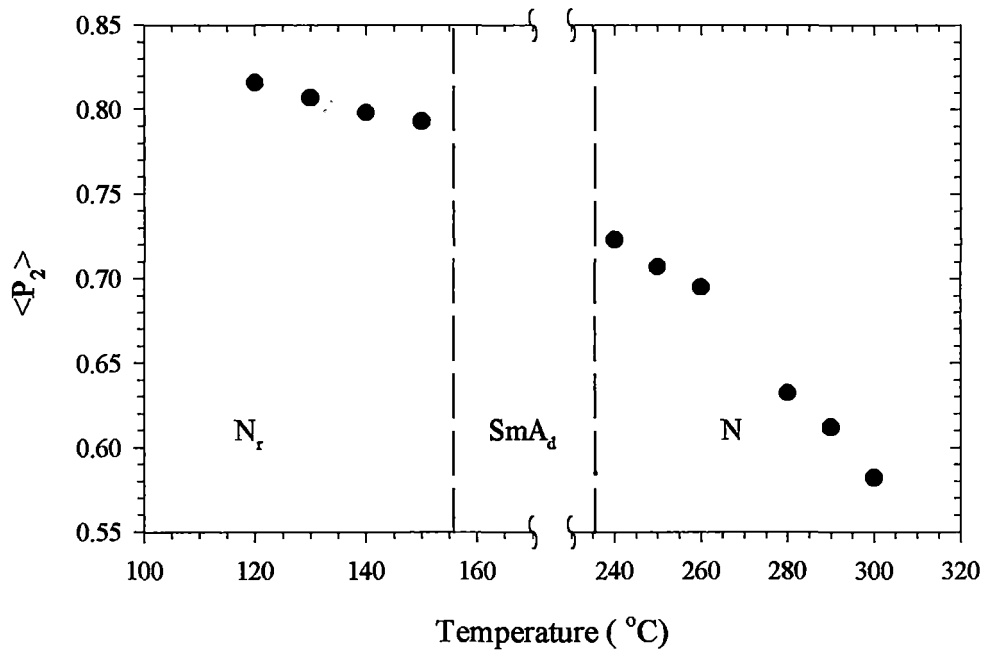

Fig. 3.8 Temperature variation of order parameter of Mixture C_1 (7CBB+8OCB)

order parameter in N_{re} and N phases change more quickly than in smectic A_d. I have tried to fit my experimental data with those calculated from the theory of McMillan[75] with α=0.58, δ = 0.14, but without much success as can be seen in Fig.-3.9. However this is not surprising since in the SmA_d phase the aliphatic chains of the molecules are being closely packed cannot remain parallel to one another. This decreases the value of the orientational order parameter with temperature significantly. It is observed that $\langle P_2 \rangle$ value at SmA–N transition is very high which is in agreement with extended McMillan's theory by Luckhurst and Timini[113]. According to them $\langle P_2 \rangle$ value near SmA–N transition lie within 0.65 and 0.75. Continuous change of $\langle P_2 \rangle$ value with temperature near N_{re}–SmA_d and SmA_d–N transitions imply that both the transitions are of second order. DSC study of this mixture confirms that both these transitions are continuous (Fig.-3.10).

The temperature variation of the density of mixture B_1, up to 170 °C, is shown in Fig.-3.11. Density variation is also continuous at N_{re}–SmA_d transition.

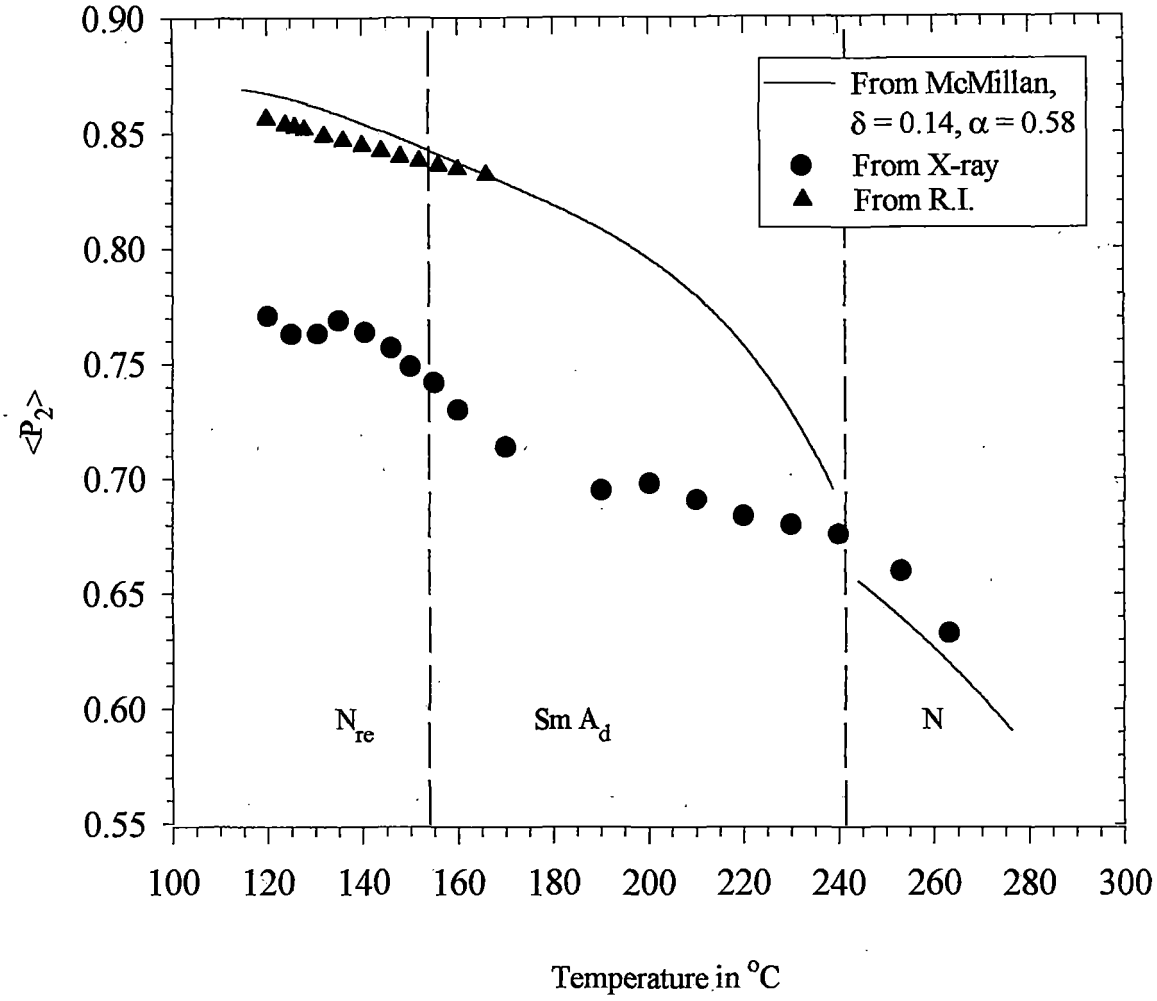

Fig. 3.9 Temperature variation of order parameter of Mixture B_1 (7OCB+7CBB)

As noted earlier I have also determined the variation of ordinary and extraordinary refractive indices at wavelength 5780Å with temperature for mixture B_1 only and is given in Fig.-3.12. The mixture shows large birefringence (~ 0.3) in the re-entrant nematic phase and the SmA_d phase as well. Again, there is no discontinuity in these values at the N_{re} to SmA_d transition temperature. All these observations indicate that the re-entrant nematic to induced smectic A_d phase transition in this mixture is of second order.

The refractive index data have been analysed to determine the polarisability values (α_e and α_o) using Neugebauer's procedure[89]. The polarisability anisotropy

($\Delta\alpha_o = \alpha_e - \alpha_o$ at 0°C) for a perfectly ordered sample, i.e., at $\langle P_2 \rangle = 1$, was obtained from these data using an extrapolation procedure given by Haller et al[92]. The order parameter $\langle P_2 \rangle$ is calculated from the well-known relation 2.27[91]

$$\langle P_2 \rangle = (\alpha_e - \alpha_o) / \Delta\alpha_o.$$

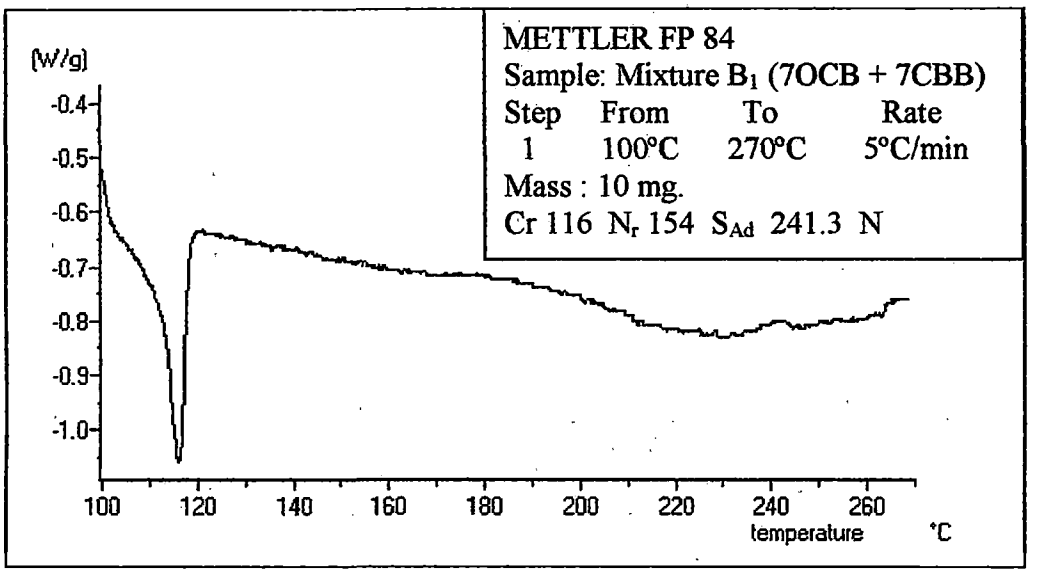

Fig. 3.10 DSC graph of Mixture B_1 (7OCB + 7CBB)

Fig.-3.9 shows the temperature variations of $\langle P_2 \rangle$ values obtained from optical birefringence study for mixture B_1 together with $\langle P_2 \rangle$ values obtained from our x-ray studies. In x-ray studies the sample could be studied upto 260°C without decomposition since the sample being taken in a sealed capillary could not react with atmospheric oxygen. In case of refractive index and density measurements, however, our systems were not sealed, hence decomposition sets in at a lower temperature, so measurements could be done upto 170°C. Moreover, above 260°C the sample could not be aligned well in the magnetic field, hence $\langle P_2 \rangle$ values from x-ray diffraction data were not calculated above that temperature. It can be seen that the order parameter values obtained from refractive index data are much larger than those obtained from our x-ray studies, though they agree quite well with the

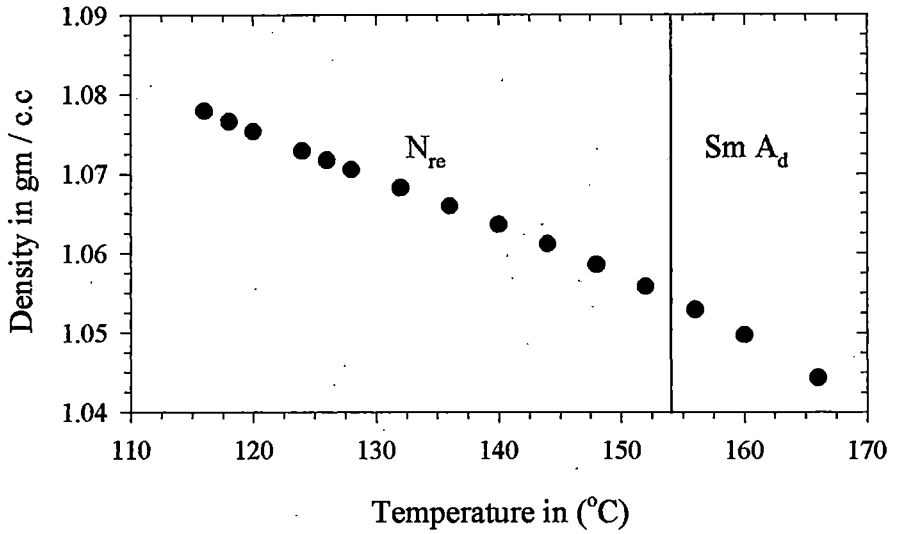

Fig. 3.11 Variation of density with temperature of Mixture B_1 (7OCB+7CBB)

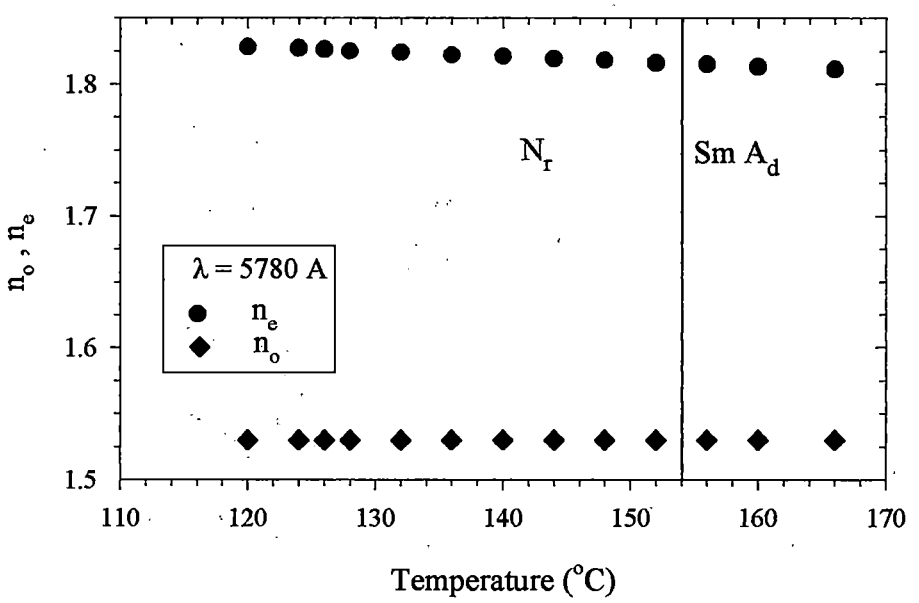

Fig. 3.12 Variation of refractive indices with temperature of Mixture B_1(7OCB+7CBB)

theoretical values. The discrepancy between the order parameter values obtained from x-ray data on one hand and refractive index or magnetic susceptibilities data on the other hand has been reported earlier by many authors[114-116]. They have also discussed probable causes for such disagreement among experimental order parameter values obtained by using different techniques. Another cause may be worth noting here. All the constituent molecules of the mixtures studied have rather long end chains. Hence, this discrepancy may be, in part, due to the fact that the rigid part and the chain part of the molecules are not collinear and hence, the x-ray diffraction pattern from an assembly of such molecules has broader outer halo than that from a linear molecular assembly. The polarisability and magnetic susceptibility anisotropies on the other hand depend mostly on the aromatic rigid part of the molecules and vary little on the orientation of the aliphatic chain part. So, the order parameter values calculated from x-ray diffraction intensities are smaller than those obtained from the other two experimental techniques. This effect of chain ordering on x-ray $\langle P_2 \rangle$ values has been evaluated by Gupta et al[117] for a few pure compounds having long end chains. However, such calculations for mixtures are much more difficult and have not been tried as yet.

Chapter - 4

STUDY OF PHYSICAL PROPERTIES OF BINARY MIXTURES OF TWO NEMATOGENS

In this chapter, study of different physical parameters of binary mixtures of two nematic liquid crystalline compounds have been reported. The compounds are p-ethoxyphenyl trans - 4- butyl cyclohexane carboxylate (EPBCC in short) and 4′-n-pentyloxy - 4- cyanobyphenyl (5OCB in short). The structural formulae and transition temperatures (°C) of them are given below:

EPBCC 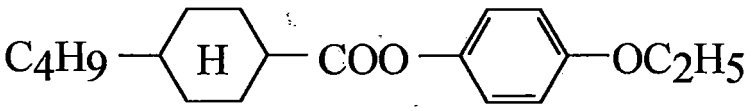

Cr 36.3 N 74.6 I

5OCB 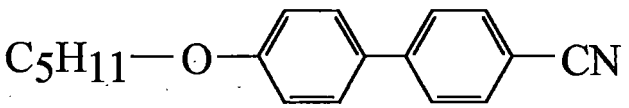

Cr2 48 Cr1 53 N 68 I

Both the samples were gifted by Hoffmann La-Roche and Co., Switzerland. I used these sample without further purification. Density[118], optical birefringence[118], apparent molecular length[116], intermolecular distance[116] and order parameters[116,118] of pure EPBCC compound had already been studied by M. Mitra et al in our laboratory. They also measured magnetic susceptibility anisotropy[119]. Anomalous behaviour in the variation of density, apparent molecular length and intermolecular distance with temperature were observed by them. Density, optical birefringence and order parameter measurements of pure 5OCB compound were done by M. Mitra et al[120]. X-ray diffraction study in this sample was performed by B. Bhattacharjee et al[107]. Crystal structure analysis was undertaken by P. Mandal et al[121].

The mixtures of 5OCB and EPBCC were prepared with four different compositions A to D (x_{5OCB} = 0.213; 0.434; 0.626; 0.818). Transition temperatures of these compositions were determined with Mettler FP 80/82 thermo-system by studying textures under a polarising microscope. The phase diagram is shown in Fig.-4.1. In all concentrations Cr – N transition temperatures could not be determined accurately and hence are not shown in the phase

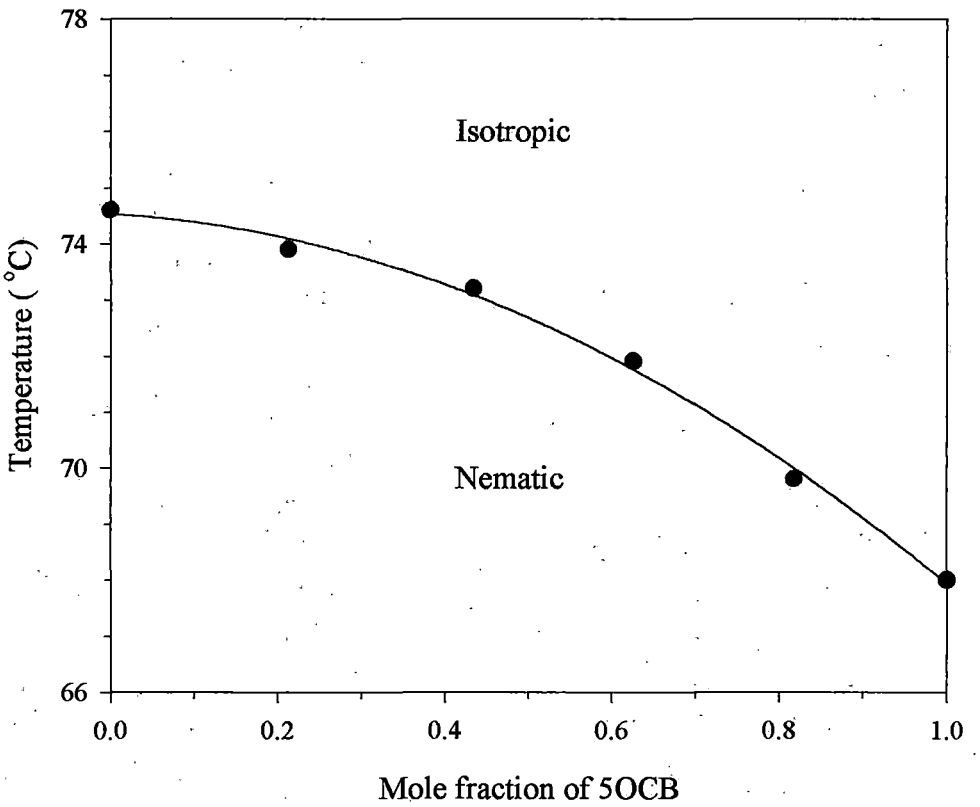

Fig. 4.1 Phase diagram of binary mixture (EPBCC + 5OCB)

diagram. The maximum and minimum Cr–N transition temperatures are ~3°C and ~16°C respectively. It is evident that N – I transition temperatures vary smoothly with concentration (c) of 5OCB and follow the equation $T_{NI} = 74.53 - 0.83c - 5.77c^2$. For all the mixtures schlieren textures were found which is characteristic of nematic phase. Cybotactic nematic phase as revealed from x-ray diffraction photographs (shown in Fig.-4.2), was observed only for the mixture B, at lower temperatures (20° – 36°). It might be worthwhile to mention here that 5CB and ME6O.5 exhibit only N phase in pure form but their mixture induces smectic phase. The details are discussed in chapter 5. The first component 5CB is having larger dipole moment (μ = 4.8 D) than 5OCB (μ =4.3 D) and the second component ME6O.5 possesses less flexible core but longer alkyl chain on both ends than EPBCC. Measurement of density, optical birefringence and x-ray diffraction study for all these mixtures were undertaken by me. Apparent

5CB 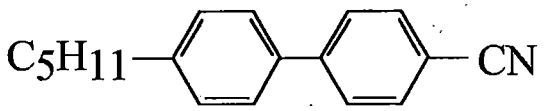

ME6O.5 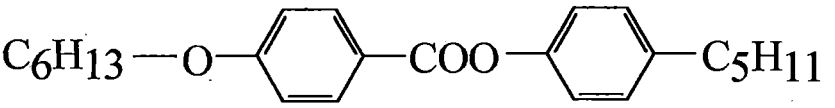

molecular length, l, orientational order parameters $\langle P_2 \rangle$ and $\langle P_4 \rangle$ for the mixtures were determined from x-ray photograph. $\langle P_2 \rangle$ are also determined from refractive index measurement. Details of the experimental techniques have been discussed in chapter 2.

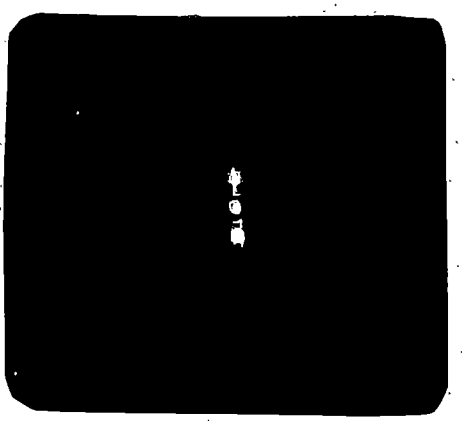

Fig. 4.2a X-ray photograph of cybotactic nematic phase at 20.5°C.

Variations of density with temperatures for all the mixtures as well as for the two pure compounds are shown in Fig.-4.3. It is observed that density of the mixtures decreases smoothly with temperature but with increasing concentration of 5OCB the density variation is quite irregular. For example over an appreciable range of temperature (43.5° to 66°C) density of mixture C almost coincides with the density of 5OCB whereas density of mixture D, in which concentration of 5OCB is maximum, deviates most from the density of 5OCB. This might be the result of anomalous density behaviours of EPBCC[118] as shown in the Fig.-4.3.

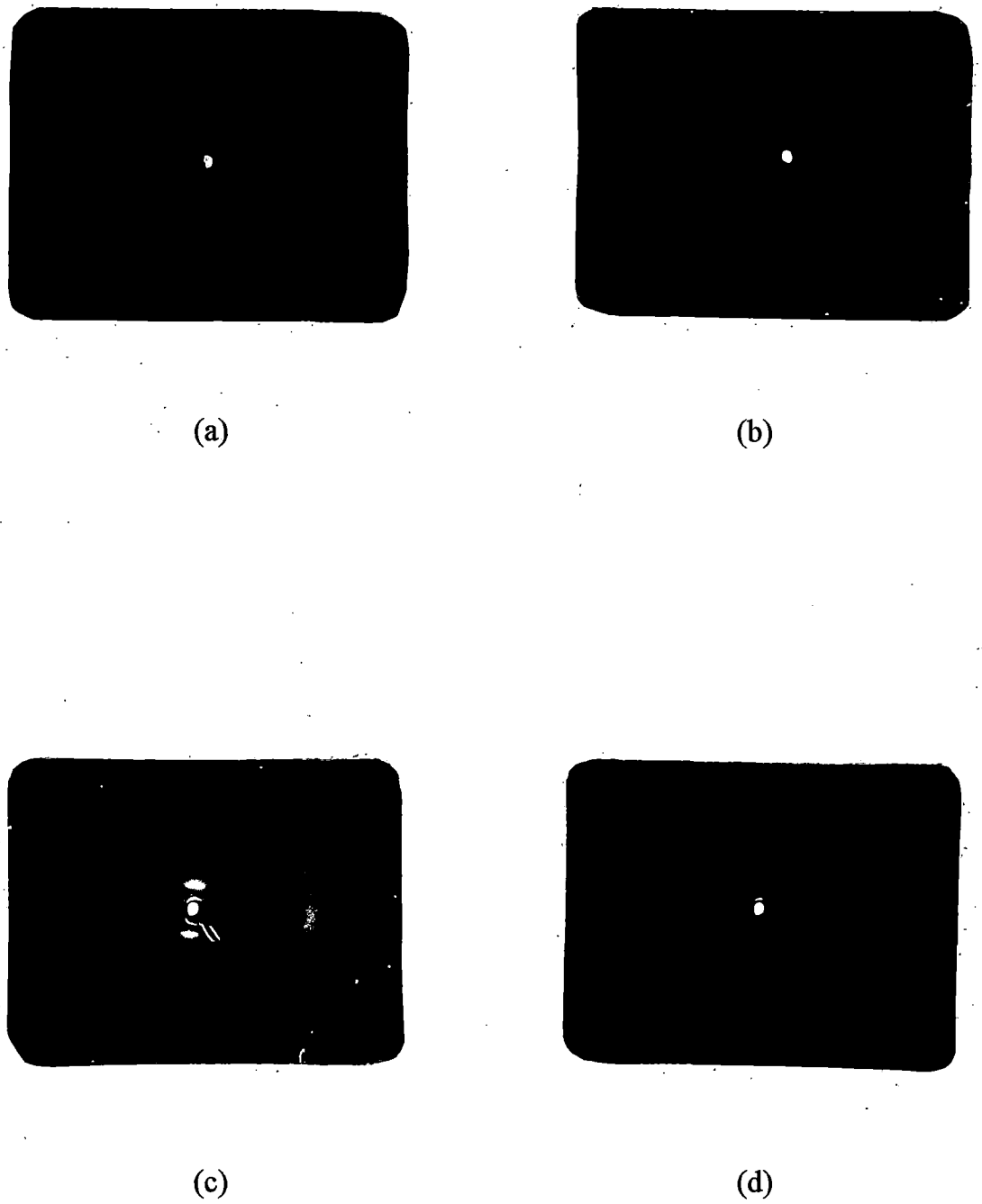

(a) (b)

(c) (d)

Fig. 4.2b X-ray photograph of nematic phase a) Mixture A at 35°C, b) Mixture B at 52.3°C, c) Mixture C at 53.4°C and d) Mixture D at 42°C

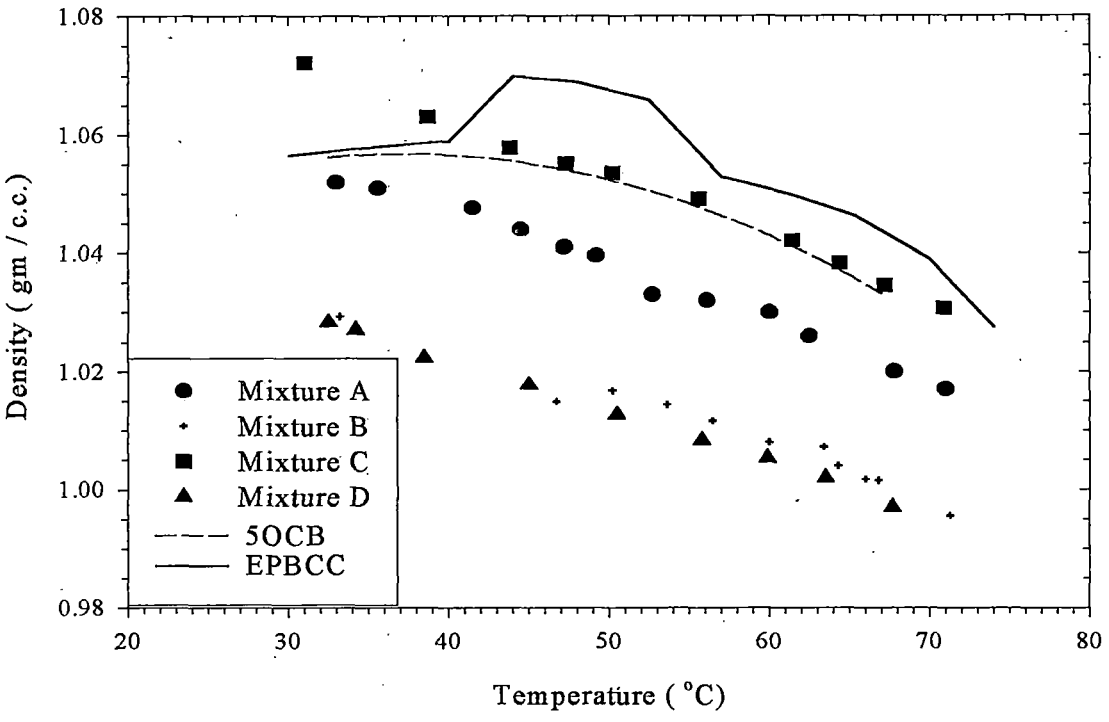

Fig. 4.3 Variation of density with temperature for the binary Mixture (EPBCC + 5OCB)

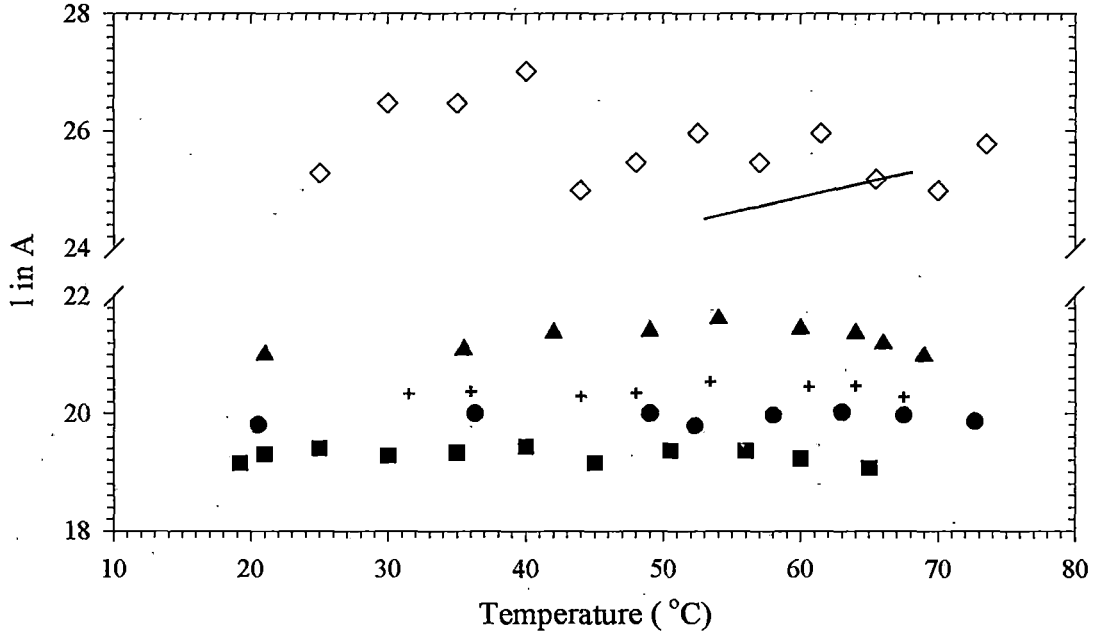

Fig. 4.4 Variation of apparent molecular length with temperature for pure compounds and the mixtures. EPBCC data are from ref.116; 5OCB data are from ref. 107 where only values of l at the ends of nematic range are given.

■ Mixture A ● Mixture B + Mixture C
▲ Mixture D ◇ EPBCC —— 5OCB

Temperature dependence of apparent molecular length for pure EPBCC and mixtures have been shown in Fig.-4.4. The molecular lengths of EPBCC (L_A) and 5OCB (L_B) determined from molecular model using a stereo model unit (Prentice Hall Inc., N.Y.) in the most elongated configuration are 19.4Å and 18.5Å respectively. The apparent molecular length for pure EPBCC varies irregularly from 25.0 Å to 27.0 Å and that for pure 5OCB varies from 24.5 Å to 25.3 Å as obtained from x-ray study[107,116]. Thus in both the cases l is about 1.3 to 1.4 times of L indicating the formation of bimolecular associations. It is noted that for all the mixtures apparent molecular lengths are nearly constant throughout the temperature range and with increasing concentration of 5OCB the l values increase regularly. However, in mixture mixture-A, where concentration of 5OCB is minimum, observed apparent molecular length is 19.3Å which is almost equal to the average molecular length (19.21 Å) obtained from the following equation and considering the mixture contains only monomers. The equation is[122-125]

$$l = x_A L_A + x_B L_B$$

where x_A and x_B are mole fractions of A and B molecules. It implies that due to addition of small amount of 5OCB bimolecular associations between the molecules break down almost completely and monomeric concentration is maximum. But in case of mixtures- B, C and D l values are 19.9 Å, 20.3 Å and 21.2 Å respectively which are greater than the respective values 19 Å, 18.84 Å and 18.66 Å obtained from the above equation. Therefore, as the concentration of 5OCB is increased, concentration of different types of dimers increases. It is obvious that these dimers are not as strongly associated as observed in pure molecules.

Variation of orientational order parameter $\langle P_2 \rangle$ and $\langle P_4 \rangle$ with temperature for all the mixtures are given in Fig.-4.5. Temperature variations of order parameters of the pure compounds obtained from refractive index study[107,110] are also shown in this figure for comparison. It is observed from the figure that below 55°C $\langle P_2 \rangle$ values determine from both the methods for mixtures as well as pure components more or less agree with Maier-Saupe theoretical values. But above 55°C $\langle P_2 \rangle$ values fall quicker than Maier-Saupe theoretical prediction. Such observations in

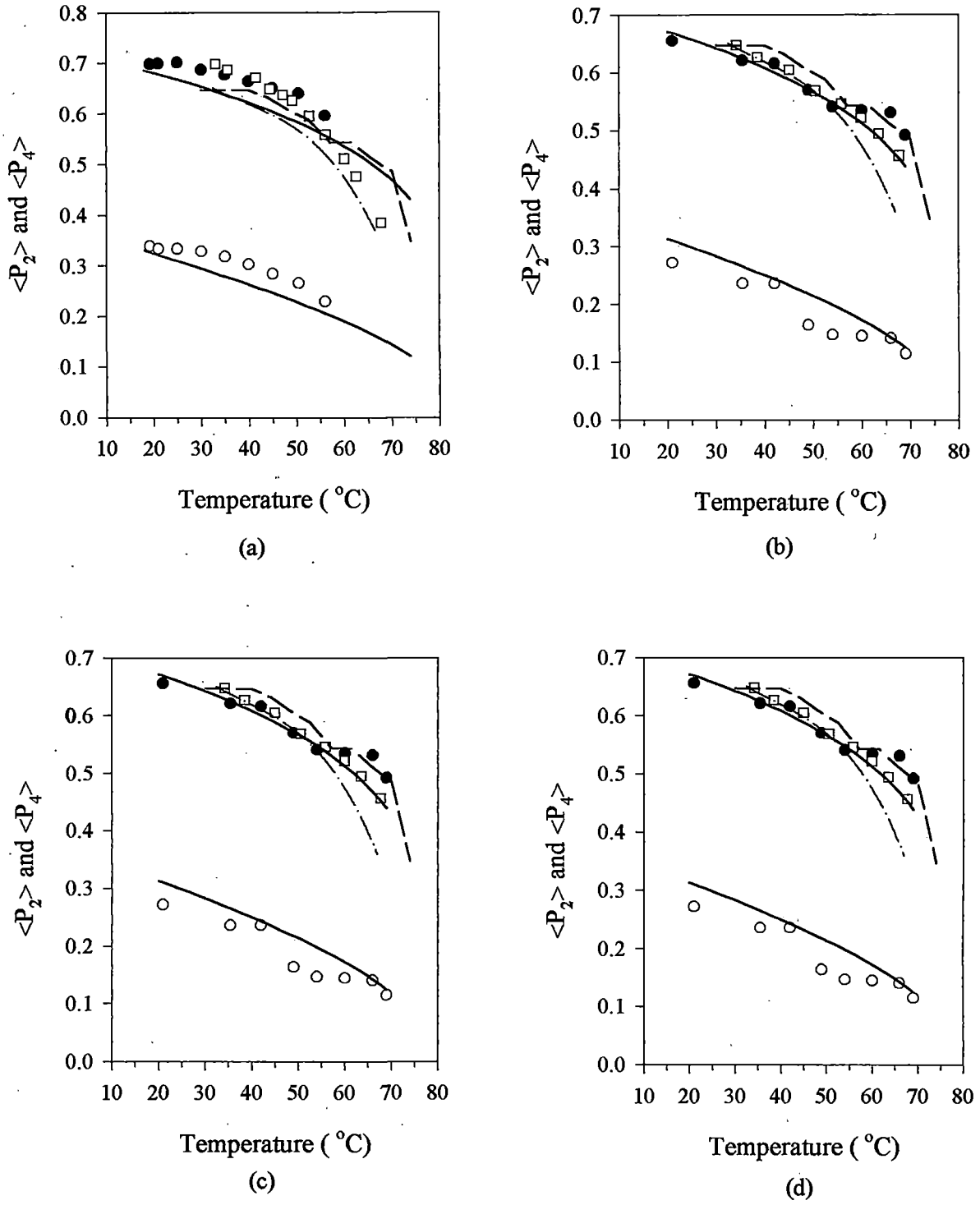

Fig. 4.5 Variation of orientational order parameter with temperature for a) Mixture A, b) Mixture B, c) Mixture C and d) Mixture D

- ● $\langle P_2 \rangle$ of mixture from x-ray
- ○ $\langle P_4 \rangle$ of mixture from x-ray
- □ $\langle P_2 \rangle$ of mixture from R.I.
- —·— $\langle P_2 \rangle$ of 5OCB from R.I
- — — $\langle P_2 \rangle$ of EPBCC from R.I
- —— Calculated value from MS Theory

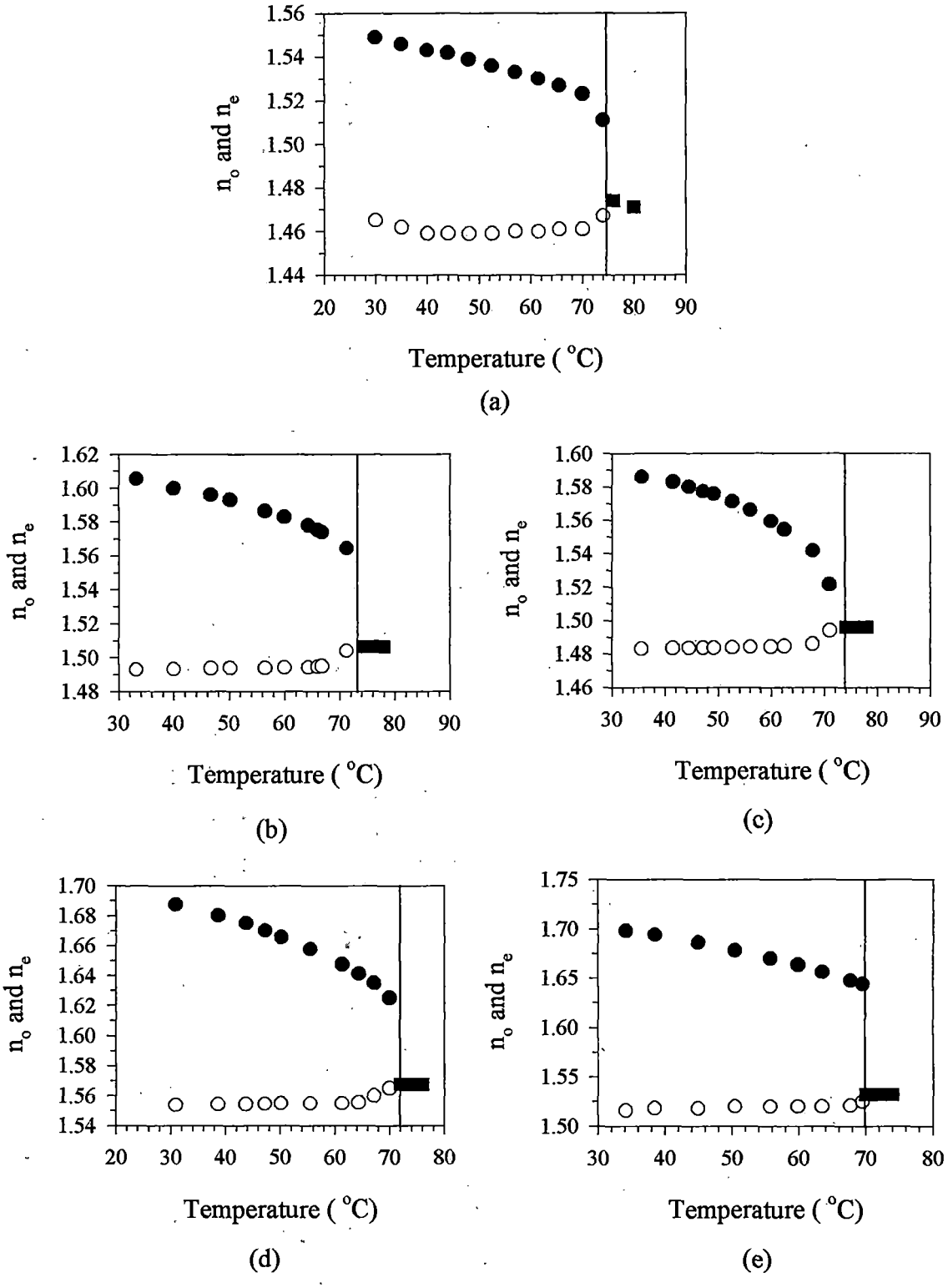

Fig. 4.6 Variation of refractive indices with temperature for a) EPBCC, b) Mixture A, c) Mixture B, d) Mixture C and e) Mixture D

● n_e ○ n_o

other compounds have been reported earlier[114,116,119,126,127]. This contradiction may be the result of different types of approximation and averaging involved in calculating orientational order parameter from experimental data obtained from x-ray studies in one hand and birefringence measurements on the other hand. Thermal fluctuation of the chain part near the clearing temperature may lowers the value of order parameter which was not taken into consideration in mean field approximation. Except mixture-A, $\langle P_4 \rangle$ values are lower than Maier-Saupe theoretical value as has been reported in other compounds.

Variation of refractive indices with temperature show typical nematic nature – presented in Fig.-4.6. Variation of $\Delta n = (n_e - n_o)$ with composition at temperatures 40°, 50° and 60°C are shown in Fig.-4.7. It decreases smoothly with decreasing concentration of 5OCB as expected from simple additivity rule.

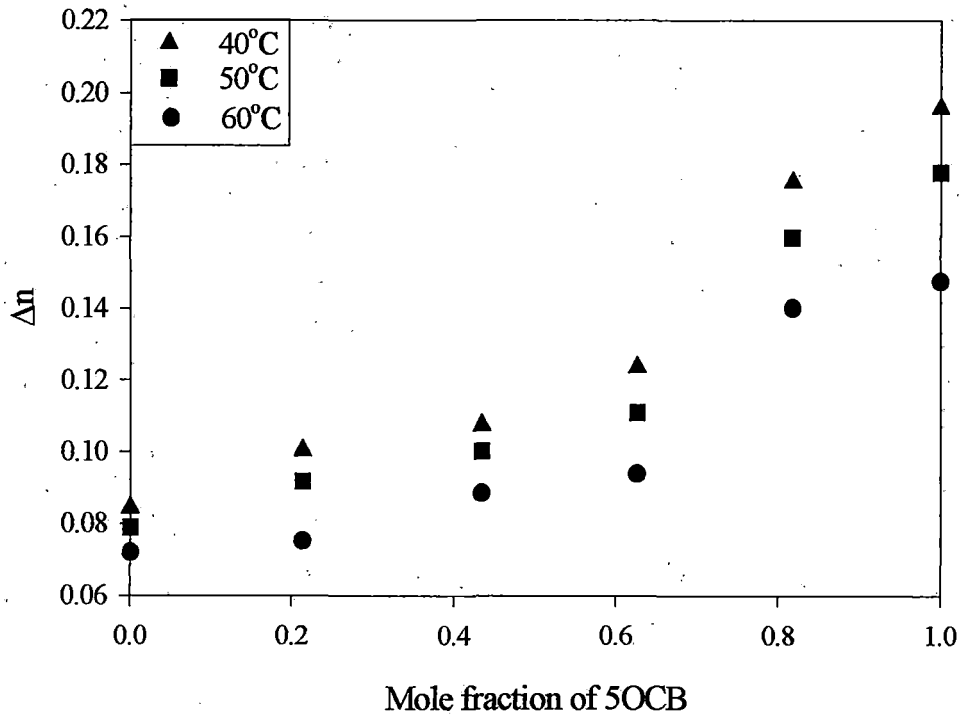

Fig. 4.7 Variation of Δn with concentration for the binary Mixture (EPBCC + 5OCB)

Chapter - 5

STUDY OF DIELECTRIC ANISOTROPY OF AN ESTER/BIPHENYL MIXTURE EXHIBITING AN INDUCED SMECTIC PHASE

5.1 INTRODUCTION

In many binary systems consisting of nematic compounds smectic A_d phase induction is observed although the components do not possess smectic properties[53,57-68,99,128-131]. The specific solute-solvent interactions are responsible for the formation of induced smectic phases.

In this paper I present the results of dielectric permittivity investigation of the binary mixtures of 4-n-pentyl 4′cyanobiphenyl (5CB) and 4-n-pentyl phenyl 4-n′ hexyloxy benzoate (ME6O.5) at different compositions along with their behaviour in pure states. The mixture shows smectic A_d phase in certain composition range. To understand the formation of the induced smectic phases and their influence on the adjacent nematic phase, study of the physical properties of this mixture had been undertaken by different workers in our laboratory. Small angle x-ray diffraction study, measurement of density and optical birefringence have been performed by Das and Paul[128,131]. The ratio of bend and splay elastic constants had been determine by Adhikari and Paul[132], magnetic susceptibility anisotropy by Pradhan and Paul[133]. The dielectric method is a powerful tool for studying the properties of mesophases. Static field measurements give information about the dielectric anisotropy which strongly depend on dipole organisation and dipole-dipole interactions in this phase.

5.2 RELATIVE PERMITTIVITY OF MESOPHASES

We can study the response of the mesogenic substances to the application of electric field by its dielectric behaviour. The liquid crystal molecules may possess permanent dipole moments. In addition induced dipoles are created when an external field is applied. Because of geometrical anisotropy in the molecular structures liquid crystals show anisotropic dielectric behaviour. One can determine $\varepsilon_{\parallel}$ and $\varepsilon_{\perp}$, parallel and perpendicular components of dielectric permittivity by applying electric field parallel and perpendicular to the director and measuring capacities of a parallel plate capacitor C_e, C_B and C_x in the air, benzene (as standard sample) and the liquid crystal respectively as the dielectric. The expression used for this is

$$\varepsilon_x = 1 + \frac{(C_x - C_e)}{(C_B - C_e)}(\varepsilon_B - 1) \qquad 5.1$$

where ε_B and ε_x are the relative permittivity of benzene and mesogenic substance — that of air is taken as 1.

5.2.1 Description of experimental set-up and measurement technique

A brief description of experimental set-up has already been given in earlier paper[134]. A cell was constructed by means of two plane tin oxide coated (thickness = 7000Å and conductivity = 10.5–11.1 Ω/□) conducting glass plates separated by glass spacers of thickness ~150 μm. A small portion of the plate was previously chosen by marking it with glass cutter to keep effective area of the liquid under consideration constant. Two glass plates were sealed together in three sides by using high temperature adhesive and was baked in an oven for several hours. The conducting glass plates were given to us as gifts by Dr Murray Bennet, Solarix Thin Film Division, USA.

The prepared cell was calibrated with benzene, p-xylene, carbon tetrachloride as standard liquid and measured dielectric permittivity value were within ±0.14% of literature values. Capacitance of the cell was measured by a digital LCR meter bridge (VASAVI ELECTRONICS, Model No. - VLCR7) at 10 kHz. Constant voltage across the capacitor was 0.35V r.m.s., low enough not to produce any electric field induced instability. The mesogenic sample was filled into the cell as isotropic liquid and slowly cooled to the desired temperature in a magnetic field of ~5 kG to get aligned sample. The cell was housed in a thermostated block and its temperature was controlled within ±0.5°C. Then $\varepsilon_{\parallel}$ and $\varepsilon_{\perp}$ were measured with the same cell at varying temperatures keeping the electric field parallel and perpendicular to the director respectively. From the values of $\varepsilon_{\parallel}$ and $\varepsilon_{\perp}$ at a temperature, one can calculate the dielectric anisotropy $\Delta\varepsilon = \varepsilon_{\parallel} - \varepsilon_{\perp}$ (for positive anisotropy) and mean relative dielectric permittivity

$$\bar{\varepsilon} = \frac{1}{3}(\varepsilon_{\parallel} + 2\varepsilon_{\perp}). \qquad 5.2$$

The principal dielectric permittivity $\varepsilon_{\parallel}$ and $\varepsilon_{\perp}$ were measured for 7CB at different temperatures as shown in Fig.-5.1 for the standardisation of the apparatus. These values agreed within 4% of the values given in references[135-137].

Both the components 5CB and ME6O.5 were gifted by E. Merck, U.K. The transition temperatures (°C) of the pure compounds are given below. Supercooling temperature is shown in parentheses.

5CB 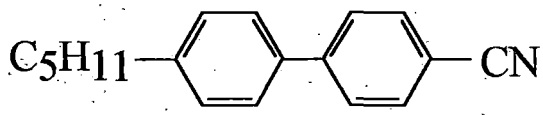

Cr 22.5 N 35.5 I

ME6O.5 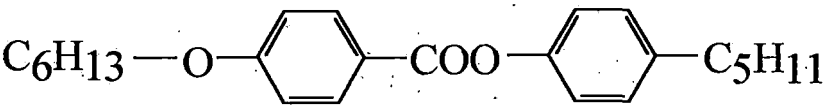

Cr (35.4) 49.5 N 62.2 I

Eight mixtures (1–8) with mole fractions of ME6O.5 equal to 0.2925, 0.3573, 0.4403, 0.5014, 0.5992, 0.6975, 0.7512 and 0.8155 were prepared by weighing the components and mixing thoroughly in their isotropic state. Phase transition of the components as well as their mixtures were studied by observing textures under crossed polarisers.

5.3 RESULTS AND DISCUSSIONS

Phase diagram of the mixtures is presented in Fig.-5.2. From x-ray diffraction study Das and Paul[128] inferred that the smectic phase is an A_d phase. I observed that SmA_d phase is induced over a wide concentration range of ME6O.5 however mixtures with ME6O.5 concentration less than 0.36 and greater than 0.82 do not induced SmA_d phase. It is also noted that maximum thermal stability of SmA_d phase is around 0.65 concentration of ME6O.5. The principal dielectric permittivities for the pure compounds 5CB and ME6O.5 are presented in Fig.-5.3a

and 5.3b. Our values of $\varepsilon_{\parallel}$ and $\varepsilon_{\perp}$ for 5CB are consistent with other published results[130,135,137]. The author is not aware of any published dielectric permittivity data for ME6O.5.

Though both the pure structure show positive dielectric anisotropy, their behaviours are different. Dielectric anisotropy ($\Delta\varepsilon$) decreases with increasing temperature in 5CB while it is almost constant in ME6O.5. For the polar compound 5CB, $\Delta\varepsilon$ is large over the entire temperature range due to the highly polar end group which lies along the director axis. Here $\bar{\varepsilon}$ is less than ε_{iso} at T_{NI}. For the weakly-polar compound ME6O.5 $\Delta\varepsilon$ is very small, ε_{iso} and $\bar{\varepsilon}$ almost coincide at T_{NI}. These facts are in conformity with the observations of Madhusudana and Chandrasekhar[138] that in N phase short range antiferroelectric order exists in systems having axial moments and no such ordering exists in non-polar system.

Variations of permittivity components with temperature for all the mixtures are shown in Fig. - 5.4 –5.4. The observed permittivity components of the mixtures in N phase are as expected from the simple rule of mixtures. However a significant jump in the parallel permittivity components at the smectic-nematic (Sm-N) transitions is observed in all cases. This is due to the increased antiparallel dipole-dipole correlation in the layered structure of SmA_d phase. The change of $\varepsilon_{\perp}$ at the Sm-N transition is continuous at the lower and higher concentrations and is discontinuous in between. Similar effects have been observed[130] in mixtures of 5CB and ME5O.5. But opposite behaviour was observed[128,131] in case of order parameters. At lower and higher concentrations, change of order parameters at Sm – N transition is first order and it is second order in between.

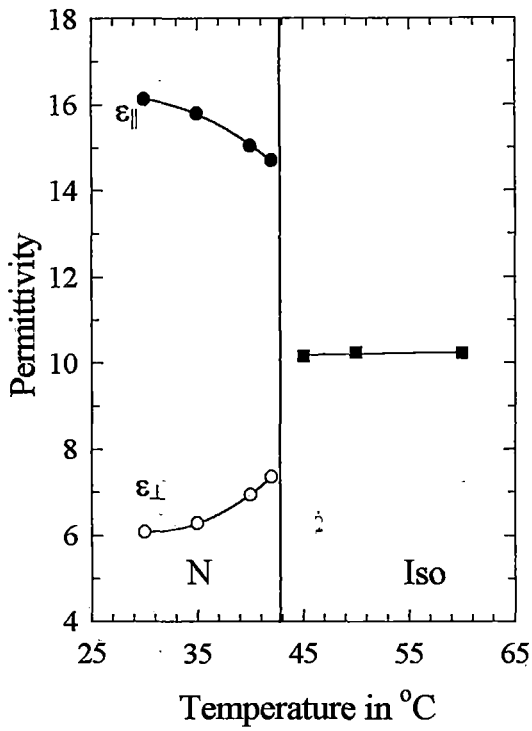

Fig. 5.1 Variation of permittivity with temperature of 7CB

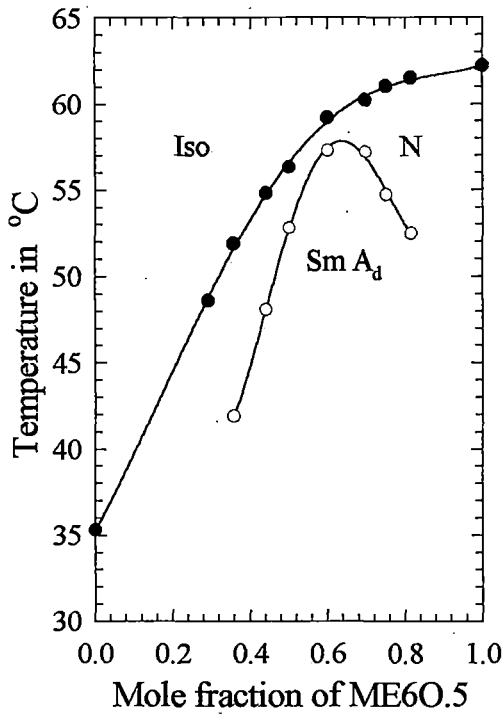

Fig. 5.2 Phase diagram of binary Mixtures (ME6O.5 + 5CB)

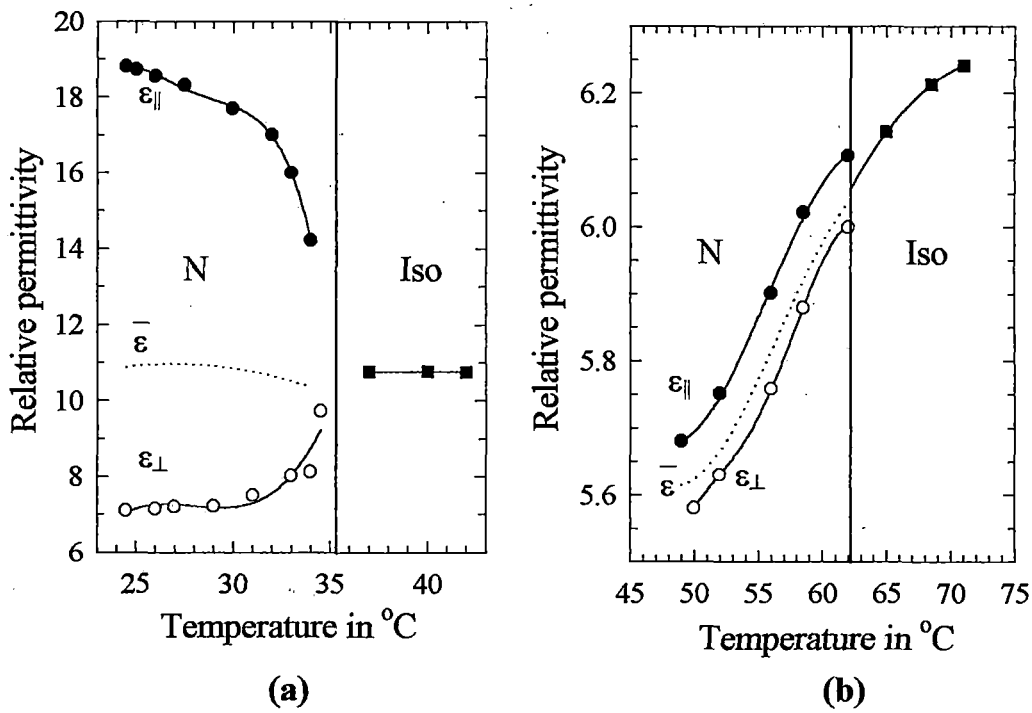

Fig 5.3 Variation of permittivity with temperature
(a) 5CB, (b) ME6O.5

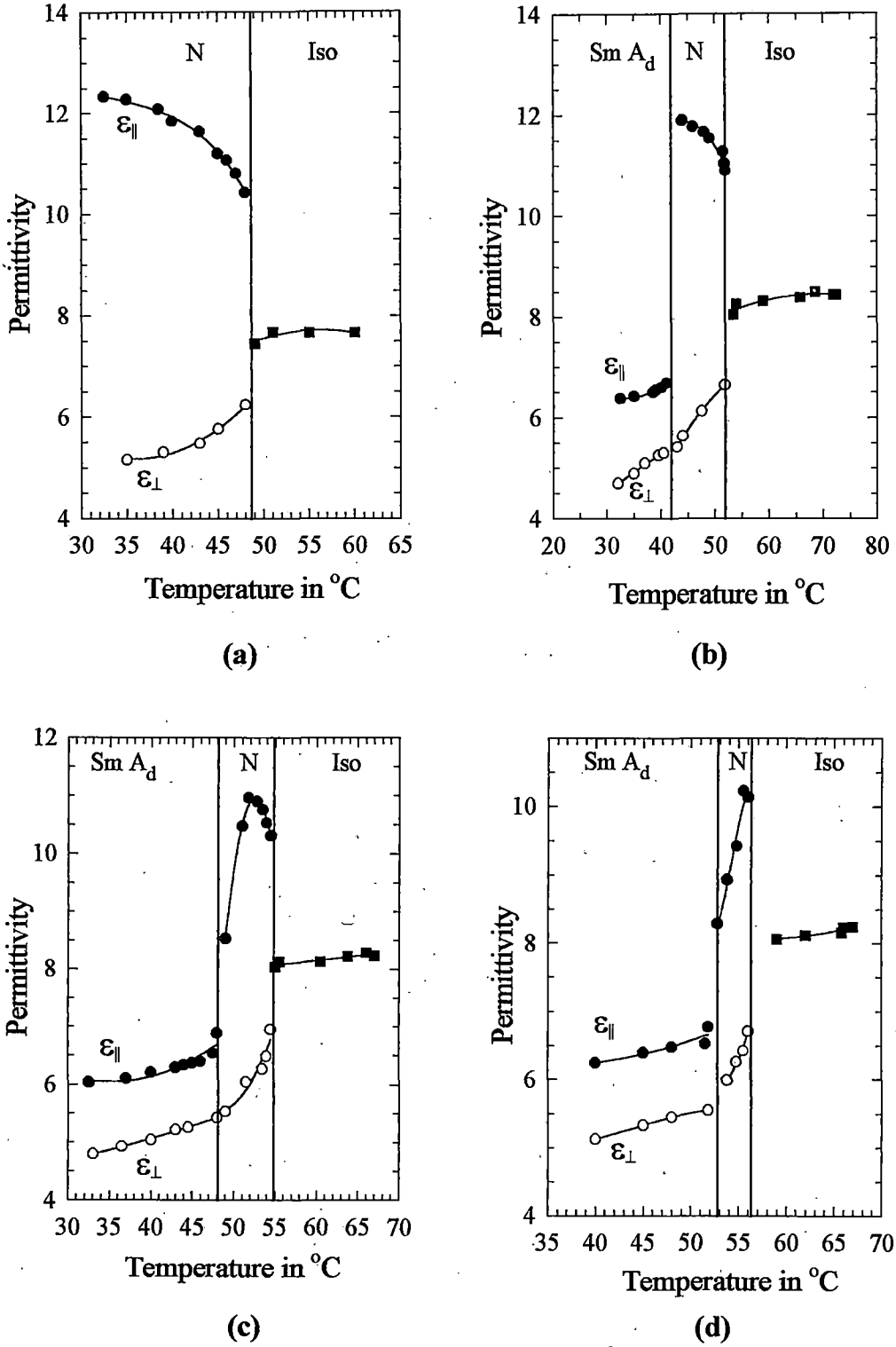

Fig. 5.4 Variation of permittivity with temperature (a) Mixture-1, (b) Mixture-2, (c) Mixture-3 and (d) Mixture-4

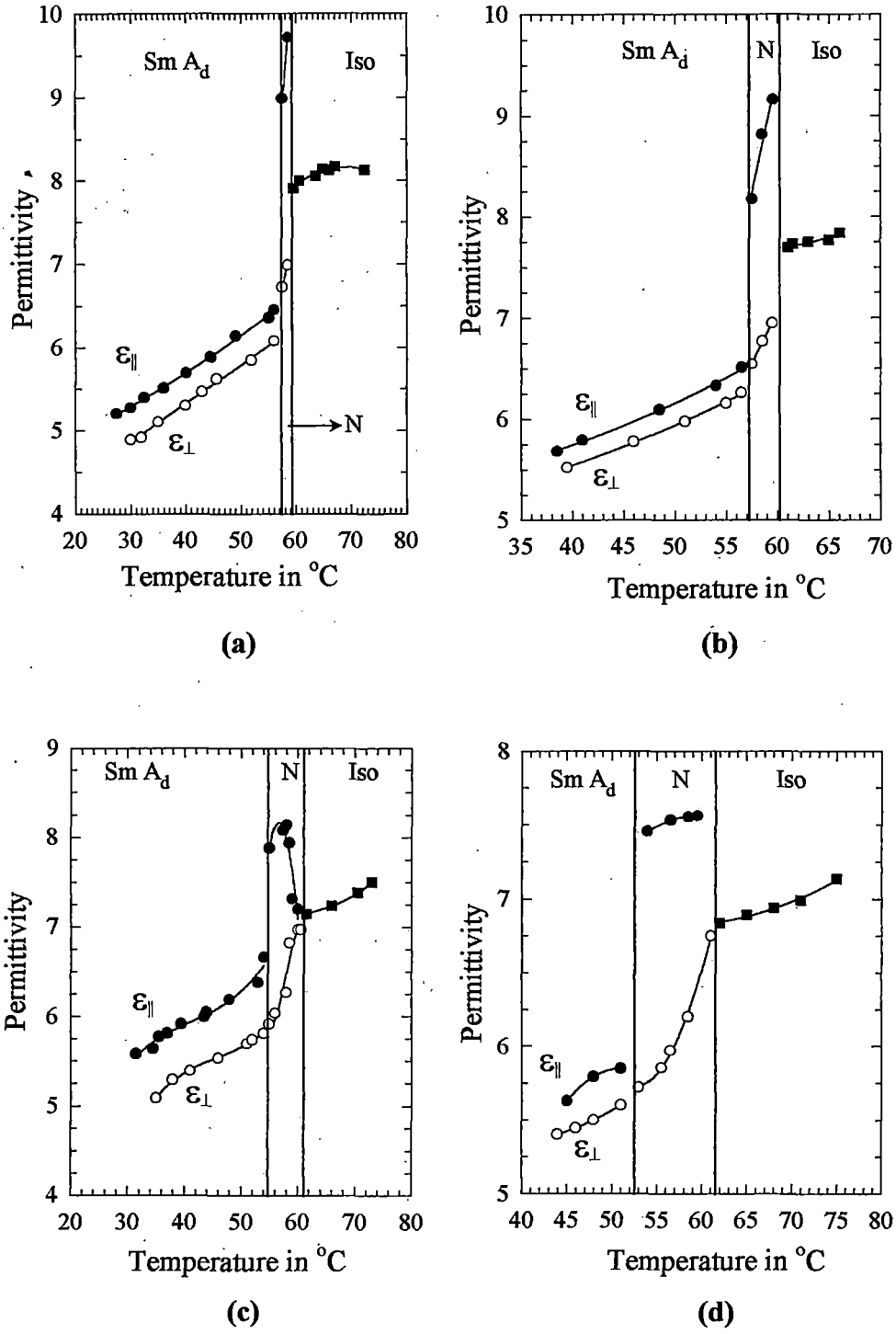

FIGURE 5 Variation of permittivity with temperature (a) Mixture-5, (b) Mixture-6, (c) Mixture-7 and (d) Mixture-8

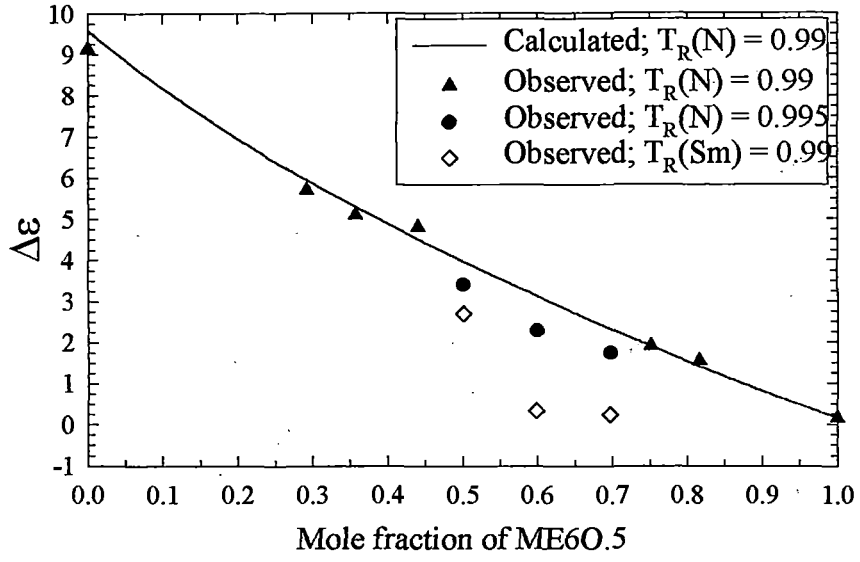

Fig. 5.6 Variation of permittivity anisotropy with mole fraction of ME6O.5

I have plotted $\Delta\varepsilon$ as a function of concentration of ME6O.5 corresponding to a reduced temperature $T_R = (T/ T_{NI}) = 0.99$ in Fig.-5.6. Since $T_R = 0.99$ for Mixtures-4, 5 and 6 is in the Sm A_d phase we have also shown data for $T_R = 0.995$ for those mixtures in N phase. I have also calculated the anisotropy $\Delta\varepsilon$ for the mixtures using the additive rule[130]

$$\Delta\varepsilon_{12} = y_1(\Delta\varepsilon_1)\left(\frac{S_{expt}}{S_{cal}}\right)_1 + y_2(\Delta\varepsilon_2)\left(\frac{S_{expt}}{S_{cal}}\right)_2$$

where $\Delta\varepsilon_{12}$ is the dielectric anisotropy of the mixture, y_1, y_2 are the volume-fractions of the components, S_1 and S_2 are the order parameters of the pure components at the same reduced temperature. However in the induced smectic region there are additional contributions to $\Delta\varepsilon$ which are not considered in the theoretical calculations. As evident from Fig.-5.6 the calculated result for the dielectric anisotropy is in fair agreement with the experiment in the nematic phase.

It is also observed that $\Delta\varepsilon$ shows a minimum around x = 0.65. Similar results have been reported earlier[130]. Variation of packing fractions, layer spacings and orientational order parameter $\langle P_2 \rangle$ from x-ray study and susceptibility measurements with molar concentration also show a minimum like this[115,128,134,139]. At this composition, it is noted earlier, that stability of the SmA_d phase is maximum. In study of other binary mixtures having induced SmA_d phase, layer spacings show maxima rather than a minima[68] at the composition of maximum stability which has been described in chapter 3.

I thus find that the degree of stabilisation of Sm A_d phase plays a major role in determining the physical properties of the binary mixtures. The minimum values are observed probably for those concentration for which monomer concentration is large, maximum occurs when dimer concentration exceeds that of monomer.

Chapter - 6

THEORY OF STRUCTURE ANALYSIS

6.1 INTRODUCTION

The discovery of x-ray and Von Laue's experiment of x-ray diffraction by a single crystal brought forth a momentous change in the concept of crystalline solids. The idea of external regular geometrical shape to be regarded as the basic feature and characteristic of crystallinity of solids was then replaced by the regularity in the arrangement of atoms and molecules in space. This new idea of crystallinity established that x-ray is capable of diffraction and bringing the inside structures of the crystalline materials. As liquid crystals show anisotropic properties like solid, to elucidate the formation and stability of mesophases, a systematic study had been undertaken by many scientists to find relations between mesophase characteristics and molecular interactions revealed in crystal structure by x-ray diffraction analysis[121,140-146].

6.2 X-RAY DIFFRACTION BY CRYSTALS

A crystal with its periodic structure was found to act as a three dimensional diffraction grating for x-rays. If the periodicity of the structure is defined by three non-coplanar unit translations a, b, c then for radiation of wavelength λ with unit vector S_o, diffracted maxima would occur along directions with unit vectors S, only when the following three Laue[147] equations are satisfied simultaneously:

a. $(S - S_o) = h\lambda$; b. $(S - S_o) = k\lambda$; c. $(S - S_o) = l\lambda$;

h, k, l being integer.

Lawrence Bragg[148,149] extended Laue's idea by showing that each diffracted beam may be considered as 'reflection' by an array of parallel lattice planes with inter planar spacing d_{HKL}, where HKL are Millar indices of the possible crystal face parallel to the array, provided that the x-ray beam is incident at a particular glancing angle θ_{HKL} to be 'reflected', naturally, at the same angle. Thus the direction of the observed maxima are given, by what we know as Bragg equation, $2d_{HKL}\sin\theta_{HKL} = \lambda$. Here HKL are same integers as in Laue's equation.

X-rays are scattered by the electrons of an atom, the nucleus has no part in it. Electrons in the atom, scattering coherently, give rise to a resultant amplitude f depending on the direction of observation. This quantity f is known as the atomic

scattering factor or form factor. Considering now all the N atoms in the unit cell, the resultant diffracted amplitude for the reflection hkl, known as the structure factors F(hkl), is given by the expression

$$F(hkl) = \sum_{j=1}^{N} f_j \exp 2\pi i \left(hx_j + ky_j + lz_j\right) \qquad 6.1$$

where f_j is the form factor of the j^{th} atom, with fractional co-ordinate x_i, y_i, and z_i.

Equation 6.1 may be written as

$$F_H = \sum_{j=1}^{N} f_j \exp\left(2\pi i \mathbf{H}.\mathbf{r}_j\right) \qquad 6.2$$

The vector $\mathbf{r}_j$ represents the position of the j^{th} atom in the unit cell and $\mathbf{H}$ the position in reciprocal space of the point (hkl). Evidently, F_H is a complex number which may be written in terms of its modulus and phase:

$$F_H = |F_H| \exp(i\phi_H)$$

Now as far as x-ray diffraction is concerned, the crystal is just a periodic distribution of electrons in three dimensions. The electron density $\rho(\mathbf{r})$ at location $\mathbf{r}$ in the crystal may then be represented by a Fourier series in three dimensions:

$$\left.\begin{aligned} \rho(\mathbf{r}) &= \frac{1}{V}\int_S F_H \exp(-2\pi i \mathbf{H}.\mathbf{r})\, ds \\ \text{or} \\ \rho(\mathbf{r}) &= \frac{1}{V}\sum_h\sum_k\sum_l F_H \exp(-2\pi i \mathbf{H}.\mathbf{r}) \end{aligned}\right\} \qquad 6.3$$

So, if one sums up the Fourier series for a fine enough grid of points spanning the entire unit cell, the structure is obtained. But measurement of intensities of the reflections provides us with $|F_H|^2$ and hence $|F_H|$, the phases ϕ_H are lost.

This is the well known **Phase Problem** in the crystallography. To overcome this problem, we generally take help of four methods viz., ① *Patterson function*, ② ***Direct methods***, ③ *Isomorphous replacement technique* and ④ *Anomalous scattering method.* Patterson map is very useful when heavy atoms are present in the unit cell. In organic crystals where there are no heavy atoms, Patterson method is quite inadequate, and usually direct methods are used.

6.3 DIRECT METHODS

Direct methods try to evaluate phases ϕ_H directly from the measured intensities I_{obs} through purely mathematical techniques. Roughly one can say that, since the crystal structure can be described by a limited numbers of parameters (the positions of the atoms) and since many more intensities can be measured, relationship among the structure factor F_H and thus among the phases ϕ_H, will exist. Therefore, the goal of the Direct methods is to identify as many of these relationship as possible. Thus if phases of two reflection were known for Σ_2 phase relations, described latter in this chapter, that of a third one related to these two can also be determined. But how can direct methods calculate phases from observed structure factor magnitudes when the amplitude and phase of a wave are physically independent quantities? $|F_H|$ and ϕ_H are linked through a knowledge of the electron density $\rho(\mathbf{r})$. Since $\rho(\mathbf{r})$ is related to structure factors by a Fourier transformation, constraints on the electron density impose corresponding constraints on the structure factors. Because the structure amplitudes are known, most constraints restrict the values of structure factor phase or, more precisely, the phases of structure invariants and seminvariants. In favourable cases, these constraints are sufficient to determine phase value directly.

6.4 STRUCTURE INVARIANTS AND SEMINVARIANTS

A structure invariant is a quantity, the value of which remains unchanged for any shift of the origin of the unit cell. A simple example is the intensity of a reflection, or F^2 because it can be measured and therefore is independent of any shift of the origin. The structure factor F is not a structure invariant since for any shift in the origin by say $\Delta\mathbf{r}$ the phase of 'F' changes by 2π $\mathbf{H}.\Delta\mathbf{r}$ radians. However, if the sum of the indices of the structure factors equals zero then it can easily be shown that the product of these structure factors is a structure invariant. Thus $F_{-H}F_KF_{H-K}$ is an example of a structure invariant and hence sum of their phases viz.,

$$\phi_{-H} + \phi_K + \phi_{H-K} = \phi(\mathbf{H},\mathbf{K}) = \phi_3 \quad \text{(say)} \qquad 6.4$$

is also an invariant. The value of structure invariant, however, is not always known, even though its values can only be a function of other structure invariants, e.g., intensities.

The structure seminvariants[150] are those linear combinations of the phase whose values are uniquely determined by the crystal structure alone, when the choice of origin is restricted within permissible values. It originates from space group symmetry. For each space group they have to be derived separately. In any space group any structure invariant is also a structure seminvariant, but reverse is always not true. A complete theory concerning this subject is given in a series of papers by Hauptman and Karle[151-153] and by Schenk[154].

6.5 SOFTWARE PACKAGES BASED ON DIRECT METHODS

Although a substantial work was done by Ott[155], Banerjee[156], Avrami[157] and Goedkoop[158], the magnum offers of crystal structure determination was the work of H. Hauptmann and J. Karle[159] of achieving it by direct methods. Different computer programs viz., MULTAN, SIMPLE[160], SHELX[161], MDM[162], MAGIC[163], RANTAN[164], MAGEX[165], YZRAC[166], MITHRIL[167] etc. are available based on direct methods — of which MULTAN (MULtiple TANgent) developed by Germain, Main and Woolfson[168] was used by me.

A systematic account of the development of the direct methods is beyond the scope of this dissertation. Only I shall discuss the basic principle and some working formulae.

6.6 STEPS TO SOLVE THE STRUCTURE

Several steps have to be taken to solve the crystal structure after intensity data collection. Steps are as follows:

I) Data reduction due to Lorentz factor and Polarisation factor

II) Absorption correction, absolute scaling and temperature factor

III) Estimation of $|E|$'s from F_{obs} values

IV) Set up phase relationships

V) Starting phase determination

VI) Phase extension and refinement

VII) Calculation of figure of merit

VIII) E-map interpretation

IX) Refinement of structures via Fourier synthesis, Difference Fourier synthesis and Least-square refinement.

Once the intensity data are collected in an automatic single crystal diffractometer (like ENRAF – Nonius, Phillips, Seifert, Rigaku) using monochromated x-ray beam, next task is to correct them for some geometric factors such as Lorentz factor, Polarisation factor and for some physical factors such as, absorption and temperature factor.

Step – I

Lorentz factor

The relation between intensity I_{hkl} and $|F_{hkl}|$ as used in diffractometric study is

$$|F_{hkl}| = \left[\frac{KI_{hkl}}{L_{hkl}\, P_{hkl}}\right]^{\frac{1}{2}}$$

where K is a constant for the experiment, but L_{hkl}, the Lorentz factor, and P_{hkl}, the polarisation factor, differ from reflection to reflection and depend on the geometry of the experimental set-up.

Lorentz factor is composed of two parts:

$$L_{hkl} = \frac{1}{\sin 2\theta_{hkl}} = \left(\frac{1}{2}\frac{1}{\sin\theta_{hkl}}\right)\left(\frac{1}{\cos\theta_{hkl}}\right)$$

the first factor is a measure of the relative intensity reflected by a unit volume at glancing angle θ and the second factor is an inverse measure of the relative rate of change, with glancing angle, of the path length. L_{hkl} can also be interpreted as the relative time opportunity for the various planes of the crystal to reflect.

Polarisation factor

This factor arises due to the nature of x-ray beam and the dependence of scattering amplitude on the orientation of electric vector **E** of the beam. For a

single electron scattering amplitude is proportional to $\sin\phi$ where ϕ is the angle between direction of the reflected beam and **E**. For parallel and perpendicular component of **E**, ϕ will be $(90° - 2\theta_{hkl})$ and 90° respectively. Thus the ratio of the amplitude is $\cos 2\theta_{hkl}$:1. The mean intensity for these two states of polarisation is defined as the polarisation factor.

$$P_{hkl} = \frac{1}{2}\left(1+\cos^2 2\theta_{hkl}\right).$$

In our case the incident beam is partially polarised during monochromatisation by reflection from the basal plane of a graphite crystal and P_{hkl} takes the form,

$$P_{hkl} = P_{erf}\frac{\cos^2 2\theta_m + \cos^2 2\theta_{hkl}}{1+\cos^2 2\theta_m} + \left(1-P_{erf}\right)\frac{\cos^2 2\theta_m + \cos^2 2\theta_{hkl}}{1+\cos 2\theta_m}$$

where P_{erf} = a constant depending on the crystal used in the monochromator (0.5 in our experiment).

θ_m = Bragg angle of reflection from the monochromator crystal.

Step – II

Absorption

To obtain the absorption correction for a reflection it is necessary to calculate the absorption of intensity for the actual path length travelled within the crystal by the beam reflecting from each infinitesimal portion of the crystal and then to integrate these results over the entire volume of the crystal[ ]. This problem cannot be solved explicitly for a crystal of general shape. In general, the practical approach has been to try to minimise the effects of absorption as much possible by crystal shaping and/or the use of more penetrating radiation, e.g., MoK_α.

Temperature factor and absolute scale

In increasing temperature, electron clouds about the nucleus spread over a large volume and thus to cause the scattering power of the real atom to fall off

more rapidly than that of the ideal, stationary model. The proper scattering factor for a real atom is, thus, not simply f_o, rather given by the expression

$$f = f_o\, e^{-B\left(\sin^2\theta\right)/\lambda^2} \qquad 6.5$$

where B is called Debye Waller Temperature factor and is related to the mean-square amplitude $\overline{u^2}$ of atomic vibration by

$$B = 8\pi^2 \overline{u^2}.$$

It is convenient to have an estimate of the average value of B for the whole structure before beginning the actual analysis. Wilson plot method[170] provides a realistic working value of B and at the same time calculates the scale factor k to place all the observed intensities on an approximately absolute basis. Expression used for the purpose is

$$\ln\left[\left\langle \left|F_{obs}\right|^2\right\rangle \Big/ \sum_{i=1}^{N} f_{oi}^2\right] = \ln k - 2B\left(\sin^2\theta\right)/\lambda^2. \qquad 6.6$$

Thus if the left side of equation 6.6 is evaluated for each of the small shells of constant f to cover the entire reciprocal space and the values are plotted against $(\sin^2\theta)/\lambda^2$, the result should be a straight line in which the slope is $-2B$ which gives the thermal parameter and the extrapolated intercept at $(\sin^2\theta)/\lambda^2 = 0$ is $\ln k$ giving the scale factor k needed to convert $|F_{obs}|$ to $|F_{abs}|$ by

$$|F_{obs}|^2 = k\,|F_{abs}|^2. \qquad 6.7$$

Step III

Estimation of |E|'s from $|F_{obs}|$ values

Since in the direct methods phases of the structure factors are estimated directly from the structure amplitudes it becomes necessary that the structure amplitudes be judged on their intrinsic merit where allowance is made for the decrease of the atomic scattering factor with increasing scattering angle. Ordinarily, the amplitudes of the different structure factors, F_H, cannot be compared directly, since the scattering factor decreases with increasing reflection angle θ. The observed $|F_H|$ is therefore modified so that they correspond to the hypothetical diffracted wave which would be obtained if atoms were stationary

point atoms. Thus the modified structure factor, called 'Normalised structure factor', E_H is defined by,

$$|E_H|^2 = \frac{|F_H|^2}{\varepsilon \sum_{j=1}^{N} f_j^2} = \frac{I_h}{\langle I \rangle} \qquad \text{and} \quad \langle |E_H|^2 \rangle = 1$$

where ε is an integer characteristic of the space group symmetry elements of the crystal. $I_h = |F_H|^2$ and $\langle I \rangle$ is the expected intensity at that value of $\sin\theta/\lambda$. Among several ways the best method to obtain expected intensity is to use the K-curve, that is plot of equation 6.6.

Extrapolating the K-curve at low angle is very important. It is always a good idea to check the scaling of E's by examining $\langle |E|^2 \rangle$ as a function of $\sin\theta/\lambda$. Values of $\langle |E|^2 \rangle$ well above unity may give rise to difficulties in phase determination.

Step IV

Set up phase relationship, phase extension and refinement

For this, phases of only the strongest reflections are required. In practice a suitable number of reflections (4 x no. of independent atoms + 100) are chosen. If the crystal is triclinic or centrosymmetric, more reflections may have to be used.

The most commonly used phase relation is a three phase structure invariant based on positivity of electron density criterion, as proposed by Karle and Karle[153]:

$$\phi_H \approx \phi_K + \phi_{H-K} \qquad 6.8$$

which for centrosymmetric structure is expressed by signs as

$$S(\mathbf{H}) \approx S(\mathbf{K})\, S(\mathbf{H} - \mathbf{K}) \qquad 6.9$$

These relationships are probability relations and the probability is high when the reflections have large |E| values in addition to satisfying the criterion $\mathbf{H} + \mathbf{K} + \mathbf{L} = 0$. These are called Σ_2 phase relations. Relation 6.8 is used to generate phases ϕ_H when the values of the phases on the right-hand side are known and it is used in a cyclic manner to propagate the phases to all the selected reflections.

The question now arises of finding the overall estimate if there are several

pairs of known phases, the estimate from each of which might well be different.

The answer to this important problem was given by Karle and Hauptman[171] (1956) when they introduced the tangent formula

$$\tan\phi_{\mathbf{H}} \approx \frac{\sum_{\mathbf{K}} k(\mathbf{H},\mathbf{K}) \sin\left(\phi_{\mathbf{K}} + \phi_{\mathbf{H}-\mathbf{K}}\right)}{\sum_{\mathbf{K}} k(\mathbf{H},\mathbf{K}) \cos\left(\phi_{\mathbf{K}} + \phi_{\mathbf{H}-\mathbf{K}}\right)} = \frac{B(\mathbf{H})}{A(\mathbf{H})} \qquad 6.10$$

where $k(\mathbf{H},\mathbf{K}) = 2\sigma_3\sigma_2^{-\frac{3}{2}} |E_{\mathbf{H}}||E_{\mathbf{K}}||E_{\mathbf{H}-\mathbf{K}}|$

$$\sigma_n = \sum_{j=1}^{N} Z_j^n$$

Z_j being the atomic number of the j^{th} atom in a unit cell containing a total of N atoms. For identical atoms $\sigma_3\sigma_2^{-\frac{3}{2}} = N^{-\frac{1}{2}}$.

In order to use the tangent formula to obtain a new phase, the value of some phases have to be known and put into the right -hand side of the tangent formula. The set of the known phases is called a starting set from which the tangent formula derives more and more new phases and refines them to self-consistency.

When $\phi_{\mathbf{K}}$ and $\phi_{\mathbf{H}-\mathbf{K}}$ are known then the distribution proposed by Cochran and Woolfson[172] for centrosymmetric structure and by Cochran[173] for non-centrosymmetric structure are as follows:

Centrosymmetric case:

$$P_+(\mathbf{H},\mathbf{K}) = \frac{1}{2} + \frac{1}{2}\tanh\left[\frac{1}{2}k(\mathbf{H},\mathbf{K})\right] \qquad 6.11$$

Non-centrosymmetric case:

$$P\left[\phi(\mathbf{H},\mathbf{K})\right] = \frac{\exp\left\{k(\mathbf{H},\mathbf{K})\ \cos\left[\phi(\mathbf{H},\mathbf{K})\right]\right\}}{2\pi I_0\left\{k(\mathbf{H},\mathbf{K})\right\}} \qquad 6.12$$

where I_0 is a zero-order modified Bessel function of the first kind.

But in this way all phases cannot be determined with acceptable reliability. It is therefore useful at this stage to eliminate about 10% of these reflections whose phases are most poorly defined by the tangent formula 6.10. An estimate of the reliability of each phase is obtained from $\alpha(\mathbf{H})$:

$$\alpha(\mathbf{H}) = \left\{A(\mathbf{H})^2 + B(\mathbf{H})^2\right\}^{\frac{1}{2}} \qquad 6.13$$

when 6.13 contains only one term, as it may in the initial stages of the phase determination, then $\alpha(\mathbf{H}) = k(\mathbf{H},\mathbf{K})$.

The larger the value of $\alpha(\mathbf{H})$, the more the reliable is the phase estimate. The relation between $\alpha(\mathbf{H})$ and the variance is given by Karle and Karle[153] (1966) as

$$\sigma^2(\mathbf{H}) = \frac{\pi^2}{3} + 4\sum_{t=1}^{\infty} \frac{(-1)^t}{t^2} \frac{I_t\{\alpha(\mathbf{H})\}}{I_0\{\alpha(\mathbf{H})\}}$$

From 6.13 it can be seen that $\alpha(\mathbf{H})$ can only be calculated when the phases are known. However, an estimate of $\alpha(\mathbf{H})$ can be obtained from the known distribution of three phase structure invariants[173]. The estimated $\alpha(\mathbf{H})$ at the initial stage is given approximately by

$$\alpha_{est}(\mathbf{H}) = \sum_{\mathbf{K}} k(\mathbf{H},\mathbf{K}) \frac{I_1\{k(\mathbf{H},\mathbf{K})\}}{I_0\{k(\mathbf{H},\mathbf{K})\}} \qquad 6.14$$

Step V

Starting phase determination

As the tangent phasing process is usually initiated with a few 'known' phases so to fix the origin and enantiomorph is the first step in phase extension. This is done imposing the condition in terms of structure factor seminvariant phases. The selection of starting phases which are involved in reliable structure invariant relationship is critical to the success of 'multisolution' methods. The generator reflections are sorted by a convergence-type process by Germain, Main and Woolfson[168] which maximises the connection between starting phases. At the end of the convergence procedure there is obtained a number of reflections sufficient to fix the origin and enantiomorphs whose phases are known and a number of few other reflections to which different phase values are assigned to create different starting points for phase extension through Σ_2 relations. The strength of convergence is that it ensures, as far as possible, that the initial phases will develop through strong and reliable phase relationships. For each starting phase set phases of all the selected strong reflections are generated and refined as explained in earlier section. Thus we get multiple phase set.

Step VII

Calculation of figure of merit

When a number of sets of phases have been developed by MULTAN it is necessary to rank them according to some Figure-of-Merit (FOM), prior to computing a Fourier map (i.e., E-map). Combining all weights from various FOM viz., Absolute Figure-of-Merit (ABSFOM), Relative Figure-of-Merit (RFOM), R-factor Figure-of-Merit (RFAC), Psi (zero) Figure-of-Merit (PSIO) etc. Combined Figure-of-Merit (CFOM) are calculated for each set. The most likely correct sets of phases are those with the highest value of CFOMs.

Step VIII

E-map interpretation

E-map are calculated using the best set of phases as indicated by the FOM. The complete interpretation of the maps is done in three stages:

a) peak search

b) separation of peaks into potentially bonded clusters

c) application of simple stereochemical criteria to identify possible molecular fragments.

The molecular fragments obtained in this way can be compared with the expected molecular structure. The computer can thus present the user with a list of peaks and their interpretation in terms of the expected molecular structure quite automatically. It is also common practice to output a picture of molecule as an easy check on the structure the computer has found.

Step IX

Refinement of structures

Generally for refinement of a model structure obtained from E-map we use following three methods, e.g., 1) Fourier synthesis, 2) Difference Fourier synthesis and 3) Least square refinement.

The Fourier synthesis gives the refined co-ordinates of the atoms and also tends to reveal the position of any atom which is not included in computing the

structure factors. The Difference Fourier map is very useful for correcting the position of an atom used in structure factor calculation. This is also very useful in locating H-atoms towards the final stages of refinement procedure. Difference Fourier synthesis is free from series termination effect which arises due to limitation in the amount of data being collected.

An analytical method of refinement of great power and generality is that based on the principle of Least Squares. In brief, Least-Square refinement consists in using the square of the difference between observed and calculated values as a measure of their disagreement and adjusting the parameters so that the total disagreement is a minimum.

An agreement between the calculated structures factors F_c and those observed, F_o, indicates the degree of refinement. The most common method of assessing the agreement is calculating the residual or reliability index of the form

$$R = \frac{\sum\left(|F_o| - |F_c|\right)}{\sum|F_o|} \qquad 6.15$$

the summation being over all the reflections. Evidently, the lower the value of R, the better is the agreement. Another form of the residual of common use is

$$R_w = \left[\frac{\sum w\left(|F_o - F_c|^2\right)}{\sum w|F_o|^2}\right]^{\frac{1}{2}} \qquad 6.16$$

where the frequently used weight is,

$$w = \frac{1}{\sigma^2(F_o)}$$

$\sigma(F_o)$ being the standard deviation of F_o.

Chapter - 7

ON THE TEMPERATURE DEPENDENCE OF CRYSTAL STRUCTURE OF TWO MESOGENIC COMPOUNDS

7.1 INTRODUCTION

The structure determination of mesogens in the crystalline state may provide correlation between crystal structures and mesophase behaviour[140,141]. Under this context the structural investigation of a number of mesogenic compounds[121,142-146] were undertaken in our laboratory. In the last twenty years many such studies on structural analysis have been reported, but the available data cannot predict the existence of definite phase. Certain trends can be concluded from the knowledge of the conformation and packing of the mesogenic molecules in crystalline state. In most cases it has been found that smectic precursors form layered structure while the nematic precursors possess imbricated structure. Disordering is frequently observed in the crystal structure of mesogenic compounds[142,174]. It seemed promising to determine the crystal structures at low temperatures. It may provide more detailed information about the thermal behaviour of the molecule.

This chapter describes the crystal structures of 5-(4-ethylcyclohexyl) -2- (4-Cyanophenyl) pyrimidine (ECCPP) at 246K and 5-(trans-4-heptylcyclohexyl)-2-(4-cyanophenyl) pyrimidine (HCCPP) at 243K. Structures of these two compounds at room temperature were determined earlier in our laboratory[142,144]. The compound ECCPP, lower member of the series, shows nematic phase (124°C) when heated to isotropic phase and HCCPP shows smectic (82°C) as well as nematic phase (158°C)[175].

7.2 EXPERIMENTAL

7.2.1 Crystal Data

Plate - shaped transparent crystals of suitable size for x-ray diffraction were obtained from a solution of acetone for both the compounds. Intensity data were collected at low temperature using an Enraf Nonius CAD - 4 diffractometer with graphite monochromated CuK_α radiation in the $\omega - 2\theta$ scan mode. A total of 5287 reflections for ECCPP and 3612 reflections for HCCPP were taken. Reflections having intensity below 2.5σ (I) level were treated as unobserved. Both the crystals belong to monoclinic system. The space group of HCCPP is $P2_1/c$

having systematic absences h0l for l odd (2n + 1) and 0k0 for k odd and the space group of ECCPP is $P2_1/n$ having h0l absent for h + l odd and 0k0 with k odd.

The reflections were corrected for Lorentz and polarisation factors but no absorption correction was made. Basic crystallographic data both at room temperature and low temperature are given in Table - 7.1. There was no indication of phase transformation on cooling the crystal. The contraction in volume at low temperature is by 2% for ECCPP and 1% for HCCPP.

Table - 7.1

Crystallographic data

	Room Temp. (for ECCPP)	Low Temp. (246 K) (for ECCPP)	Room Temp. (for HCCPP)	Low Temp. (243 K) (for HCCPP)
Crystal system	Monoclinic	Monoclinic	Monoclinic	Monoclinic
Space group	$P2_1/n$	$P2_1/n$	$P2_1/c$	$P2_1/c$
a / Å	15.959	15.6149	13.0422	13.0171
b / Å	33.469	33.4043	17.7464	17.7024
c / Å	6.210	6.2376	9.5950	9.5620
β / deg	90.335	91.4622	107.170	107.5498
Z	8	8	4	4
V / $Å^3$	3316.90	3252.50	2121.81	2100.85
d_{cal} / gm-cm^{-3}	1.17	1.19	1.13	1.14

7.2.2 Structure determination and refinement

The structures were solved by direct method using the PC version of program Multan-80 of NRCVAX package[176]. 450 structure amplitudes were selected for initial phase determination for ECCPP with $E \geq 1.83$ and for HCCPP with $E \geq 1.53$. E-map with the highest figure of merit showed fragments of the molecules. Remaining carbon atoms were located by successive Fourier synthesis. I had great difficulty in locating the positions of atoms of one of the two molecules of ECCPP but for HCCPP atomic position are located easily. Successive Fourier

and difference Fourier were applied several times to arrive at the trial structure. The positions of the hydrogen atoms were determined from the known geometry around carbon atoms and also with the help of difference Fourier map. The structures were refined by full matrix least squares method. The final R_w-value for ECCPP and HCCPP were found to be 0.096 (R = 0.099) and 0.061 (R = 0.62) respectively. I could not get crystals of very good quality and the R values are therefore somewhat high.

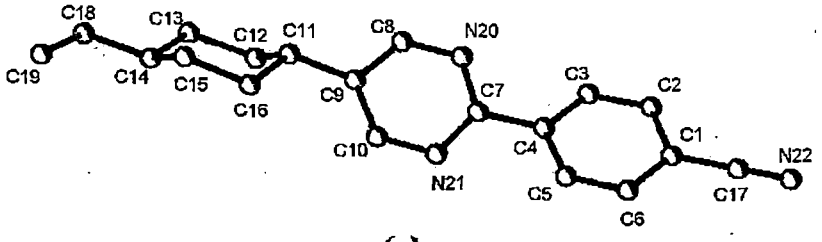

(a)

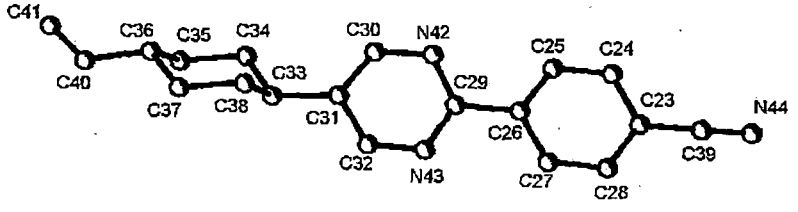

(b)

EPPCC Molecule

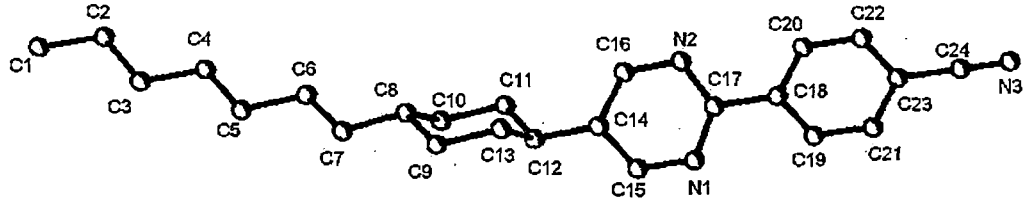

HCCPP Molecule

Fig. 7.1 Molecular structure of ECCPP and HCCPP

7.3 RESULTS AND DISCUSSION

7.3.1 Molecular structure

Molecular structure of ECCPP and HCCPP are shown in Fig.-7.1 with the atom numbering scheme. Final positions and thermal parameters of the non hydrogen atoms at low temperature are listed in Table - 7.2 – 7.3 and the bond lengths and bond angles at both temperatures in Table - 7.4 – 7.7. In both the cases values of bond lengths and bond angles are comparable with the structures determined at room temperature[142,144] except the cyclohexane ring of the molecule B of the compound ECCPP. In the room temperature structure, the cyclohexane ring of the molecule A has a normal chair conformation, however in the molecule B, it is approximately planar — this was the result of disorder, in which two mirrored chair conformations of about equal weight are involved. This disorder is also manifested in anomalous bond distances and angles involving the cyclohexane atoms and abnormally large temperature parameters for some of these atoms. The most remarkable feature of the low temperature structure is the conformational change of the cyclohexane ring of molecule B from planar to chair form. Its bond lengths and bond angles agree with reported values for cyclohexane rings[144,146,174,177]. The cyclohexane rings for HCCPP are in chair conformation at both the temperatures. The relative positions of the successive rings within the molecules are shown in the Newman's projections of Fig.-7.2 and 7.3.

For ECCPP, the dihedral angle between the phenyl and the pyrimidine rings are 16.3° (A molecule) and 7.8° (B molecule), the room temperature values being 15.2° and 6.9° respectively. For HCCPP this angle is 15° in both the cases.

7.3.2 Molecular Packing

Projections of the structure along [001] and [010] for ECCPP are shown in Fig.-7.4. Intermolecular distances smaller than the sum of the Van der Waal's radii of the atoms involved have been calculated. There were short contacts between AA and AB molecules as have been found in room temperature analysis. At low temperature the shortest distance of approach between AA molecules is 3.41Å

ECCPP Molecule

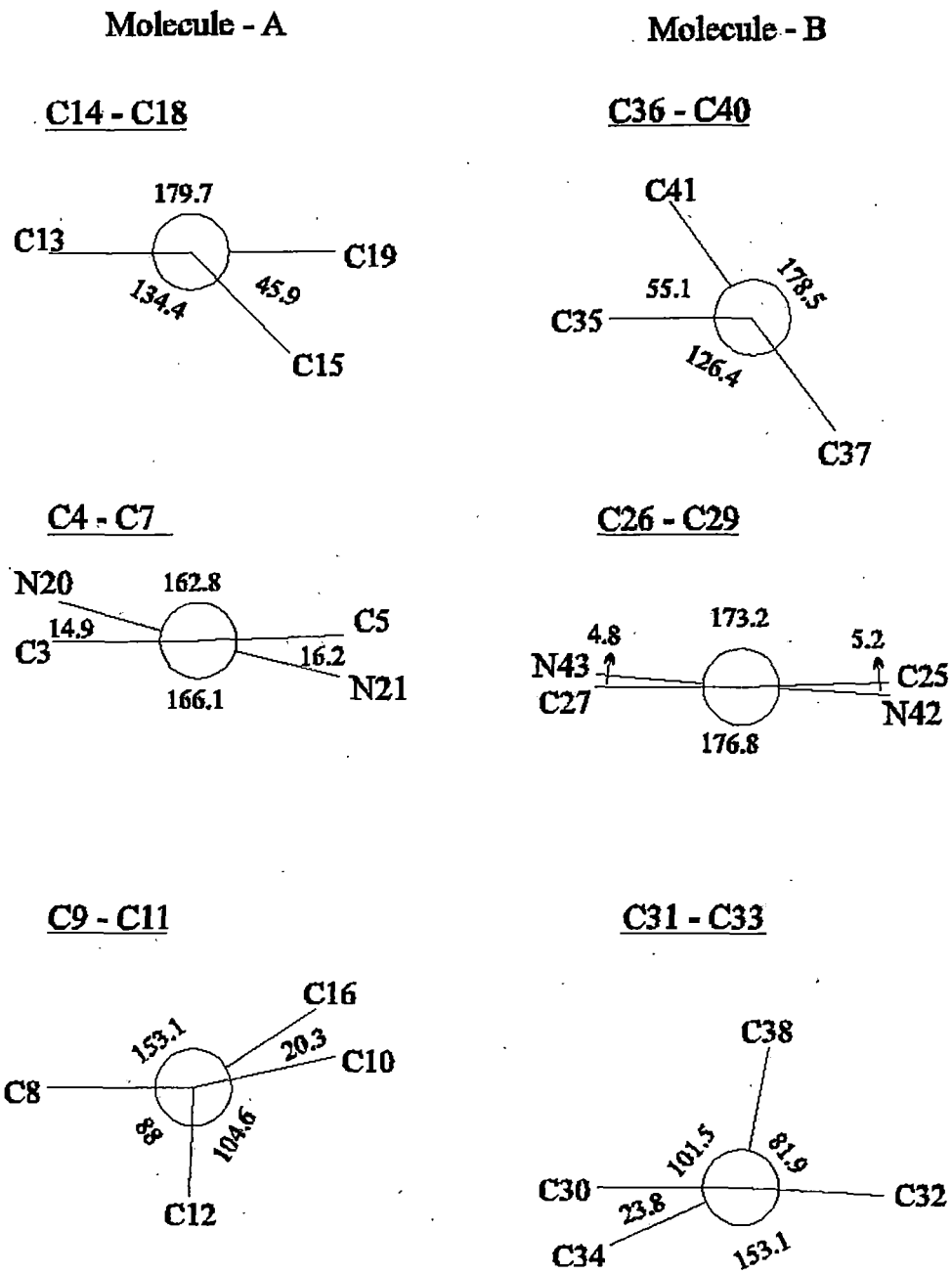

Fig. 7.2 Newman's projection of ECCPP molecule

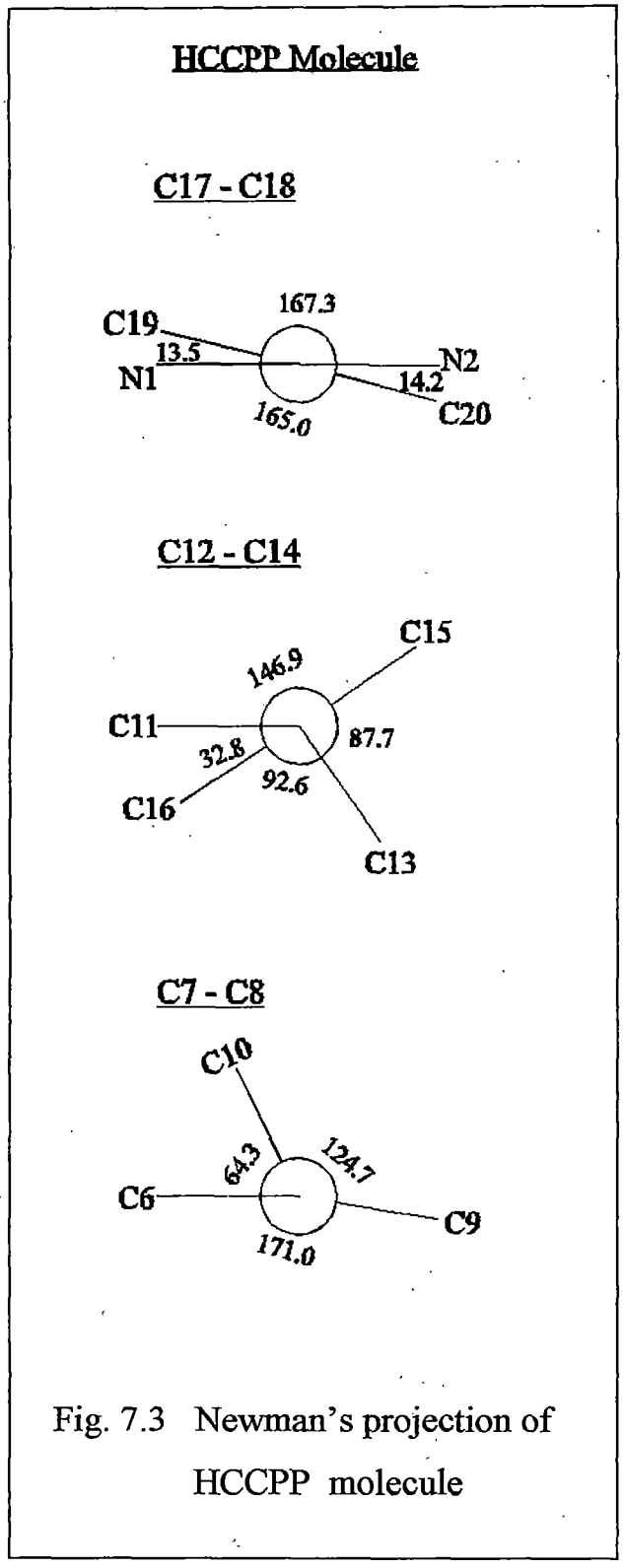

Fig. 7.3 Newman's projection of HCCPP molecule

and that of AB molecules is 3.31Å. These are about 0.04Å less than those found at room temperature. The interaction of AA and AB are both of dipolar nature. The associated pair lengths of AA is 23.1Å and that of AB is 30.9Å. From x-ray diffraction photographs of nematic phase, the apparent length of pairs of associated molecule is found to be about 25.0 Å. I, therefore, conclude that AA type association plays a crucial role in mesophase formation. Pairs of molecules related by a centre of symmetry give rise to a sheet of parallel molecule in the plane (100) and these sheets are stacked in an imbricated fashion along the c-axis.

The projections of the structures of HCCPP along [001] and [010] are shown in the Fig.-7.5. Intermolecular short contacts occur between molecules related through a centre of symmetry (½, 0, ½). These short contacts suggest that associated pairs of molecules are bound together by weak interactions between benzenes, pyrimidines and cyano groups. Total length of this pair is 32Å which becomes 33.7Å in smectic phase and 37Å in nematic phase. The molecules are arranged in layers in (101) planes and the layers

are stacked along [010]. The molecular packing therefore fulfils the geometrical prerequisite for smectic phase formation on melting as was found in the room temperature structure.

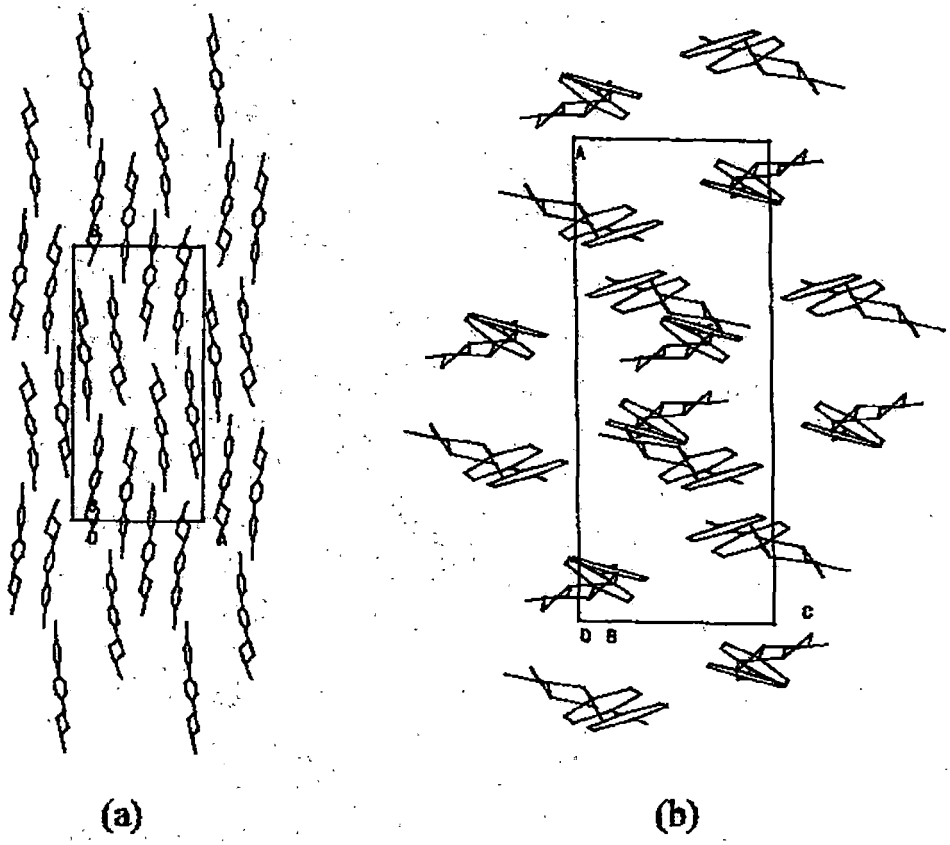

Fig. 7.4 Projection of the structure of ECCPP along a) [001] and b) [010]

7.3.3 Molecular thermal vibrations

Thermal ellipsoid plot of the molecules using the program ORTEP[178] for both the compounds at low and at room temperatures are shown in Fig.-7.6 and Fig.-7.7. Thermal ellipsoids are at 50% probability level. I find that ellipsoids enclosing hydrogen atoms are consistently larger than those for the C and N atoms. For ECCPP molecules ORTEP drawing at low and room temperatures differ significantly, specially in the molecule B, which is highly disordered at room temperature.

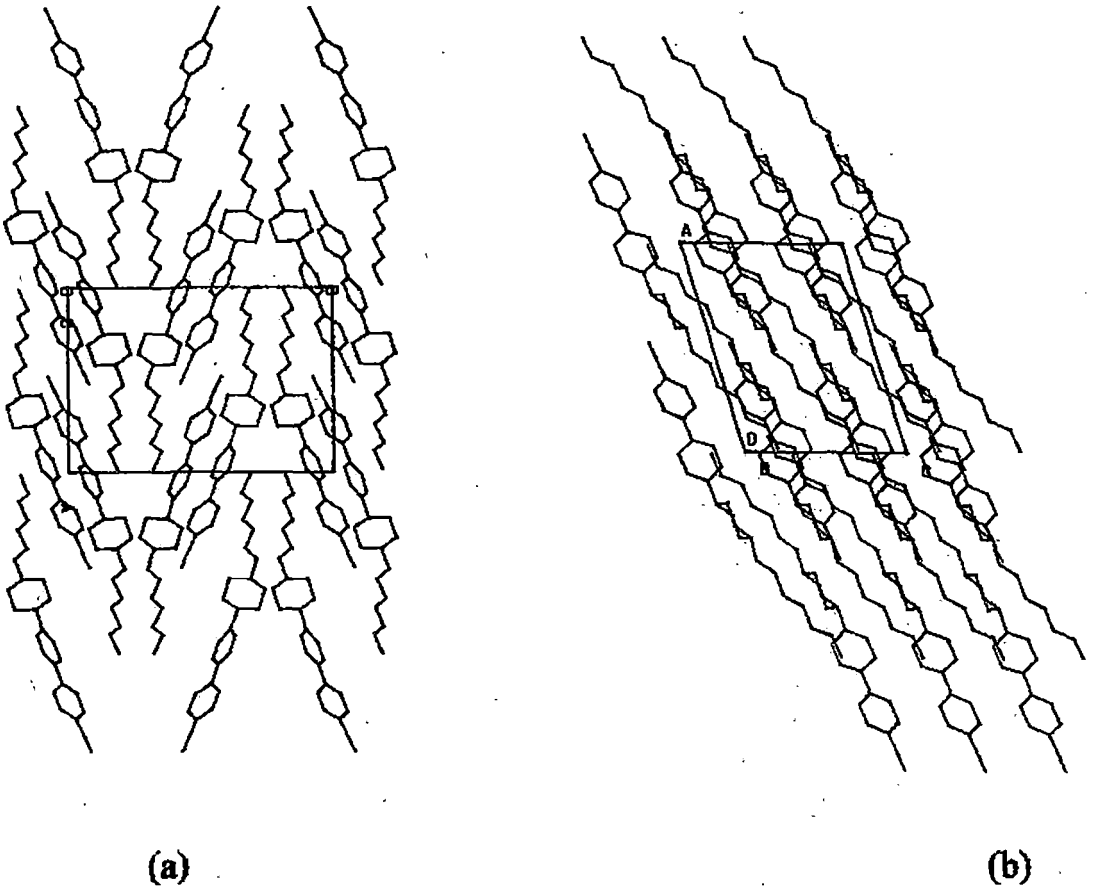

Fig. 7.5 Projection of the structure of HCCPP along a) [001] and b) [010]

It was shown by Cruickshank[179] and Schoemaker and Trueblood[180], that a linear least square analysis of the anisotropic displacement parameters of the individual atoms in a molecule that might be assumed to behave as a rigid body, could provide librational (L) and translational (T) tensors describing the overall motion of the molecules. The anisotropic displace parameters of the two compounds were fitted to the rigid body model. A computer program was written in our laboratory. The analysis was carried out at low and room temperatures treating the entire molecule as a rigid body and the molecular fragment consisting of the cyanophenyl pyrimidine as rigid body. The mean square amplitudes of

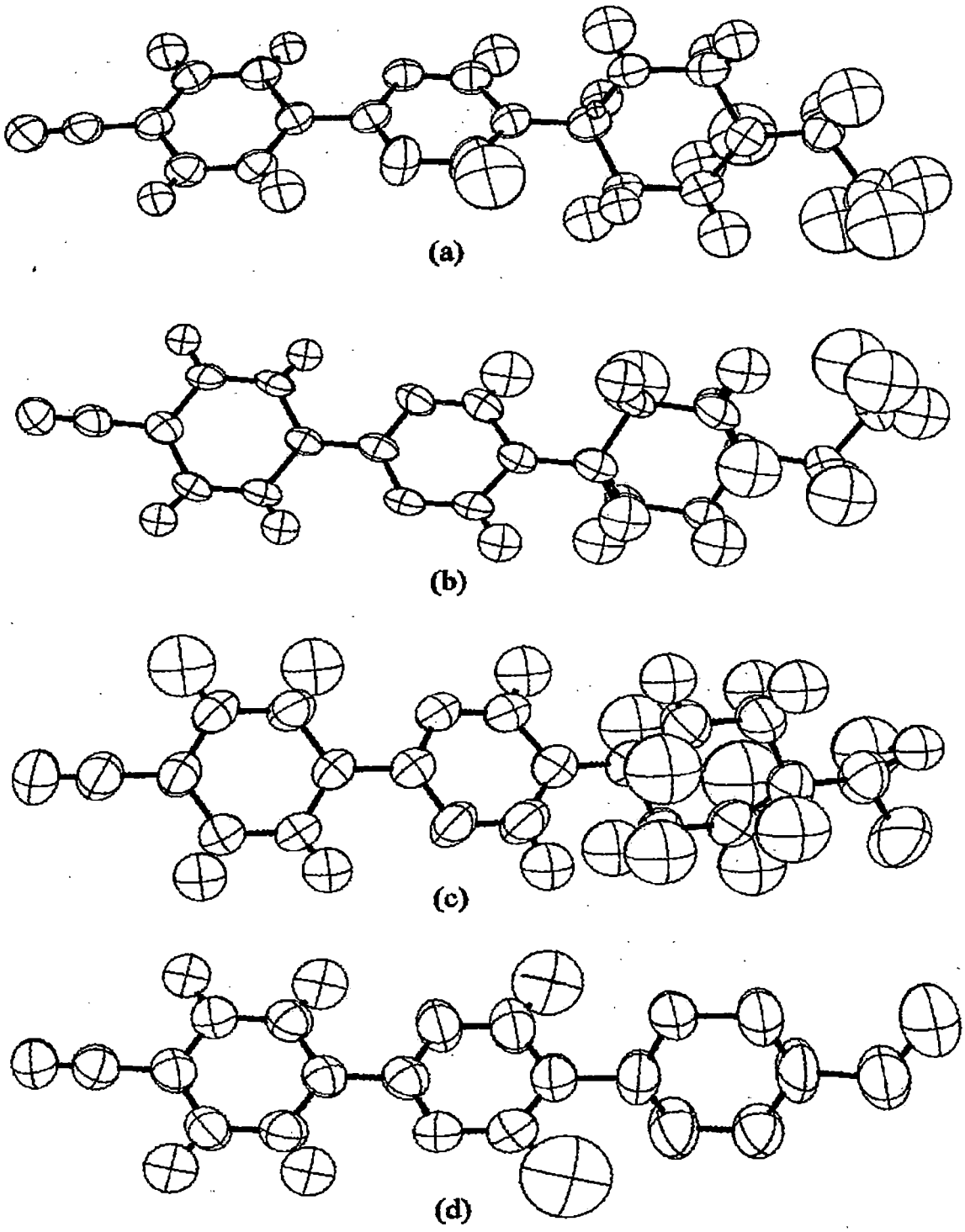

Fig. 7.6 ORTEP drawing for ECCPP a) molecule A at low temperature, b) molecule B at low temperature, c) molecule A at room temperature and d) molecule B at room temperature

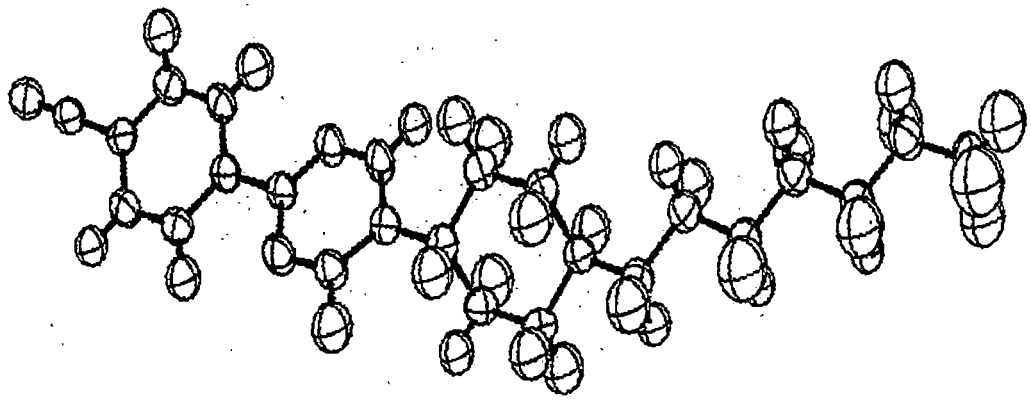

(a)

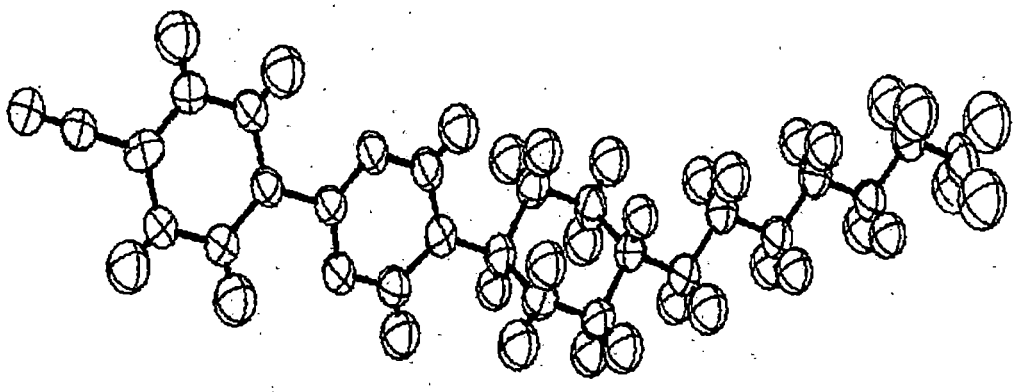

(b)

Fig. 7.7 ORTEP drawing for HCCPP a) at low temperature and b) at room temperature

translational motion and angular libration corresponding to three principal axes of T and L ellipsoids are given in the Table - 7.8. These motions are referred to cartesian axes with molecular centre of mass as origin. The X-axis is taken to the best fitted line in the least square plane of the cyano phenyl pyrimidine group and passing through the para position of the molecules. Y-axis is in this plane perpendicular to X-axis and Z-axis is perpendicular to the plane. I have also

calculated the moment of inertia (M.I) of the molecules. The principal axes about which eigen value of M.I tensor is minimum, is the long axis of the molecule. L_3 is the libration about the long molecular axis. From the table it is found that for the compound HCCPP values of the librational motions are very low at both the temperatures when the whole molecule is concerned. When the ring system is considered it is found that L_3 is rather large. At low temperature this L_3 value is about 0.6 times of that of high temperature value. For ECCPP molecules (A and B) L_3 values are comparatively large for both the ring system and when the whole molecule is considered. At low temperature this L_3 values is smaller than that at room temperature. In all cases the mean squares amplitudes of translational motions have the smallest values along the stacking directions and largest along the molecular axes. At low temperatures these values are much smaller than those at room temperature. The translational vibration is much larger at room temperature in the case of molecule B when the whole molecule is considered. This is consistent with the disorder in the crystal structure.

Since the molecules considered in these analyses are not strictly rigid, I cannot have a simple interpretation of motion in terms of translation and libration. However the results indicate that the molecular motion is anisotropic and is mainly translational in character.

To investigate the orientational behaviour of the two compounds at different temperatures the orientational order parameters for the principal molecular axes have been calculated. The order parameter in principle could be evaluated using

$$S = \frac{1}{N}\left\langle \sum_{i=1}^{N}\left(\frac{3}{2}\mathrm{Cos}^2\theta_i - \frac{1}{2}\right)\right\rangle$$

where θ_i is the angle of the axis of the i^{th} molecule with the director. The director, **n** is found by diagonalisation of the ordering tensor Q, for the principal molecular axis. Q is defined as[181]

$$Q_{\alpha\beta} = \frac{1}{N}\sum_i\left(3a_{i\alpha}a_{i\beta} - \frac{1}{2}\delta_{\alpha\beta}\right)$$

where N is the number of molecules, a_α and a_β are the components of a unit vector a_i associated with the long axes of the individual molecule. Calculations were carried out for 108 molecules. For ECCPP at room temperature molecules A and B have S values of 0.980 and 0.978 respectively. At low temperature the values increase to 0.991 and 0.986. S values for HCCPP at low temperature is 0.940 and at room temperature it is 0.926. For long range ordered crystalline state S should be 1. However, S is only unambiguously defined for rigid molecules. In reality, typical mesogenic molecules are neither rigid nor highly symmetric. The flexible chain part at the end often has low symmetry and more degrees of freedom and as a result it can take different conformations. As the chain becomes larger, the flexibility increases. This causes a lowering of order parameter of HCCPP molecule.

I calculated the correction to the order parameter for the libration about the axis transverse to the long molecular axis, using the following equation for the average value of $\langle \mathrm{Cos}^2\theta \rangle$.

$$\left\langle \mathrm{Cos}^2\theta \right\rangle = \frac{\omega}{2\pi} \int_0^{2\pi/\omega} \mathrm{Cos}^2\left(\theta_0 + \theta_1 \,\mathrm{Cos}\,(\omega t)\right) \mathrm{d}t$$

where θ_0 is the angle between the molecule and the director, θ_1 is the mean square librational amplitude perpendicular to the long molecular axes. When θ_1 is very small above equation can be written as

$$\left\langle \mathrm{Cos}^2\theta \right\rangle = \mathrm{Cos}^2\theta_0 - \frac{\theta_1^2}{2}\,\mathrm{Cos}^2 2\theta_0$$

The correction to the order parameters at both the temperatures were of the order of 10^{-3} .

7.4 CONCLUSIONS

A systematic study of the molecular and crystalline structure of mesogenic material is of considerable interest in the interpretation of the physical properties of liquid crystalline phases. The molecular arrangement in any liquid crystalline

phase is specific and is quite often related to the packing in the respective crystal phase.

It is often found that molecules of these mesomorphic compounds have certain translatory movements which eventually lead to disorder in the structure. In the compound ECCPP such disordering have been observed in the cyclohexane ring of the molecule B. Thermal motions are at 273K and 323K show significant difference. It is expected that if the crystal is further heated the molecule will have increased thermal and conformational disorder.

Crystal structure for a number of mesogenic compounds have been determined to establish rules concerning the relation between solid phase and mesomorphic phases. But the structural studies of mesomorphic compounds at different temperatures in the solid phase are few.

I do not have experimental set-up for collecting diffraction data at high temperatures. Single crystal structural analysis near the melting point could have given us more insight into the fluctuations of the physical properties at solid – mesophasic transition.

Table -7.2

Fractional co-ordinates of the non-hydrogen atoms for the HCCPP molecule at low temp.

	x	y	z	Biso
C1	0.0139(3)	0.8159(3)	0.7082(4)	5.92(20)
C2	0.1158(3)	0.8485(2)	0.6907(4)	4.65(14)
C3	0.8105(2)	0.1572(2)	0.5762(3)	3.96(12)
C4	0.2594(2)	0.8454(2)	0.5623(3)	4.04(12)
C5	0.3093(2)	0.8045(2)	0.4594(3)	3.97(12)
C6	0.4150(2)	0.8386(7)	0.4541(3)	3.88(12)
C7	0.4718(2)	0.7925(2)	0.3650(3)	3.94(12)
C8	0.5840(2)	0.8202(1)	0.3706(3)	3.28(11)
C9	0.6406(2)	0.7645(2)	0.2969(3)	4.09(13)
C10	0.5822(2)	0.8981(2)	0.3030(3)	3.85(12)
C11	0.6932(2)	0.9245(2)	0.3020(3)	3.96(13)
C12	0.7467(2)	0.8687(2)	0.2253(3)	3.28(11)
C13	0.7518(2)	0.7907(2)	0.2960(3)	3.92(12)
C14	0.8549(2)	0.8943(1)	0.2170(3)	3.12(10)
C15	0.8915(2)	0.8759(2)	0.0989(3)	3.72(12)
C16	0.9271(2)	0.9382(2)	0.3241(3)	3.81(12)
C17	1.0479(2)	0.9405(1)	0.1945(2)	3.08(10)
C18	1.1513(2)	0.9672(1)	0.1798(2)	3.12(10)
C19	1.1941(2)	0.9367(2)	0.0754(3)	3.66(11)
C20	1.2073(2)	1.0255(2)	0.2690(3)	3.78(11)
C21	1.2892(2)	0.9628(2)	0.0593(3)	3.70(11)
C22	1.3024(2)	1.0524(2)	0.2540(3)	3.95(12)
C23	1.3439(2)	1.0217(1)	0.1484(3)	3.22(10)
C24	1.4414(2)	1.0522(1)	0.1301(3)	3.45(11)
N1	0.9858(2)	0.8974(1)	0.0852(2)	3.82(10)
N2	1.0221(2)	0.9617(1)	0.3144(2)	3.80(10)
N3	1.5181(2)	1.0784(1)	0.1153(3)	4.30(10)

Table - 7.3

Fractional co-ordinates of non-hydrogen atoms for the ECCPP molecule at low temp.

	x	y	z	Biso
C1	0.1118 (2)	0.4435 (1)	0.1663 (6)	3.91(15)
C2	0.0898 (2)	0.4660 (1)	0.3453 (6)	4.12(17)
C3	0.0854 (2)	0.5068 (1)	0.3303 (5)	3.89(17)
C4	0.1030 (2)	0.5266 (1)	0.1390 (5)	3.34(14)
C5	0.1257 (2)	0.5035 (1)	-0.0373 (5)	3.96(16)
C6	0.1306 (2)	0.4628 (1)	-0.0256 (5)	4.08(17)
C7	0.0948 (2)	0.5703 (1)	0.1220 (5)	3.70(15)
C8	0.0413 (3)	0.6283 (1)	0.2502 (6)	5.16(21)
C9	0.0720 (3)	0.6501 (1)	0.0790 (6)	5.22(22)
C10	0.1174 (3)	0.6271 (2)	-0.0647 (7)	6.08(24)
C11	0.0465 (4)	0.6936 (2)	0.0567 (7)	6.6 (3)
C12	0.1009 (4)	0.7195 (2)	0.1957 (7)	7.1 (3)
C13	0.0790 (3)	0.7638 (1)	0.1818 (7)	5.74(23)
C14	0.0698 (4)	0 .7791(1)	-0.0479 (7)	6.5 (3)
C15	0.0198 (4)	0.7529 (2)	-0.1861 (8)	7.3 (3)
C16	0.0465 (3)	0.7089 (1)	-0.1731 (6)	5.21(21)
C17	0.1151 (3)	0.4006 (1)	0.1800 (6)	4.73(19)
C18	0.0507 (3)	0.8233 (1)	-0.0528 (8)	5.72(21)
C19	0.0398 (4)	0.8424 (2)	-0.2699 (10)	8.3 (3)
N20	0.0522 (2)	0.5895 (1)	0.2740 (5)	4.55(16)
N21	0.1297 (2)	0.5881 (1)	-0.0477 (5)	5.27(17)
N22	0.1173 (3)	0.3665 (1)	0.1922 (6)	6.39(21)
C23	0.2007 (3)	0.3138 (1)	0.7193 (6)	4.21(16)
C24	0.2245 (3)	0.2985 (1)	0.9221 (6)	4.46(17)
C25	0.2199 (3)	0.2580 (1)	0.9579 (6)	4.28(17)
C26	0.1920 (2)	0.2320 (1)	0.7975 (6)	3.80(15)
C27	0.1688 (2)	0.2478 (1)	0.5954 (6)	4.17(17)
C28	0.1733 (3)	0.2882 (1)	0.5590 (6)	4.29(17)
C29	0.1842 (2)	0.1885 (1)	0.8420 (6)	4.12(17)
C30	0.1981 (4)	0.1375 (2)	1.0784 (8)	7.2 (3)
C31	0.1602 (3)	0.1112 (1)	0.9378 (6)	5.24(22)
C32	0.1382 (3)	0.1277 (1)	0.7428 (6)	5.65(24)
C33	0.1379 (3)	0.0680 (1)	0.9819 (7)	5.38(22)
C34	0.1264 (3)	0.0582 (1)	1.2170 (6)	5.32(22)
C35	0.0991 (3)	0.0149 (2)	1.2494 (7)	6.15(25)
C36	0.1594 (3)	-0.0147 (1)	1.1517 (8)	5.93(23)
C37	0.1777 (3)	-0.0039 (1)	0.9196 (7)	5.60(22)
C38	0.2021 (4)	0.0395 (2)	0.8900 (8)	6.7 (3)
C39	0.2059 (3)	0.3562 (1)	0.6846 (6)	4.81(20)
C40	0.1312 (3)	-0.0580 (1)	1.1662 (8)	5.74(22)
C41	0.1129 (5)	-0.0735 (2)	1.3856 (10)	9.1 (4)
N42	0.2118 (3)	0.1762 (1)	1.0349 (6)	6.43(19)
N43	0.1494 (2)	0.1656 (1)	0.6921 (5)	5.13(18)
N44	0.2102 (3)	0.3902 (1)	0.6619 (6)	6.58(23)

Biso is the Mean of the Principal Axes of the Thermal Ellipsoid

Table - 7.4

Bond distances (Å) of the non-hydrogen atoms with standard deviations in parentheses for molecule HCCPP at low temperature.

C(1)-C(2)	1.502(4)	C(8)-C(10)	1.522(4)	C(14)-C(16)	1.398(3)	C(19)-C(21)	1.375(4)
C(2)-C(3)	1.515(4)	C(9)-C(13)	1.522(4)	C(15)-N(1)	1.328(3)	C(20)-C(22)	1.373(4)
C(3)-C(4)	1.508(4)	C(10)-C(11)	1.522(4)	C(16)-N(2)	1.334(3)	C(21)-C(23)	1.398(3)
C(4)-C(5)	1.516(4)	C(11)-C(12)	1.519(4)	C(17)-C(18)	1.472(3)	C(22)-C(23)	1.391(3)
C(5)-C(6)	1.517(4)	C(12)-C(13)	1.530(4)	C(17)-N(1)	1.349(3)	C(23)-C(24)	1.437(3)
C(6)-C(7)	1.522(4)	C(12)-C(14)	1.505(3)	C(17)-N(2)	1.343(3)	C(24)-N(3)	1.148(3)
C(7)-C(8)	1.526(3)	C(14)-C(15)	1.390(3)	C(18)-C(19)	1.391(3)	C(18)-C(20)	1.396(3)
C(8)-C(9)	1.524(4)						

Table - 7.5

Bond angles (deg.) of the non-hydrogen atoms with standard deviations in parentheses for molecule HCCPP at low temperature.

C(1)-C(2)-C(3)	115.39(25)	C(11)-C(12)-C(14)	113.69(20)	C(17)-C(18)-C(20)	120.25(20)
C(2)-C(3)-C(4)	113.43(22)	C(13)-C(12)-C(14)	112.22(19)	C(19)-C(18)-C(20)	118.49(22)
C(3)-C(4)-C(5)	115.08(22)	C(9)-C(13)-C(12)	111.19(21)	C(18)-C(19)-C(21)	121.28(22)
C(4)-C(5)-C(6)	113.74(22)	C(12)-C(14)-C(15)	121.87(21)	C(18)-C(20)-C(22)	120.93(22)
C(5)-C(6)-C(7)	113.85(22)	C(12)-C(14)-C(16)	124.17(21)	C(19)-C(21)-C(23)	119.56(22)
C(6)-C(7)-C(8)	115.47(21)	C(15)-C(14)-C(16)	113.96(21)	C(20)-C(22)-C(23)	120.03(22)
C(7)-C(8)-C(9)	111.58(20)	C(14)-C(15)-N(1)	124.52(22)	C(21)-C(23)-C(22)	119.70(22)
C(7)-C(8)-C(10)	112.56(20)	C(14)-C(16)-N(2)	123.65(21)	C(21)-C(23)-C(24)	120.74(21)
C(9)-C(8)-C(10)	109.72(20)	C(18)-C(17)-N(1)	117.40(20)	C(22)-C(23)-C(24)	119.55(22)
C(8)-C(9)-C(13)	113.53(21)	C(18)-C(17)-N(2)	117.62(20)	C(23)-C(24)-N(3)	178.2(3)
C(8)-C(10)-C(11)	112.82(20)	N(1)-C(17)-N(2)	124.97(21)	C(15)-N(1)-C(17)	116.20(20)
C(10)-C(11)-C(12)	112.20(21)	C(17)-C(18)-C(19)	121.24(21)	C(16)-N(2)-C(17)	116.69(20)
C(11)-C(12)-C(13)	109.83(20)				

Table - 7.6

Bond distances (Å) of the non-hydrogen atoms with standard deviations in parentheses for molecule ECCPP at low temperature.

C(1)-C(2)	1.3960(3)	C(11)-C(16)	1.5223(3)	C(29)-N(42)	1.3328(5)
C(1)-C(6)	1.3966(3)	C(12)-C(13)	1.51859(14)	C(29)-N(43)	1.3145(5)
C(1)-C(17)	1.43707(12)	C(13)-C(14)	1.5250(3)	C(30)-C(31)	1.3659(5)
C(2)-C(3)	1.36723(11)	C(14)-C(15)	1.4441(6)	C(30)-N(42)	1.33783(12)
C(3)-C(4)	1.3989(3)	C(14)-C(18)	1.50750(13)	C(31)-C(32)	1.3712(4)
C(4)-C(5)	1.3973(4)	C(15)-C(16)	1.52903(16)	C(31)-C(33)	1.51200(15)
C(4)-C(7)	1.46781(12)	C(17)-N(22)	1.14031(9)	C(32)-N(43)	1.31861(11)
C(5)-C(6)	1.36381(11)	C(18)-C(19)	1.5019(3)	C(33)-C(34)	1.5181(3)
C(7)-N(20)	1.3361(6)	C(23)-C(24)	1.4059(4)	C(33)-C(38)	1.5074(8)
C(7)-N(21)	1.3412(5)	C(23)-C(28)	1.3746(4)	C(34)-C(35)	1.52352(17)
C(8)-C(9)	1.3887(4)	C(23)-C(39)	1.43606(11)	C(35)-C(36)	1.5054(7)
C(8)-N(20)	1.31458(11)	C(24)-C(25)	1.37118(11)	C(36)-C(37)	1.5267(4)
C(9)-C(10)	1.3885(6)	C(25)-C(26)	1.3866(4)	C(36)-C(40)	1.51423(17)
C(9)-C(11)	1.51223(16)	C(26)-C(27)	1.4048(4)	C(37)-C(38)	1.50885(15)
C(10)-N(21)	1.32210(11)	C(26)-C(29)	1.48579(12)	C(39)-N(44)	1.14664(9)
C(11)-C(12)	1.4784(7)	C(27)-C(28)	1.37110(11)	C(40)-C(41)	1.4971(4)

Table -7.7

Bond angles (deg.) of the non-hydrogen atoms with standard deviations in parentheses for molecule ECCPP at low temperature.

C(2)-C(1)-C(6)	19.917(17)	C(12)-C(13)-C(14)	113.354(12)	C(26)-C(29)-N(43)	118.036(13)
C(2)-C(1)-C(17)	119.875(8)	C(13)-C(14)-C(15)	113.17(3)	N(42)-C(29)-N(43)	125.534(22)
C(6)-C(1)-C(17)	120.208(9)	C(13)-C(14)-C(18)	111.208(10)	C(31)-C(30)-N(42)	124.009(12)
C(1)-C(2)-C(3)	119.615(8)	C(15)-C(14)-C(18)	118.59(3)	C(30)-C(31)-C(32)	113.991(25)
C(2)-C(3)-C(4)	121.371(9)	C(14)-C(15)-C(16)	114.08(3)	C(30)-C(31)-C(33)	126.536(10)
C(3)-C(4)-C(5)	117.913(17)	C(11)-C(16)-C(15)	111.458(16)	C(32)-C(31)-C(33)	119.408(20)
C(3)-C(4)-C(7)	120.982(11)	C(1)-C(17)-N(22)	179.5	C(31)-C(32)-N(43)	124.504(14)
C(5)-C(4)-C(7)	121.068(7)	C(14)-C(18)-C(19)	116.771(10)	C(31)-C(33)-C(34)	114.553(12)
C(4)-C(5)-C(6)	121.628(8)	C(7)-N(20)-C(8)	117.227(10)	C(31)-C(33)-C(38)	112.12(4)
C(1)-C(6)-C(5)	119.546(10)	C(7)-N(21)-C(10)	116.013(19)	C(34)-C(33)-C(38)	109.10(4)
C(4)-C(7)-N(20)	117.965(11)	C(24)-C(23)-C(28)	119.941(19)	C(33)-C(34)-C(35)	111.945(15)
C(4)-C(7)-N(21)	117.438(16)	C(24)-C(23)-C(39)	118.658(9)	C(34)-C(35)-C(36)	112.98(4)
N(20)-C(7)-N(21)	124.59(3)	C(28)-C(23)-C(39)	121.401(11)	C(35)-C(36)-C(37)	111.20(3)
C(9)-C(8)-N(20)	123.968(18)	C(23)-C(24)-C(25)	119.403(9)	C(35)-C(36)-C(40)	114.64(4)
C(8)-C(9)-C(10)	113.42(3)	C(24)-C(25)-C(26)	121.061(12)	C(37)-C(36)-C(40)	110.228(15)
C(8)-C(9)-C(11)	118.70(3)	C(25)-C(26)-C(27)	118.820(20)	C(36)-C(37)-C(38)	113.476(12)
C(10)-C(9)-C(11)	127.596(9)	C(25)-C(26)-C(29)	120.226(11)	C(33)-C(38)-C(37)	112.80(4)
C(9)-C(10)-N(21)	124.728(11)	C(27)-C(26)-C(29)	120.925(11)	C(23)-C(39)-N(44)	178.4
C(9)-C(11)-C(12)	111.26(3)	C(26)-C(27)-C(28)	120.298(9)	C(36)-C(40)-C(41)	116.527(14)
C(9)-C(11)-C(16)	113.731(16)	C(23)-C(28)-C(27)	120.475(12)	C(29)-N(42)-C(30)	115.572(16)
C(12)-C(11)-C(16)	109.99(3)	C(26)-C(29)-N(42)	116.409(11)	C(29)-N(43)-C(32)	116.299(12)
C(11)-C(12)-C(13)	114.24(3)				

Table - 7.8

Eigen values and eigen vectors of libration (L in deg.) and translation (T in $Å^2$)

	Room Temperature				Low Temperature			
	Eigen value	Direction Cosines			Eigen value	Direction Cosines		
Compound ECCPP								
Molecule A								
Whole Molecule								
T	0.0783	0.6519	0.7209	-0.2358	0.0706	0.8949	-0.3681	-0.2519
	0.0737	-0.7409	0.5384	-0.4021	0.0650	0.3950	0.9152	-0.0673
	0.0548	-0.1629	0.4367	0.8847	0.0275	0.2057	-0.1603	0.9651
L	1.81	0.9815	-0.1752	0.0767	1.45	0.0751	0.0282	-0.7083
	9.36	0.1649	0.9784	0.1245	7.31	-0.1332	0.9863	-0.0933
	1.90	-0.0969	-0.1096	0.9893	1.40	0.6964	0.1601	0.6993
Cyano phenyl pyrimidine								
T	0.0479	0.6547	-0.5137	-0.5545	0.0359	0.6971	0.2673	-0.6646
	0.0779	0.3623	0.8571	-0.3662	0.0653	-0.1932	0.9631	0.1881
	0.0630	0.6634	0.0389	0.7437	0.0183	0.6891	-0.0008	0.7232
L	1.62	0.9586	-0.2834	0.0268	1.40	0.9790	0.2010	-0.0250
	9.50	0.2774	0.9511	0.1358	8.63	-0.2010	0.9780	-0.0410
	3.19	-0.0640	-0.1228	0.9904	3.13	0.0160	0.0460	0.9990
Molecule B								
Whole Molecule								
T	0.1429	0.9149	0.0013	0.3934	0.0655	0.8290	0.5290	-0.1780
	0.0804	0.2464	0.7776	-0.5784	0.0674	-0.4700	0.8330	0.2880
	0.0717	-0.3067	0.6287	0.7146	0.0364	0.3010	-0.1550	0.9400
L	1.90	0.8687	0.1317	-0.4774	0.8100	0.8042	0.0334	0.5930
	8.323	0.1063	0.9911	0.0800	7.8970	0.1094	0.9729	-0.2031
	1.510	0.4837	-0.0188	0.8750	1.510	-0.5840	0.2283	0.7780
Cyano phenyl pyrimidine								
T	0.0387	0.8954	0.1734	-0.4101	0.0272	0.7949	-0.2062	0.5760
	0.0717	0.1339	0.7735	0.6195	0.0645	0.1970	0.9770	0.0853
	0.0810	0.4247	-0.6096	0.6695	0.0428	-0.5810	0.0436	0.8120
L	1.40	0.9750	0.2094	0.0741	3.992	0.9610	-0.2600	0.0833
	11.47	0.2209	0.9489	0.2255	9.655	0.2710	0.9490	-0.1550
	4.47	-0.0231	-0.2662	0.9714	3.38	-0.0435	0.1729	0.9830
Compound HCCPP								
Whole Molecule								
T	0.0558	0.8274	-0.0325	0.5607	0.0528	0.9980	0.0255	-0.0444
	0.0494	-0.4159	0.6355	0.6505	0.0452	-0.0374	0.9558	-0.2915
	0.0536	-0.3774	-0.7714	0.5123	0.0346	0.0350	0.2920	0.9553
L	5.72	0.9486	0.2374	-0.2094	2.63	0.9860	0.1645	0.0264
	0.628	-0.1994	0.9618	0.1875	0.512	-0.1570	0.8640	0.4770
	0.850	0.2458	-0.1361	0.9597	0.1150	0.0556	-0.4743	0.8785
Cyano phenyl pyrimidine								
T	0.0541	0.8864	0.4177	0.1996	0.0524	0.9678	-0.2482	0.0410
	0.0497	-0.4231	0.9059	-0.0166	0.0467	0.2512	0.9454	-0.2074
	0.0431	-0.1878	-0.0697	0.9797	0.0292	0.0127	0.2110	0.9772
L	8.223	0.9508	0.2991	-0.0877	4.928	0.9912	0.1293	-0.0364
	1.718	-0.2694	0.9270	0.2611	0.4438	-0.0892	0.8171	0.5295
	1.415	0.1553	-0.2264	0.9619	0.2560	0.9872	-0.5617	0.8214

Chapter - 8

SPLAY AND BEND ELASTIC CONSTANTS OF TWO NEMATOGENS

8.1 INTRODUCTION

Numerous experiments in nematic liquid crystals based on field induced Fréedericksz transition have been performed in last thirty years keeping in mind that liquid crystal display devices depends among other things on its elastic properties. To formulate liquid crystals to meet device requirements it is desirable to understand the factors which determines the elastic constants. New types of non-polar as well as weakly polar nematic liquid crystals with alkenyl side chains have been prepared by Schadt et al[182-184]. The compounds have low optical anisotropy, low viscosity but high elastic constants and thus be used in display devices with short response times. With this view in mind I have undertaken this measurements of elastic constants of two alkenyl compounds namely, 3E-n-butane-phenyl- (4-cyclohexane-4′-n-propane) -ether (3CPOD(3)1 in short) and 3E - n - butane - phenyl - (4-cyclohexane-4′-n-pentane) -ether (5CPOD(3)1 in short). The structural formulae and the corresponding transition temperatures (°C) are given below:

3CPOD(3)1 : 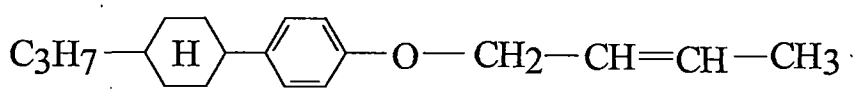

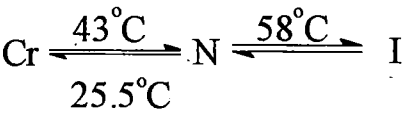

5CPOD(3)1 : 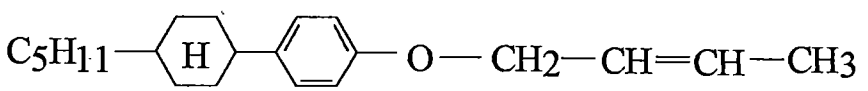

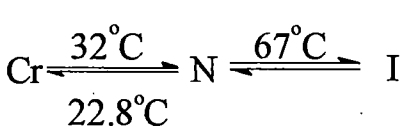

Study of different physical properties of these two compounds had been undertaken by different workers in our laboratory. Using x-ray diffraction techniques, order parameters $\langle P_2 \rangle$, $\langle P_4 \rangle$ and other physical parameters have been determined by A.

Nath et al[185,186]. They have also measured density, refractive indices and $\langle P_2 \rangle$ from optical birefringence study. N. K. Pradhan et al determined diamagnetic susceptibility anisotropy[133]. Elastic constants of the compound 3CPOD(3)1 has also been measured by Schadt[184,187,188]. This compound has negative dielectric anisotropy as has been reported by them. Samples of negative dielectric anisotropy are useful for positive contrast guest host displays and also for electric field controlled birefringence displays[189].

8.2 ELASTIC CONSTANTS AND DISTORTION FREE ENERGY OF NEMATIC LIQUID CRYSTALS

The elastic properties of a liquid crystal are generated due to restoring torques which become apparent when the system is perturbed from its equilibrium position by some external stimuli like magnetic or electric field for instance. The director pattern is no longer uniform in space, but curved. If n(**r**) changes noticeably only over large distances compared with the molecular dimensions, these curvatures can be described in terms of a continuum theory which disregards the details of the structure on a molecular scale. Based upon this point of view Zocher[190,191] and Oseen[192] initiated a phenomenological theory which was further developed by Frank[193]. This theory is in fact analogue to the continuum theory of elasticity of solids. According to the continuum theory of liquid crystals, the elastic part of the internal energy density of a perturbed liquid crystal is given by the equation

$$F_d = \frac{1}{2}\left[k_{11}(\nabla.\mathbf{n})^2 + k_{22}(\mathbf{n}.\nabla\times\mathbf{n})^2 + k_{33}(\mathbf{n}\times\nabla\times\mathbf{n})^2\right] \qquad 8.1$$

The coefficients k_{11}, k_{22} and k_{33} in this expression, the so called elastic constants are associated with the three basic types of distortions, viz., splay, twist and bend. The above equation is fundamental formula for the continuum theory of nematics. It is possible to generate deformations that are pure splay, pure twist or pure bend. Thus each constants should be positive, if not, the undistorted nematic conformation would not correspond to a minimum of the free energy F_d.

8.3 FRÉEDERICKSZ TRANSITION

The term Fréedericksz transition refers to the deformation of a thin layer of nematic liquid crystal with a uniform director field, in an external electric[194-196] or magnetic[197-203] field. It was first observed by Fréedericksz that such a layer would undergo an abrupt change in its optical properties when the strength of an external magnetic field, applied normal to the director, exceeded a well defined threshold value, known as the critical field. If the nematic liquid crystals have positive diamagnetic anisotropy or dielectric anisotropy, then as the field exceeds the critical value, the director starts to align along the external field. Depending on various geometrical arrangements one can determine splay, twist and bend elastic constants as shown in the Fig. - 8.1.

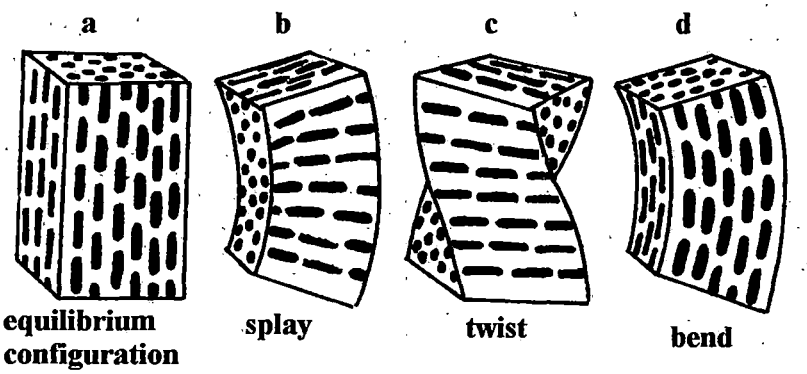

Fig. 8.1 a) An ordered liquid crystal in equilibrium configuration. The deformation states — b) splay, c) twist and d) bend

Fréedericksz transitions can be used to measure directly the elastic constants, provided the geometry i.e., the boundary conditions and the direction of the applied field are chosen in the appropriate way. Attentions are to be paid to the calculation of the threshold values belonging to different geometries. From the geometry of arrangement as shown in the Fig.-8.2 we can determine splay, twist or bend elastic

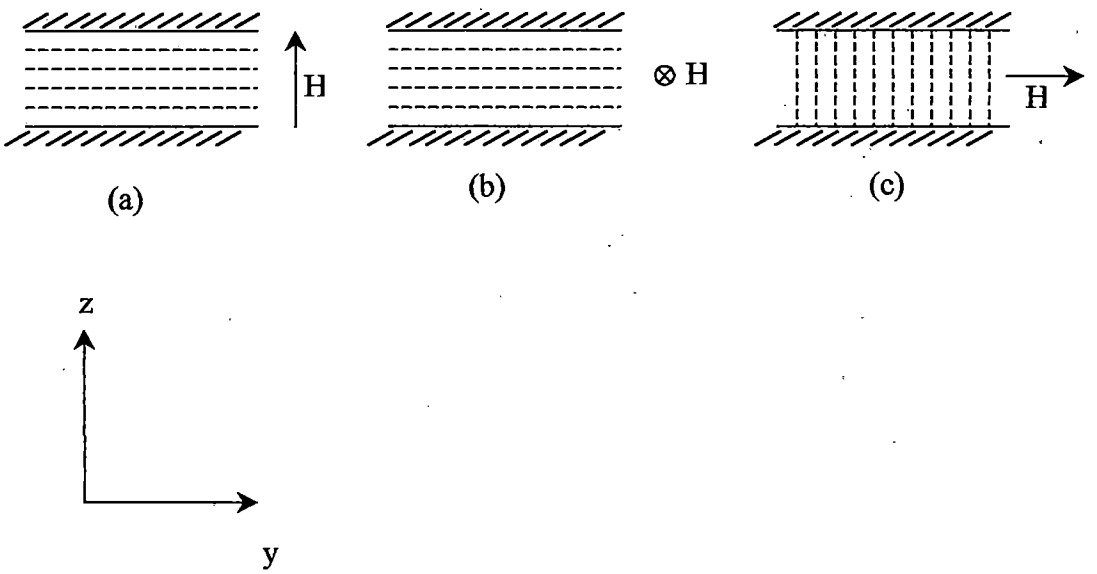

Fig. 8.2 Schematic experimental set-up for the determination of elastic constants from Fréedericksz transition: a) splay, b) twist and c) bend

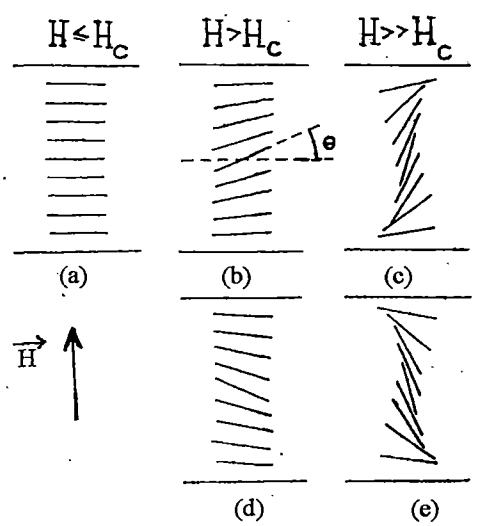

Fig. 8.3 Deformation of the director pattern above the threshold field in the splay mode

constants in the magnetic field H. The critical magnetic field for Fréedericksz transition is

$$(H_c)_i = \left(\frac{k_{ii}}{\Delta\chi}\right)^{1/2} \frac{\pi}{d} \qquad 8.2$$

where d is the sample thickness, $\Delta\chi$ is the diamagnetic anisotropy, the subscript i = 1, 2, 3 refers to splay, twist and bend deformation respectively. In splay mode, for a magnetic field $H>H_c$, applied along Z direction, the uniform planar structure (Fig.-8.3a) is unstable and the system jumps into one of the two possible states Fig. - 8.3b or 8.3d. If the field is increased further these states develop into Fig. - 8.3c and 8.3e respectively. In my calculation $\Delta\chi$ values have been taken from N. K. Pradhan's work[133].

8.4 EXPERIMENTAL TECHNIQUE AND SET-UP FOR DETERMINATION OF K_{11} AND K_{33}

The apparatus for the determination of the elastic constants (k_{11} and k_{33}) has been designed and fabricated in our laboratory by Das and Paul[204]. The block diagram of the set-up has been shown in Fig.-8.4. Details of the cell preparation

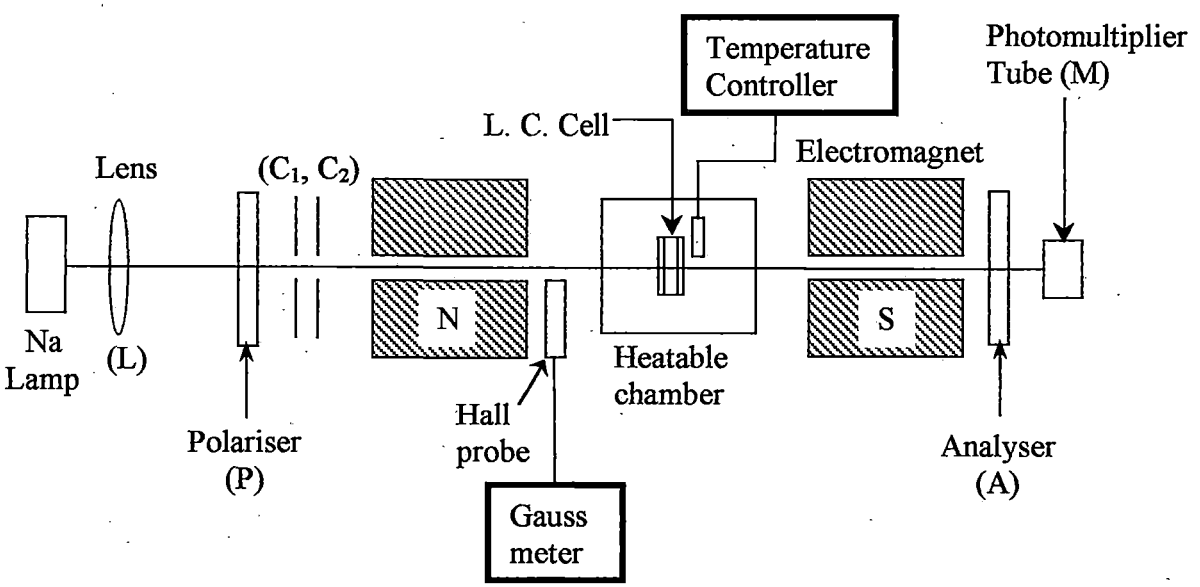

Fig. 8.4 Block diagram of experimental set-up for measuring elastic constants by Fréedericksz transition

technique has been given by de Jeu[205]. The splay elastic constant was measured by using homogeneous planar aligned cell where inner side of both the glass plates were treated by ~ 1% PVA solution, dried and gently rubbed the layer in one direction by bond paper. For bend elastic constant measurement, homeotropic aligned cell was taken. In this case inner sides of the cell were treated by lecithin. Filled in cell with the sample was placed inside a thermostated block. Sample thickness was measured with the help of screw gauge. Temperature was measured and controlled within an accuracy of ± 0.5 °C by means of a copper-constantan thermocouple inserted in the brass block and temperature controller (Indotherm Model 457). A sodium D light was used as a source which was allowed to incident on the sample through a lens (L), polariser (P) and collimating circular slits (C_1, C_2). The polariser (P) and the analyser (A) (i.e., a combination of quarter wave ($\lambda/4$) plate and a linear polariser) were crossed at ± 45° relative to the vertical axis for better sensitivity. The transmitted light was monitored by photomultiplier tube (M) which counts photon and corresponding current was measured by a nano-ammeter. Applied magnetic field was set always perpendicular to the aligned sample and during experiment it was changed slowly so that the nematic orientation remains in equilibrium with the applied magnetic field. To ensure this exact alignment, the brass block was mounted on a specially constructed platform whose alignment with respect to the field could be adjusted to an accuracy of 1-2′ of arc. Further, the platform itself rested on levelling screw so that the alignment of the sample could be varied in every possible manner. For a desired temperature, when field (H) exceeded critical value (H_c), an abrupt change in current corresponding to abrupt change in optical properties took place. We could measure H_c from field H versus intensity curve within an accuracy of ± 10 Gauss. The magnetic field was measured using a Hall-probe Gaussmeter (Model DGM-102).

If the field was increased gradually beyond its critical value, the transmitted light intensity exhibits oscillations due to the change of phase relation.

In our present set-up it is not possible to measure k_{22} till now. The threshold value for twist deformation cannot be detected optically when viewed along the twist axis. Due to the large birefringence of the medium for this direction of

propagation, the state of polarisation of the transmitted beam is indistinguishable from that of the emerging beam from the untwist nematics. A total internal reflection technique can be used to measure the k_{22} values of the twist deformation.

Both the chemicals were donated by Hoffmann La-Roche, Switzerland. I have used these samples without further purification. Transition temperatures of the pure compounds were determined with the help of Mettler Fp 80/82 thermo system by observing the texture under polarising microscope.

8.5 RESULTS AND DISCUSSIONS

Elongation of the molecular shape is a vital factor for elastic curvature. It can occur in two ways — by elongation of rigid core of structurally similar thermotropic liquid crystals (TLC) or by elongation of alkyl chain part. It is well known that elastic constants of the molecules with flexible chain part is something special due to the contribution of chain part to the elasticity of the molecule. In previous experimental works[201,203] k_{33}/k_{11} has been found to increase when rigid core of structurally similar TLCs is elongated. But for homologous samples where elongation of the molecules take place due to increase in chain length, k_{33}/k_{11} has been observed to decrease with the increase of alkyl chain length[199,206-212].

The temperature variations of both the elastic constants are shown in Fig. - 8.5 – 8.6 for the compounds. It is found that both k_{11} and k_{33} decrease with increasing temperature (Table 8.1 – 8.4) which is in agreement with other reported values. The ratio k_{33}/k_{11} is also found to decrease with increasing temperature as shown in Fig. - 8.7 and Table 8.5 – 8.6. It is noted that k_{33} is larger than k_{11} for both the samples over the entire range. This is consistent with the observation of previous workers[201,208,211,212]. It is also noted that k_{33}/k_{11} is larger in 3CPOD(3)1 than in 5CPOD(3)1 in accordance with previous observation that the ratio decrease with increasing chain lengths in a homologous series. In addition I observe that temperature variation of k_{33}/k_{11} for 5CPOD(3)1 is much smaller than that for 3CPOD(3)1.

Theoretical calculations for rigid rods[213] based on spherocylindrical model, predicts that k_{33}/k_{11} should decrease if the molecular aspect ratio R = (L-W)/W

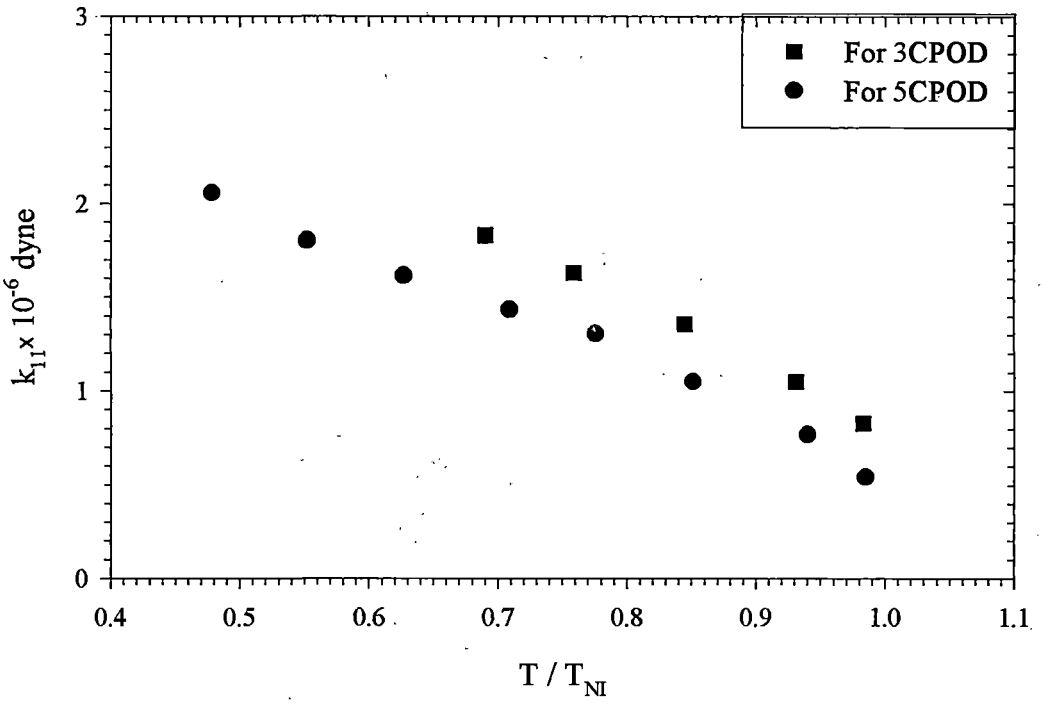

Fig. 8.5 Variation of splay elastic constant (k_{11}) with temperature

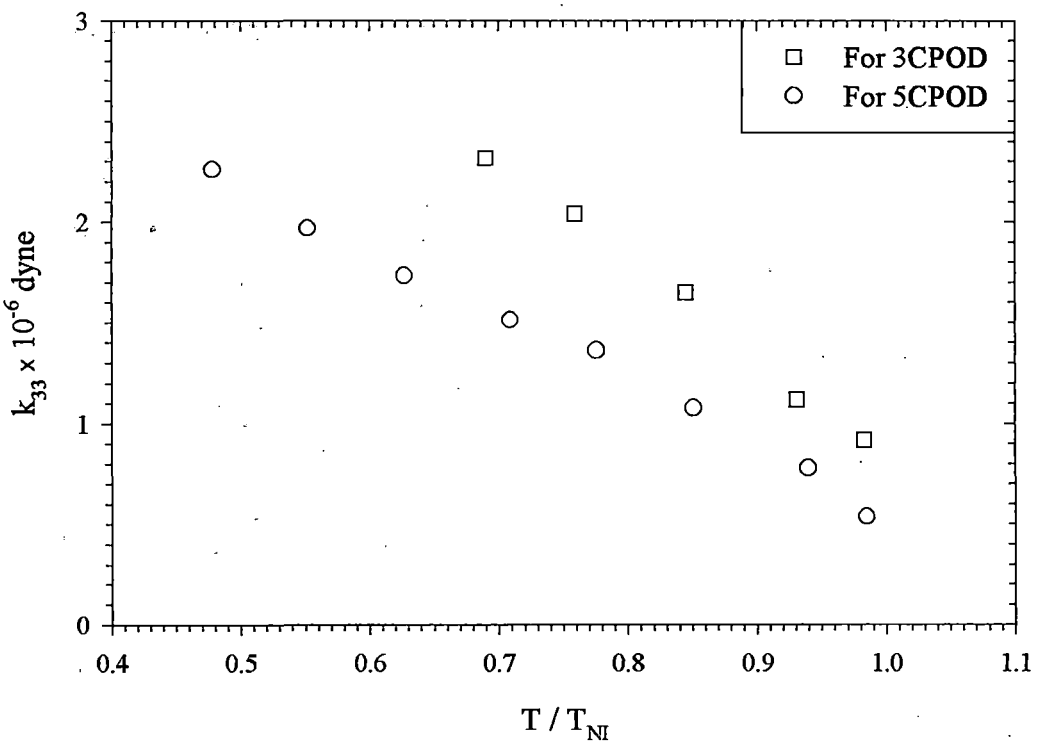

Fig. 8.6 Variation of bend elastic constant (k_{33}) with temperature

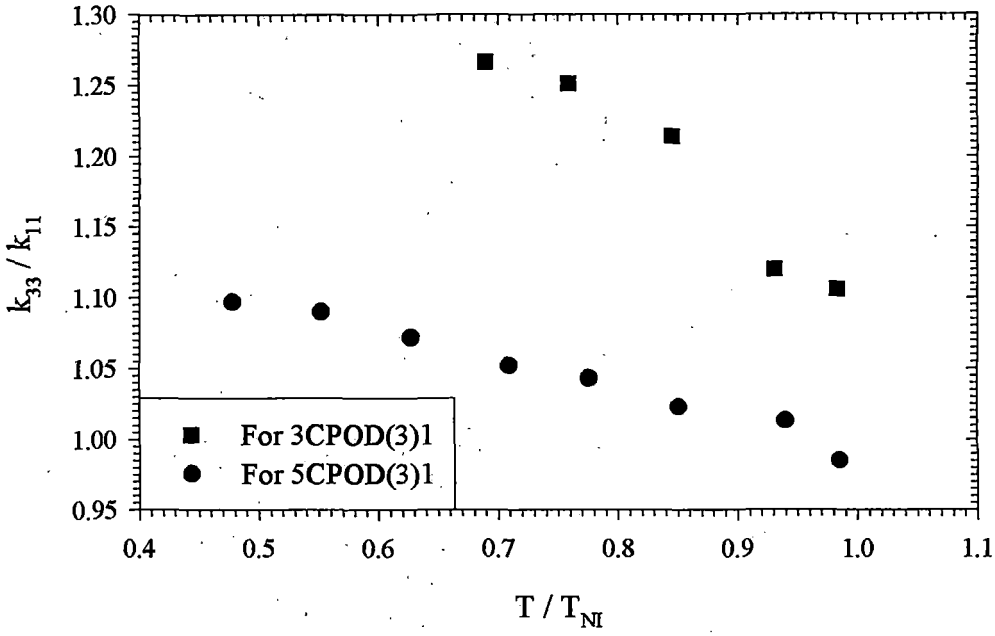

Fig. 8.7 Variation of k_{33} / k_{11} with temperature for sample 3CPOD(3)1 and 5CPOD(3)1

decreases where L and W represent the molecular length and width respectively. Though Leenhouts' previous work[201] supports this but later[203] his experimental results contradict it. Generally the width of the molecule is taken to be the nearly same as the width of the rigid core (≅ 4.83 Å) if the chain has five or less carbon atoms in it[203]. Apparent molecular length of two molecules 3CPOD(3)1 and 5CPOD(3)1 are 16.8 Å and 19.1 Å respectively. So according to the theory in my case k_{33}/k_{11} should decrease with decrease in R which is in contradiction to the experimental result.

Thus it is concluded that calculations based on spherocylindrical model is not so useful for explanation of experimental results. It is better to consider the suggestion proposed by de Jeu et al[208] and Karat et al[199] that the lengthening of the alkyl chain leads to an increase of the positional correlation in a plane perpendicular to the director and is the cause for decreasing the ratio of k_{33}/k_{11}.

Table - 8.1

Experimental values of splay elastic constant (k_{11}) for different values of temperature T / T_{NI} for sample 3CPOD(3)1

T_{NI} = 58.0°C, Sample thickness = 162 μm

T / T_{NI}	H_c in Gauss	$\Delta\chi$ x 10^{-8} cgs unit*	k_{11} x 10^{-6} dyne
0.983	770	5.255	0.8293
0.931	830	5.731	1.0508
0.845	880	6.595	1.3594
0.759	930	7.086	1.6313
0.690	960	7.465	1.8312

*data have been taken from reference [133].

Table - 8.2

Experimental values of splay elastic constant (k_{33}) for different values of temperature T / T_{NI} for sample 3CPOD(3)1

T_{NI} = 58.0° C , Sample thickness = 162 μm .

T / T_{NI}	H_c in Gauss	$\Delta\chi$ x 10^{-8} cgs unit	k_{33} x10^{-6} dyne
0.983	810	5.255	0.918
0.931	880	5.731	1.180
0.845	970	6.595	1.650
0.759	1040	7.086	2.040
0.690	1080	7.465	2.318

Table - 8.3

Experimental values of splay elastic constant (k_{11}) for different values of temperature T / T_{NI} for sample 5CPOD(3)1

T_{NI} = 67.0° C , Sample thickness = 162 μm

T / T_{NI}	H_c in Gauss	$\Delta\chi$ x 10^{-8} cgs unit	k_{11} x 10^{-6} dyne
0.985	690	4.2965	0.544
0.940	790	4.6355	0.770
0.851	870	5.2266	1.053
0.776	940	5.5538	1.306
0.709	965	5.7965	1.437
0.627	995	6.1370	1.617
0.552	1025	6.4600	1.806
0.478	1060	6.8960	2.060

Table - 8.4

Experimental values of splay elastic constant (k_{33}) for different values of temperature T / T_{NI} for sample 5CPOD(3)1

T_{NI} = 67.0° C, Sample thickness = 162 μm

T / T_{NI}	H_c in Gauss	$\Delta\chi$ x 10^{-8} cgs unit	k_{33} x10^{-6} dyne
0.985	685	4.2965	0.537
0.940	795	4.6355	0.780
0.851	880	5.2266	1.077
0.776	960	5.5538	1.362
0.709	990	5.7965	1.512
0.627	1030	6.1370	1.733
0.552	1070	6.4600	1.969
0.478	1110	6.8960	2.260

Table - 8.5

Ratio of bend to splay (k_{33} / k_{11}) elastic constants of sample 3CPOD(3)1 for various T / T_{NI} values.

T / T_{NI}	k_{11} x 10^{-6} dyne	k_{33} x 10^{-6} dyne	k_{33} / k_{11}
0.983	0.8293	0.918	1.106
0.931	1.0508	1.180	1.120
0.845	1.3594	1.650	1.214
0.759	1.6313	2.040	1.251
0.690	1.8312	2.318	1.266

Table - 8.6

Ratio of bend to splay (k_{33} / k_{11}) elastic constants of sample 5CPOD(3)1 for various T / T_{NI} values.

T / T_{NI}	k_{11} x 10^{-6} dyne	k_{33} x 10^{-6} dyne	k_{33} / k_{11}
0.985	0.544	0.537	0.985
0.940	0.770	0.780	1.013
0.851	1.053	1.077	1.023
0.776	1.306	1.362	1.043
0.709	1.437	1.512	1.052
0.627	1.617	1.733	1.072
0.552	1.806	1.969	1.090
0.478	2.060	2.260	1.097

Chapter - 9

SUMMARY AND CONCLUSION

The growing demand for hand-held consumer electronic products and portable display systems has given a fillip to the Liquid crystal display (LCD) market due to their low power consumption. To apply liquid crystals in technological field it is essential to know its physical properties. In the present dissertation I have reported the physical properties of different liquid crystalline samples as observed from x-ray diffraction, optical birefringence, dielectric anisotropy and elastic constant measurements. Here, I am describing, in a nutshell, the salient features of different works undertaken by me. The format adopted in the present work is as follows.

In chapter 1, I have presented a short review on liquid crystals especially, thermotropic liquid crystals. Among the different modifications I have concentrated my discussions only on those phases which are studied by me, namely, N and SmA. A few words about other liquid crystals have been discussed as an overview on this topic.

In chapter 2, different theories of LCs which can be verified by x-ray diffraction and optical birefringence studies, have been described. Brief description of the experimental techniques employed in this work have been reported. Methods of calculations of different physical parameters viz., orientational order parameter $\langle P_2 \rangle$ and $\langle P_4 \rangle$, apparent molecular length, intermolecular distance, refractive indices, molecular polarizabilities etc. have been outlined in this chapter.

In chapter 3, the experimental values of three bicomponent mixture systems have been reported. I have presented results on mixtures A (7CBB+6OCB) with five different compositions, mixtures B (7CBB+7OCB) with seven different compositions and mixtures C (7CBB+8OCB) with five different compositions. Mixtures A and B show induced smectic A_d phase and mixtures C show enhanced smectic A_d phase. Mixtures A_1, B_1 and C_1 show re-entrant nematic phase as well. These experiments reveal that the homo- and hetero-dimer formation is the main cause for the formation of smectic A_d phase. In all mixtures layer thickness values in SmA_d phase are almost temperature independent. But average apparent molecular lengths in N_{re} and N phases decrease with decreasing temperature. At a constant temperature for all the three mixture systems flat maxima in layer thickness is

observed when plotted against concentration near the position of maximum thermal stability of SmA_d phase. Average layer thickness of all the mixtures have been calculated assuming the presence of monomers and homo- and hetero-dimers and these are in good agreement with the observed values. Refractive index measurement was possible only for mixture B_1 in N_{re} phase and to some extent in SmA_d phase. From both x-ray diffraction, refractive indices, density and DSC studies it is confirmed that N_{re}–SmA_d transition is of second order.

In chapter 4, results of another mixture system (EPBCC+5OCB) at four different compositions have been described and their properties have been compared with those of the pure compounds. It has been widely observed that bicomponent mixtures of nematic compounds — one strongly dipolar and another weakly polar or non-polar — produces induced smectic phase. But in this experiment I have observed the formation of cybotactic structures rather than induced smectic phase. Density of mixtures decreases smoothly with temperature but with increasing concentration of 5OCB the density variation is quite irregular. This might be the effect of anomalous density behaviour of pure EPBCC. In pure state both the samples form strong association in the mesophase, the observed ratio of apparent molecular length to molecular model length (l/L) being 1.3 to 1.4. Mixture A with lowest concentration of 5OCB shows no such association at all. In other mixtures, where 5OCB concentration is increased, bimolecular association is found to exist but the nature is quite weak, l/L ratio being ~1.1.

In chapter 5, dielectric permittivity study on two compounds 5CB and ME6O.5 and their mixtures of several compositions have been discussed with brief discussions on the relevant theories and experimental techniques. Mixture of the polar 5CB and the weakly polar ME6O.5 produce induced SmA_d phase in certain concentration region. Both the samples show positive dielectric anisotropy, in both N and induced SmA_d phases, which is larger in polar compound than in weakly polar compound. $\bar{\varepsilon}$ near N – I transition is less than ε_{iso} for the polar compound and is almost equal for weakly polar compound. Observed permittivity components of the mixtures are as expected from simple additivity rule. But prominent jump in $\varepsilon_{\|}$ component is observed at Sm–N transition, which is greater than the jump of $\varepsilon_{\perp}$ at

that point. These have been explained as the effect of anti-parallel dipole-dipole associations. The change of $\varepsilon_{\perp}$ at the Sm–N transition is, however, continuous at the lower and higher concentrations and is discontinuous in between. Variation of $\Delta\varepsilon$ with mole fraction of ME6O.5 shows a minima near mole fraction of 0.65 where the thermal stability of SmA_d phase is maximum. Observation of similar minimum in orientational order parameter ($\langle P_2 \rangle$), apparent molecular length, packing fraction, Δn etc. had been reported earlier at the concentration of maximum thermal stability of SmA_d phase. Maxima in layer spacings at the concentration of maximum thermal stability had been reported in chapter - 3 and other mixtures. Thus it is concluded that thermal stabilisation of SmA_d phase plays a major role in determining the physical properties of binary mixtures. Minimum values in certain physical parameters are observed when monomer concentration is high and maximum values in physical parameters are observed when dimer concentration is high.

Chapter 6 deals with theoretical background of crystal structure analysis. Here I have discussed mainly the Direct Methods and procedures of structure solution by using the package program MULTAN.

In chapter 7, crystal structure of two mesogens ECCPP and HCCPP at low temperatures (246K and 243K respectively) have been presented. I have undertaken the crystal structure determination of these two compounds at low temperatures in an anticipation that this study may provide some information about the thermal behaviour of the molecules. These two structures were determined at room temperature in our laboratory. At room temperature, of the two independent molecules in the unit cell, the cyclohexane ring of one of the molecules of ECCPP showed planar configuration. While in other molecule it was in chair configuration. This planar configuration transformed into chair form at low temperature. Structure of HCCPP does not show any significant change. Order parameter $\langle P_2 \rangle$ calculations and analysis of the anisotropic displacement parameters were carried out at both temperatures. At low temperature translational and librational motion are lower than at room temperature. In all cases the mean squares amplitudes of translational motions have the smallest values along the stacking directions and largest along the

molecular axes. Order parameter $\langle P_2 \rangle$ for HCCPP is lower than that of ECCPP at both the temperatures. This is due to the flexibility of the long alkyl chain.

Chapter 8 presents splay (k_{11}) and bend (k_{33}) elastic constants of two alkenyl compounds 3CPOD(3)1 and 5CPOD(3)1 of a homologues series with a brief discussions on the theory of elastic constants, Freedericksz transition and experimental techniques. For both the samples k_{33} is greater than k_{11}. k_{11}, k_{33} and k_{33}/k_{11} decrease gradually with increasing temperature. Variation of k_{33}/k_{11} with chain length agrees with others experiments reported so far. From rough estimates of molecular aspect ratio it has been observed that theoretical model based on effective spherocylinders by Nehring and Saupe does not allow an explanation of the experimentally observed trends for molecules with flexible hydrocarbon chains. It is better to accept the suggestion proposed by de Jeu et al and Karat et al, who attributed the decrease of k_{33}/k_{11} with increasing chain length to an increasing degree of short range positional order in a plane perpendicular to the director **n**.

REFERENCES

1. F. Reinitzer, *Monatsch Chem.*, **9**, 421 (1888).
2. O. Lehmann, *Z. Physikal Chem.*, **4**, 462 (1889).
3. D. Demus, H. Demus and H. Zaschke, *Flussige Kristalle in Tabellen*, VEB, Deulscher Verlag Fur Grundstoffindustrie (Leipzig) (1974).
4. G. H. Brown, *J. Electronic Materials*, **2**, 402 (1973).
5. H. Kelkar and R. Hatz, *"Hand Book of Liquid Crystals"*, Verlag Chemie, Chapter 1, 6 (1980).
6. G. Friedel and E. Friedel, *Z. Krist.*, **79**, 1 (1931).
7. S. Chandrasekhar, *"Liquid Crystals"*, Cambridge Univ. Press, Cambridge, (1992).
8. B. Bahadur, *"Liquid Crystals – applications and uses"*, vol.-1, World Scientific, Singapore (1990).
9. Xin - Jin Wang, Kun Tao, Jing - An Zhao and Liang - Yu Wang, *Liq. Cryst.*, **5(2)**, 563 (1989).
10. T. Niori, T. Sekine, J. Watanabe, T. Furukawa and H. Takezoe, *J. Mater. Chem.*, **6**, 1231 (1996).
11. W. Weissflog, Ch. Lischka, I. Benne, T. Scharf, G. Pelzl, S. Diele and H. Kruth, *SPIE*, **3319**, 14 (1998).
12. M. A. Osipov and S. A. Pikin, *Mol. Cryst. Liq. Cryst.*, **103**, 57 (1983).
13. L. A. Blinov, M. A. Osipov and S. A. Pikin, *Mol. Cryst. Liq. Cryst.*, **158A**, 3 (1988).
14. J. Przedmojski, K. Czuprynski and E. Gorecka, *SPIE*, **3319**, 133 (1998).
15. A. Pegenau, P. Goring, S. Diele and C. Tschierske, *SPIE*, **3319**, 70 (1998).
16. M. Watanabe, M. Eguchi, K. Kakimoto and T. Hibiya, *J. Crystal Growth*, **133**, 23 (1993).
17. E. B. Priestley, *"Introduction to Liquid Crystals"*, Plenum Press, New York (1975).
18. G. H. Brown and J. J. Wolken, *"Liquid Crystals and Biological Structures"*, Academic Press, New York (1979).
19. S. Friberg, *"Lyotropic Liquid Crystals"*, Acs, Washington (1976).

20. V. Luzzati and Taredieu, *Annual Review of Physical Chemistry*, **25**, 79 (1974).
21. W. Helfrich and G. Heppke, *"Liquid Crystals of One and Two Dimensional Order"*, Springer - Verlag, 265 (1980).
22. P. G. de Gennes and J. Prost, *"The Physics of Liquid Crystals"*, Clarendon Press, Oxford, 2nd Edn. (1993).
23. G. Friedel, *Ann. Physique*, **18**, 273 (1922).
24. A. de Vries, *Mol. Cryst. Liq. Cryst.*, **10**, 31 (1970).
25. A. de Vries, *Mol. Cryst. Liq. Cryst.*, **10**, 219 (1970).
26. J. Malthéte, L. Liebert, A. M. Levelut and Y. Galerne, *C. R. Adac. Sc. Paris*, **303**, 1073 (1986).
27. K. Praefcke, B. Kohne, B. Gundogan, D. Singer, D. Demus, S. Diele, G. Pelzl and U. Bakowsky, *Mol. Cryst. Liq. Cryst.*, **198**, 393 (1991).
28. L. J. Lu and A. Saupe, *Phys. Rev. Lett.*, **45**, 1000 (1980).
29. H. Sackmann and D. Demus, *Mol. Cryst. Liq. Cryst.*, **21**, 239 (1973).
30. S. Diele, P. Brand and H. Sackmann, *Mol. Cryst. Liq. Cryst.*, **16**, 105 (1972).
31. D. Demus, S. Diele, M. Klapperstuck, V. Link and H. Zaschke, *Mol. Cryst. Liq. Cryst.*, **15**, 161 (1971).
32. P. S. Pershan, *"Structure of liquid crystal phases"*, Worrld Scientific Lexture Notes in Physics — vol. 23, Singapore, (1988).
33. A. de Vries, *Proc. of the International Liquid Crystal Conference*, Bangalore, December, Pramana Supplement I, 93 (1973).
34. F. D. Saeva (Ed.), *"Liquid Crystals: The Fourth State of Matter"*, Marcel Dekker, New York (1979).
35. G. R. Luckhurst and G. W. Gray (Eds.), *"The molecular physics of liquid crystals"*, Academic Press, London (1979).
36. S. Chandrasekhar (Ed.), *"Liquid Crystals"*, Heyden, London (1980).
37. A. L. Tsykalo, *"Thermophysical properties of liquid crystals"*, Gordon and Breach Science Publishers, (1991).
38. P. J. Collings and M. Hird, *"Introduction to liquid crystals chemistry and physics"*, Taylor and Francis, UK. (1997).

39. J. Prost, *Advances in Physics*, **33**, 146 (1984).

40. B. R. Ratna, R. Shashidhar and V. N. Raja, *Phys. Rev. Lett.*, **54(14)**, 1476 (1985).

41. S. Chandrasekhar, B. K. Sadashiv and A. K. Suresh, *Pramana*, **9**, 471 (1977).

42. S. Chandrasekhar, *Phil. Trans. R. Soc. A*, **309**, 93 (1983).

43. S. Chandrasekhar, *Liq. Cryst.*, **14**, 3 (1993).

44. C. Destrade, P. Foucher, H. Gasparoux, H. T. Nguyen, *Mol. Cryst. Liq. Cryst.*, **106**, 121 (1984).

45. C. Destrade, H. T. Nguyen, H. Gasparoux, J. Malthete and A. M. Levelut, *Mol. Cryst. Liq. Cryst.*, **71**, 111 (1981).

46. S. Meiboom, M. Sammon, *Phys. Rev. Lett.*, **44**, 882 (1980).

47. M. Brodzik and R. Dabrowski, *Liq. Cryst.*, **18**, 61 (1995).

48. H. Stegemeyer, Th Blumel, K. Hiltrop, H. Onusseit and F. Porsch, *Liq. Cryst.*, **1**, 1 (1996).

49. G. Pelzl, H. Sackmann, *Z. Phys. Chem.*, **254**, 354 (1973).

50. P. E. Cladis, *Phys. Rev. Lett.*, **35**, 48 (1975).

51. P. E. Cladis, *"Liquid Crystals"*, Ed. S. Chandrasekhar, Heyden, London, p 105 (1980).

52. H. T. Nguyen, F. Hardouin, C. Destrade, *J. Phys. (Paris)*, **43**, 1127 (1982).

53. J. W. Park, C. S. Bak and M. M. Labes, *J. Amer. Chem. Soc.*, **97**, 4398 (1975).

54. G. Heppke and E. J. Richter, *Z. Naturforsch*, **A33**, 185 (1978).

55. B. Engelen, G. Heppke, R. Hopt and F. Schneider, *Ann. de Phys.*, **3**, 403 (1978).

56. J. W. Goodby, R. Blinc, N. A. Clark, S. T. Lagerwall, M. A. Osipov, S. A. Pikin, T. Sakurai, K. Yoshino and B. Zeks, *"Ferroelectric Liquid Crystals: Principles, Properties and Applications"*, Gordon and Breach, Philadelphia (1991).

57. C. S. Oh, *Mol. Cryst. Liq. Cryst.*, **42**, 1 (1977).

58. M. Domon and J. Billard, *J. Phys. (Paris)*, **40**, C3-413 (1979).

59. K. P. L. Moodithaya and N. V. Madhusudana in *"Liquid Crystals"*, Proc. Int. Liq. Cryst. Conf., Bangalore, Dec. 8, (1979), Ed. S. Chandrasekhar (Heyden, London 1980) p. 297.

60. F. Schneider and N. K. Sharma, *Z. Naturforch.*, **36a**, 1086 (1981).

61. K. Araya and Y. Matsunaga, *Mol. Cryst. Liq. Cryst.*, **62**, 153 (1981).

62. G. Derfel, *Mol. Cryst. Liq. Cryst.*, **82**, 277 (1982).

63. J. Szabon and S. Diele, *Crystal Res. Tech.*, **17**, 1325 (1982).

64. K. W. Sadowska, A. Zywocinski, J. Stecki and R. Dabrowski, *J. Phys. (Paris)*, **43**, 1673 (1982);

65. W. Waclawek, R. Dabrowski and A. Domagala, *Mol. Cryst. Liq. Cryst.*, **84**, 255 (1982).

66. A. Boij and P. Adomenas, *Mol. Cryst. Liq. Cryst.*, **95**, 59 (1983).

67. E. Chino and Y. Matsunaga, *Bull. Chem. Soc. Japan*, **56**, 3230 (1983).

68. S. K. Giri, N. K. Pradhan, R. Paul, S. Paul, P. Mandal, R. Dabrowski, M. Brodzik and K. Czuprynski, *SPIE*, **3319**, 149 (1998).

69. L. Longa and W. H. de Jeu, *Phys. Rev., Mol. Cryst. Liq. Cryst.*, **A26**, 1632 (1982).

70. R. R. Netz and A. N. Berker, *Phys. Rev. Lett.*, **68**, 333 (1992).

71. M. Born, Sitz d., *Phys. Math.*, **25**, 614 (1916).

72. L. D. Landau, *"On the Theory of Phase Transition, Part - I and II"*, Collected papers of L. D. Landau, Ed. D. ter Haar, Gordon and Breach, Science Publishers, N. Y., 2nd Edn., p. 93 (1967).

73. L. Onsager, *Ann. N. Y. Acad. Sci.*, **51**, 627 (1949).

74. W. Maier and A. Saupe, *Z. Naturforch*, **13a**, 564 (1958); ibid., **14a**, 882 (1959); ibid., **15a**, 287 (1960).

75. W. L. McMillan, *Phys. Rev.*, **A4**, 1238 (1971); ibid **A6**, 936 (1972).

76. R. L. Humphries, P. G. James and G. R. Luckhurst, *J. Chem. Soc., Faraday Trans. II*, **68**, 1031 (1972).

77. K. K. Kobayashi, *J. Phys. Soc. (Japan)*, **29**, 101 (1970).

78. K. K. Kobayashi, *Mol. Cryst. Liq. Cryst.*, **13**, 137 (1971).

79. B. Jha and R. Paul, *Proc. Nucl. Phys. and Solid State Phys. Symp.*, India, **19c**, 491 (1976).

80. L. V. Azároff and C. A. Schuman, *Mol. Cryst. Liq. Cryst.*, **122**, 309 (1985).

81. H. P. Klug and L. E. Alexander, *"X-ray diffraction procedures"*, John Wiley and Sons, N. Y., p. 114 and 473 (1994).

82. A. J. Leadbetter and E. K. Norris, *Mol. Phys.*, **38**, 669 (1979).

83. R. Paul and G. Chaudhuri, Abstract in the 14th International Liquid Crystal Conference, Pisa, (1992), Abs. no. - H- P23.

84. E. Dorn, *Z. Physik*, **11**, 111 (1910).

85. G. Pelzl and H. Sackmann, *Mol. Cryst. Liq. Cryst.*, **15**, 75 (1971).

86. G. Pelzl and H. Sackmann, *Symp. Faraday Soc.*, **5**, 68 (1971).

87. Y. Galerne, S. T. Lagerwall and I. W. Smith, *Opt. Commun.*, **19**, 147 (1976).

88. S. K. Giri, N. K. Pradhan, R. Paul, S. Paul, P. Mandal, R. Dabrowski, M. Brodzik and K. Czuprynski, *Mol. Cryst. Liq. Cryst.*, (1999) (in Press).

89. H. E. Neugebauer, *Canad. J. Phys.*, **32**, 1 (1954).

90. M. F. Vuks, *Optics and Spectroscopy*, **20**, 361 (1966).

91. P. G. de Gennes, *Mol. Cryst. Liq. Cryst.*, **12**, 193 (1971).

92. I. Haller, H. A. Huggins, H. R. Lilienthal and T. R. McGuire, *J. Phys. Chem.*, **77**, 950 (1973).

93. A. K. Zeminder, S. Paul and R. Paul, *Mol. Cryst. Liq. Cryst.*, **61**, 191 (1980).

94. M. Brodzik and R. Dabrowski, *Liq. Cryst.*, **18**, 61 (1995).

95. M. Brodzik and R. Dabrowski, *Liq. Cryst.*, **20**, 99 (1996).

96. M. Brodzik and R. Dabrowski, *J. Phys. II France*, **5**, 1805 (1995).

97. S. Chandrasekhar, *Mol. Cryst. Liq. Cryst.*, **124**, 1 (1985).

98. A. C. Griffin, T. R. Britt, N. W. Buckley, R. F. Fisher, S. J. Havens and D. W. Goodman, *Liquid Crystals and Order Fluids*, Vol. - 3, Eds. J. F. Johnson and R. S. Porter, Plenum Press, New York, 61 (1978).

99. B. Engelen and F. Schneider, *Z. Naturforch.*, **33A**, 1077 (1978).

100. B. Engelen, G. Heppke, R. Hopf and F. Schneider, *Ann. Phys.*, **3**, 403 (1978).

101. L. J. Yu and M. M. Labes, *Mol. Cryst. Liq. Cryst.*, **54**, 1 (1979).

102. P. E. Cladis in *"Liquid Crystals"*, Proc. Int. Conf. Bangalore (1979), Ed. S. Chandrasekhar, Heyden, London, 105 (1980).
103. P. E. Cladis, *Mol. Cryst. Liq. Cryst.*, **67**, 177 (1981).
104. P. E. Cladis, D. Guillon, F. R. Bouchet and P. L. Finn, *Phys. Rev.*, **23a**, 2594 (1981).
105. W. H. de Jeu, L. Longa and D. Demus, *J. Chem. Phys.*, **84**, 6140 (1986).
106. M. Brodzik, *PhD thesis* submitted in Wojskowa Akademia Techniczna, (1995).
107. B. Bhattacharjee, S. Paul and R. Paul, *Mol. Cryst. Liq. Cryst.*, **89**, 181 (1982).
108. M. K. Das, S. Paul and R. Paul, *Mol. Cryst. Liq. Cryst.*, **264**, 89 (1995).
109. G. J. Brownsey and A. J. Leadbetter, *Phys. Rev. Lett.*, **44(24)**, 1608 (1980).
110. N. V. Madhusudana and J. Rajan, *Liq. Cryst.*, **7**, 31 (1990).
111. A. S. Govind and N. V. Madhusudana, *Liq. Cryst.*, **23**, 327 (1997).
112. N. V. Madhusudana, *Brazilian J. Phys.*, **28(4)**, 1 (1998).
113. G. R. Luckhurst and B. A. Timini, *Mol. Cryst. Liq. Cryst.*, **64**, 253 (1981).
114. M. Mitra, S. Paul and R. Paul, *Pramana - J. Phys.*, **29**, 409 (1987).
115. M. K. Das, R. Paul and D. Dunmur, *Mol. Cryst. Liq. Cryst.*, **258**, 239 (1995).
116. M. Mitra, R. Paul and S. Paul, *Mol. Cryst. Liq. Cryst.*, **177**, 71 (1989).
117. S. Gupta. R. Paul and S. Paul, *Mol. Cryst. Liq. Cryst.*, **262**, 485 (1995).
118. M. Mitra, S. Paul and R. Paul, *Liq. Cryst.*, **3(1)**, 123 (1988).
119. M. Mitra and R. Paul, *Mol. Cryst. Liq. Cryst.*, **148**, 185 (1987).
120. M. Mitra, R. Paul and S. Paul, *Acta Physica Polonica*, **A78**, 453 (1990).
121. P. Mandal and S. Paul, *Mol. Cryst. Liq. Cryst.*, **131**, 223 (1985).
122. J. E. Lydon and C. J. Coakley, *J. Phys., Paris*, **C1-36**, 45 (1975).
123. S. Diele, L. Nasta and H. Sackmann, *Kristall u Technik*, **12**, 10 (1979).
124. S. Diele, U. Baumeister and D. Demus, *Z. Chem.*, **21**, 27 (1980).
125. S. Diele, K. Billich and Z. Przedmojski, *Z. Chem.*, **26**, 26 (1986).
126. R. Chang, *Mol. Cryst. Liq. Cryst.*, **30**, 155 (1975).
127. N. V. Madhusudana, R. Shashidhar and S. Chandrasekhar, *Mol. Cryst. Liq. Cryst.*, **13**, 61 (1971).
128. M. K. Das and R. Paul, *Phase Trans.*, **48**, 255 (1994).

129. J. S. Dave, P. R. Patel and K. L. Vasant, *Mol. Cryst. Liq. Cryst.*, **8**, 93 (1969).

130. D. A. Dunmur, R. G. Walker and P. Palffy-Muhoray, *Mol. Cryst. Liq. Cryst.*, **122**, 321 (1985).

131. M. K. Das and R. Paul, *Phase Trans.*, **46**, 185 (1994).

132. B. Adhikari and R. Paul, *Mol. Cryst. Liq. Cryst.*, **301**, 419 (1997).

133. N. K. Pradhan, PhD thesis entitled *"Study of Physical Properties of Liquid Crystals and their Mixtures"* submitted in North Bengal University, (1998).

134. S. K. Giri, P. K. Mandal and S. Paul, *Mol. Cryst. Liq. Cryst.*, (1999) (in press).

135. S. R. Sharma, *Mol. Phys.*, **78**, 733 (1993).

136. D. A. Dunmur, M. R. Manterfield, W. H. Miller and J. K. Dunleavy, *Mol. Cryst. Liq. Cryst.*, **45**, 127 (1978).

137. M. Davies, R. Moutram, A. H. Price, M. S. Beevers and G. Williams, *J. Chem. Soc. Faraday Tran II*, **72**, 1447 (1976).

138. N. V. Madhusudana, K. L. Savithramina, S. Chandrasekhar, *Pramana*, **8**, 22 (1977).

139. M. K. Das, B. Jha and R. Paul, *Mol. Cryst. Liq. Cryst.*, **261**, 95 (1995).

140. R. F. Bryan, *J. Structural Chem.*, **23**, 128 (1982).

141. A. J. Leadbetter and M. A. Mazid, *Mol. Cryst. Liq. Cryst.*, **51**, 85 (1979).

142. P. Mandal, S. Paul, C. H. Stam and H. Schenk, *Mol. Cryst. Liq. Cryst.*, **180B**, 369 (1990).

143. P. Mandal, S. Paul, H. Schenk and K. Goubitz, *Mol. Cryst. Liq. Cryst.*, **210**, 21 (1992).

144. S. Gupta, P.Mandal, S. Paul, M. Wit, K. Goubitz and H. Schenk, *Mol. Cryst. Liq. Cryst.*, **195**, 149 (1991).

145. S. Gupta, A. Nath, S. Paul, H. Schenk and K. Goubitz, *Mol. Cryst. Liq. Cryst.*, **257**, 1 (1994).

146. A. Nath, S. Gupta, P. Mandal, S. Paul and H. Schenk, *Liq. Cryst.*, **20**, 765 (1996).

147. M. V. Laue, *"Sitzungberichte der (kgl) Bayerische Akademic der Wissenschaften"*, p. 308 (1982).

148. W. L. Bragg, *Proc. Camb. Phil. Soc.*, **17**, 43 (1913).

149. W. L. Bragg, *Proc. Roy. Soc.*, **A89**, 249 (1913).

150. M. F. C. Ladd and R. A. Palmer, *"Theory and practice of Direct methods in Crystallography"*, Plenum Pub. Co., N. Y., (1980).

151. H. Hauptman and J. Karle, *Acta Cryst.*, **9**, 45 (1956); ibid., **12**, 93 (1959).

152. J. Karle and H. Hauptman, *Acta Cryst.*, **14**, 217 (1961).

153. J. Karle and I. L. Karle, *Acta Cryst.*, **21**, 849 (1966).

154. H. Schenk, *"Computing Methods in Crystallography"*, Eds. R. Diamond, S. Ramaseshan and K. Venkatesan, Indian Academy of Science (1980).

155. H. Ott, *Zskrist*, **66**, 136 (1927).

156. K. Banerjee, *Proc. Roy. Soc.*, **A141**, 188 (1933).

157. M. Avrami, *Phys. Rev.*, **54**, 300 (1938).

158. A. J. Goedkoop, *Acta Cryst.*, **5**, 60 (1952).

159. H. Hauptman and J. Karle, *Acta Cryst.*, **6**, 136 (1953).

160. A. R. Overbeek and H. Schenk, *"In computing in crystallography"*, Edited by Schonok et al., Delft University Press, (1978).

161. G. M. Sheldrick, *"Crystallographic program system"*, University of Cambridge, England, (1976).

162. J. Lajzerowicz and J. Lajzerowicz, *Acta Cryst.*, **21**, 8 (1966).

163. J. P. Declercq, G. Germain and M. M. Woolfson, *Acta Cryst.*, **A31**, 367 (1975).

164. Y. Jia-Xing, *Acta Cryst.*, **A37**, 642 (1981).

165. Z. Shao-Hui and M. M. Woolfson, *Acta Cryst.*, **A38**, 683 (1982).

166. J. P. Declercq, G. Germain, M. M. Woolfson and H. Wright, *Acta Cryst.*, **A37**, 237 (1981).

167. C. J. Gilmore, *J. App. Cryst.*, **17**, 42 (1984).

168. G. Germain, P. Main and M. M. Woolfson, *Acta Cryst.*, **B26**, 274 (1970).

169. W. R. Busing and H. A. Levy, *Acta Cryst.*, **10**, 180 (1957).

170. A. J. C. Wilson, *Nature*, **150**, 152 (1942).

171. J. Karle and H. Hauptman, *Acta Cryst.*, **9**, 635 (1956).

172. W. Cochran and M. M. Woolfson, *Acta Cryst.*, **8**, 1(1955).

173. W. Cochran, *Acta Cryst.*, **8**, 473 (1955).

174. B. Bhattacherjee and G. A. Jeffrey, *Mol. Cryst. Liq. Cryst.*, **101**, 247 (1983).

175. S. Gupta, B. Majumdar, P. Mandal, R. Paul and S. Paul, *Phase Trans.*, **40**, 73 (1992).

176. P. S. White, *PC version of NRCVAX*, University of New Brunswick, Canada (1988).

177. W. Hasse and H. Paulus, *Mol. Cryst. Liq. Cryst.*, **100**, 111 (1983).

178. C. K. Johnson, *ORNL - 3794*, Oak Ridge National Laboratory, Tennesse (1970).

179. D. W. Cruickshank, *Acta Cryst.*, **9**, 754 (1950).

180. V. Schoemaker and K. N. Trueblood, *Acta Cryst.*, **B24**, 63 (1968).

181. R. Eppenga and D. Frenkel, *Mol. Phys.*, **52**, 1303 (1984).

182. M. Schadt, M. Petrzilka, P. R. Gerber and A. Villiger, *Mol. Cryst. Liq. Cryst.*, **122**, 241 (1985).

183. M Schadt, R. Buchecker and K. Muller, *Liq. Cryst.*, **5**, 293 (1989).

184. M. Schadt, R. Buchecker, F. Leenhouts, A. Boller, A. Villiger and M. Petrzilka, *Mol. Cryst. Liq. Cryst.*, **139**, 1 (1986)..

185. A. Nath, P. Mandal and S. Paul, *Mol. Cryst. Liq. Cryst.*, **299**, 483 (1997).

186. A. Nath, *PhD thesis submitted to University of North Bengal*, (1995).

187. M. Schadt, *Liq. Cryst.*, **14(1)**, 73 (1993).

188. S. M. Kelly, M. Schadt and H. Seiberle, *Liq. Cryst.*, **18**, 581 (1995).

189. M. Schadt, R. Buchecker and A. Villiger, *Liq. Cryst.*, **7(4)**, 519 (1990).

190. H. Zocher, *Z. Physik*, **28**, 790 (1927).

191. H. Zocher, *Trans. Faraday Soc.*, **29**, 945 (1933).

192. W. Oseen, *Trans. Faraday Soc.*, **29**, 883 (1933).

193. C. Frank, *Discussions Faraday Soc.*, **25**, 19 (1958).

194. H. Gruler, T. J. Schiffer and G. Meier, *Z. Naturforch*, **27a**, 966 (1972).

195. H. Gruler and L Chaung, *J. Appl. Phys.*, **46**, 5097 (1975).

196. M. J. Bradsahaw and E. P. Rayens, *Mol. Cryst. Liq. Cryst.*, **72**, 35 (1980).

197. V. Freedericksz and V. Tesvetkov, *Phys. Z. Soviet Union*, **6**, 490 (1934).

198. V. Freedericksz and V. Zolina, *Trans. Faraday Soc.*, **29**, 919 (1933).

199. P. Karat and N. V. Madhusudana, *Mol. Cryst. Liq. Cryst.*, **40**, 239 (1977).

200. Hp. Schad and M. A. Osman, *J. Chem. Phys.*, **75(2)**, 880 (1981).

201. F. Leenhouts, H. J. Roebers, A. J. Dekker and J. J. Jonker, *J. Phys. (Paris)*, **40**, C3-291 (1979).

202. Hp. Schad, G. Bauer and G. Maier, *J. Chem. Phys.*, **67**, 3705 (1977).

203. F. Leenhouts and A. J. Dekker, *J. Chem. Phys.*, **74**, 1956 (1981).

204. M. K. Das and R. Paul, *Mol. Cryst. Liq. Cryst.*, **259**, 13 (1995).

205. W. H. de Jeu, *"Physical Properties of Liquid Crystalline Materials"*, Gordon and Breach Science Publishers, N. Y. 24 (1980).

206. P. Karat and N. V. Madhusudana, *Mol. Cryst. Liq. Cryst.*, **36**, 51 (1976).

207. M. J. Bradshaw, E. P. Raynes, J. D. Bunning and T. E. Faber, *J. Physique*, **46**, 1513 (1985).

208. W. H. de Jeu and W. A. P. Claassen, *J. Chem. Phys.*, **67**, 3705 (1977).

209. Hp. Schad, G. Bauer and G. Meier, *J. Chem. Phys.*, **70**, 2770 (1979).

210. M. Schadt and F. Muller, *J. Phys. (Paris)*, **14**, 265 (1979).

211. G. Marrucci et al, *Mol. Cryst. Liq. Cryst.*, **206**, 17 (1991).

212. I. P. Kolomiets, A. M. Ovsipyan and S. K. Filipov, *Mol. Cryst. Liq. Cryst.*, **301**, 343 (1997).

213. J. Nehring and A. Saupe, *J. Chem. Phys.*, **56**, 5527 (1972).

LIST OF PAPERS (Published, communicated and presented)

1. "Small angle x-ray diffraction study of mixtures showing re-entrant nematic phase and induced smectic A_d phase", S. K. Giri, N. K. Pradhan, R. Paul, S. Paul, P. Mandal, R. Dabrowski, M. Brodzik and K. Czuprynski, *SPIE*, **Vol. 3319**, 149–153 (1998).

2. "Study of dielectric anisotropy of an ester/biphenyl mixture exhibiting an induced smectic phase", S. K. Giri, P. Mandal and S. Paul – Presented at the National Seminar on Liquid Crystal - 98 held at Goa University, Goa, India and accepted for publication in the journal *Mol. Cryst. Liq. Cryst.*

3. "Refractive index, density and order parameter of two binary mixtures showing re-entrant nematic phase", S. K. Giri, N. K. Pradhan, R. Paul, S. Paul, P. Mandal, R. Dabrowski, M. Brodzik and K. Czuprynski – presented at 17th International Liquid Crystal Conference-98 held at Strasbourg, France and accepted for publication in the journal *Mol. Cryst. Liq. Cryst.*

4. "Small angle x-ray diffraction study of mixtures showing re-entrant nematic phase and induced smectic A_d phase", S. K. Giri, N. K. Pradhan, R. Paul, S. Paul, P. Mandal, R. Dabrowski, M. Brodzik and K. Czuprynski – presented at the National Seminar on Liquid Crystals - 97 in Jammu, India.

5. "On the temperature dependence of crystal structures of two mesogenic compounds", S. K. Giri, P. K. Mandal, S. Paul and R. Paul, – presented at the National Seminar on Liquid Crystals - 97 in Jammu, India.

6. " Small angle x-ray diffraction study of mesomorphic mixtures of 7CBB and 7OCB", S. K. Giri, R. Paul, S. Paul, P. K. Mandal, R. Dabrowski, M. Brodzik and K. Czuprynski – presented at the European Conference on Liquid Crystals - Science and Technology, March 1997, held at Zakopane, Poland.

7. "The structure and properties of 5-(*trans*-4-heptylcyclohexyl)-2- (4- cyanophenyl) pyrimidine (HCCPP)", S. K. Giri, P. K. Mandal, S. Paul and R. Paul – presented at 17th International Liquid Crystal Conference-98 in France.

8. "Anomalous behaviour as observed from density measurements and optical studies for a binary mixture of 5OCB + EPBCC", S. K. Giri, P. K. Mandal and S. Paul – presented at The National Seminar on Liquid Crystals - 95 of Indian Liquid Crystal Society held in Vadodara, Baroda, Gujarat, India, (to be communicated).